



JAGIELLONIAN UNIVERSITY
IN KRAKOW

Self-localization and time reversal
symmetry breaking effects in
ultra-cold atomic gases

by

Katarzyna Targońska

Ph.D. thesis

under supervision of prof. dr hab Krzysztof Sacha

Kraków, 2013

Wydział Fizyki, Astronomii i Informatyki Stosowanej
Uniwersytet Jagielloński

Oświadczenie

Ja niżej podpisana Katarzyna Targońska (nr indeksu: 1060650) doktorantka Wydziału Fizyki, Astronomii i Informatyki Stosowanej Uniwersytetu Jagiellońskiego oświadczam, że przedłożona przeze mnie rozprawa doktorska pt. „Self-localization and time reversal symmetry breaking effects in ultra-cold atomic gases” jest oryginalna i przedstawia wyniki badań wykonanych przeze mnie osobiście, pod kierunkiem prof. dr hab. Krzysztofa Sachy. Pracę napisałam samodzielnie.

Oświadczam, że moja rozprawa doktorska została opracowana zgodnie z Ustawą o prawie autorskim i prawach pokrewnych z dnia 4 lutego 1994 r. (Dziennik Ustaw 1994 nr 24 poz. 83 wraz z późniejszymi zmianami).

Jestem świadoma, że niezgodność niniejszego oświadczenia z prawdą ujawniona w dowolnym czasie, niezależnie od skutków prawnych wynikających z ww. ustawy, może spowodować unieważnienie stopnia nabytego na podstawie tej rozprawy.

Kraków, dnia

Acknowledgements

Przede wszystkim chciałabym ogromnie podziękować prof. dr hab. Krzysztofowi Sacha. Przez lata doktoratu stał się dla mnie niezwykłym oparciem i wzorem do naśladowania.

Dziękuję również prof. dr hab. Jakubowi Zakrzewskiemu, za wskazówki, współpracę i ratunek w opresjach.

Dziękuję za pomoc i odpowiedzi na różne moje pytania dr Romanowi Marcinkowi i niezwykłą życzliwość Danusi Myrek.

Chciałabym podziękować doktorantom: Marcinowi Płodzieniowi, Michałowi Maikowi i Łukaszowi Skowronkowi, których błyskotliwości i dowcip zapewniały mi dużą dawkę rozrywki i obcowanie z ich nietuzinkowym spojrzeniem na świat.

Dziękuję moim rodzicom i braciom Michałowi i Ryškowi, za ich czujną i opiekuńczą obecność.

Chciałabym wyrazić wdzięczność Stefanowi i Jolancie Dousom oraz Tadeuszowi Stopce za pomoc i opiekę.

Dziękuję również ojcu Jordanowi za mądrość, wyrozumiałość i czas.

Last, but definitely not least, I would like to thank Zoran Hadzibabic for putting his sanity on the line in supporting my endeavour.

Abstract

The thesis contains a theoretical description of phenomena related mainly to Bose-Fermi mixtures of ultra-cold atoms. Due to the great experimental control, such mixtures can be studied in a variety of environments and for a variety of intra- and inter-species interactions. We first study ultra-cold gases in an optical lattice potential that, due to modulations that break time-reversal symmetry, enables the realisation of complex tunnelling amplitudes. We show that a superfluid Fermi gas in a two dimensional triangular lattice potential with complex tunnelings acquires a spatially varying complex phase of the pairing function. In the case of Bose-Fermi mixtures, of bosonic molecules and unbound fermions in the lattice, the two sub-systems can impose a spatially varying phase onto each other. In the presence of bosons the Fermi system can reveal both gapped and gapless superfluidity. In the second part of the thesis, we consider the self-localisation of a small number of Bose particles immersed in a large homogeneous mixture of fermions in two different spin states. We observe the self-localisation for repulsive interactions between bosons and fermions in three dimensions. In the one-dimensional case, bosons also self-localise for attractive interactions, thereby forming, together with a pair of fermions at the bottom of the Fermi sea, a vector soliton. We also analyse thermal effects and show that a small non-zero temperature affects the pairing function of the Fermi sub-system but has little influence on the self-localisation phenomena. However, the critical value of the self-localisation can change when the Fermi system is superfluid. This effect could also provide a novel experimental probe of fermionic superfluidity.

Preface

The thesis is organised as follow. **Chapter 1** contains the background on the main concepts studied throughout the thesis. We first provide the general information on ultra-cold atoms, such as the concepts of bosons and fermions, condensation, fermion pairing and Feshbach resonances. We also summarise the most important aspects in the derivation of the mean-field BCS theory of fermionic superfluidity, as well as some key ideas regarding superfluidity in ultra-cold atomic gases.

Chapter 2 provides a description of a shaken triangular optical lattice from the theoretical perspective. We show how time reversal symmetry can be broken for a given shaking protocol. We then study, using a mean-field approach, a mixture of fermions in the lattice with complex tunnelling amplitudes. We also theoretically explore a Bose-Fermi mixture coupled by a photo-association process.

Chapter 3 is devoted to the study the phenomenon of self-localisation. As an introduction, we discuss the instability of a homogeneous mixture of fermions and bosonic impurities coupled to each other by the density-density interaction. We then present the results of mean-field calculations for interactions of different strengths and signs. With some caution, we speculate on the possible interplay of self-localisation and superfluidity in the Bose-Fermi system. In the part devoted to one-dimensional regime, we focus on an analytical model that pictures the coupling of two sub-systems by the set of soliton-like solutions.

Some of the results presented here were published in scientific journals in the following papers:

K. Targońska, K. Sacha, *Self-localization of a small number of Bose particles in a superfluid Fermi system*, Phys. Rev A **82**, 033601 (2010)

K. Sacha, K. Targońska, and J. Zakrzewski, *Frustration and time-reversal symmetry breaking for Fermi and Bose-Fermi systems*, Phys. Rev A **85**, 053613 (2012)

The research presented in this thesis was partly supported by Polish National Center for Science funds received through Grant No. DEC-2011/01/N/ST2/00424.

Contents

Acknowledgements	iii
Abstract	iv
List of Figures	ix
Abbreviations	xi
1 Introduction	1
1.1 Ultra-cold atoms	1
1.2 Indistinguishable particles	3
1.2.1 Bosons	3
1.2.2 Fermions	5
1.3 Interactions	8
1.3.1 Feshbach Resonances	10
1.4 Theoretical many-body methods	13
1.4.1 Gross–Pitaevskii equation	13
1.4.2 Bogoliubov transformation	13
1.4.2.1 Homogeneous BCS system	17
1.4.2.2 Critical temperature	18
1.5 Bosonic vs. fermionic superfluidity	19
2 Effects of time reveals symmetry breaking for fermions and Bose-Fermi mixtures in a triangular lattice	23
2.1 Introduction	23
2.2 Background	25
2.2.1 Triangular lattice	25
2.2.1.1 The triangular lattice and frustration	25
2.2.1.2 Triangular optical lattice	26
2.2.1.3 Layered two-dimensional system	27
2.2.2 Fermion and Bosons on a lattice	28
2.2.2.1 The single particle states	28

2.2.2.2	Many-body Hamiltonian	29
2.2.2.3	Local order parameter and long-range order	31
2.3	Periodically driven lattices	32
2.3.0.4	Is a driven lattice in equilibrium?	33
2.3.1	Realisation of complex tunnellings	35
2.3.1.1	A shaken one-dimensional optical lattice	36
2.3.2	Triangular optical lattice with complex tunnelings - simulating classical magnetism	40
2.4	Fermions in the triangular lattice	42
2.5	Mixture of fermions and molecular dimers on the triangular lattice	45
2.5.1	The limit of dominant number of molecular dimers	45
2.5.2	Effects of variation of the number of molecular dimers	48
2.5.2.1	Results	52
2.5.2.2	Gapless superfluidity	57
2.6	Conclusions	58
3	Self-localisation of a small number of Bose particles in a superfluid Fermi system	59
3.1	Introduction	59
3.2	Instability of Bose-Fermi mixtures	62
3.3	Model description of Bose-Fermi mixtures	65
3.4	Results in three dimensions	69
3.4.1	Repulsive boson-fermion interaction	69
3.4.1.1	General characteristics of self-localisation	69
3.4.1.2	Non-zero temperature	72
3.4.1.3	Self-localisation as a probe of superfluidity?	74
3.4.1.4	The effects of the inclusion of boson-boson interactions	77
3.4.2	Attractive boson-fermion interaction	79
3.5	Results in one dimension	80
3.5.1	Attractive boson-fermion interactions	82
3.5.1.1	Simple model	83
3.5.1.2	Simple model with inclusion of boson-boson interactions	87
3.6	Final remarks	89
A	Appendix for Chapter 2	91
A.1	The steepest-descent method	91
A.2	Calculation for the Sec. 2.5.2	92
B	Appendix for Chapter 3	94
B.1	Pairing function in one dimension	94
B.2	The regularisation of the pairing function in 3D	96

Bibliography

List of Figures

1.1	Excitation spectrum	18
2.1	The phase diagram	24
2.2	The triangular plaquette and frustration	25
2.3	Creation of a 2D triangular lattice	27
2.4	Layered two-dimensional systems	28
2.5	Hubbard Hamiltonian	30
2.6	Tunnelings parameter as a function of driven strength s_1	39
2.7	Triangular Bravais lattice	41
2.8	Mapping phase of the BEC on the $x - y$ spin model	42
2.9	The Fourier transform of the BCS pairing function for the isolated Fermi system	45
2.10	Position of the BCS pairing function in the momentum space for the complex tunnelling during the crossover	49
2.11	Contour plot of the positions of the Fourier peaks of the BCS pairing function and the BEC wave function as a function of number of bosons n_b and γ coupling	53
2.12	Crossover regime for the BEC wave function	54
2.13	Crossover regime for the paring function	56
2.14	The region of gapless superfluidity.	57
3.1	Schematic picture of a polaron	60
3.2	An example of an inhomogeneous binary mixture that has lower energy than a homogeneous system	64
3.3	Self-localisation of ^{23}Na atoms in a superfluid mixture of ^{40}K atoms at zero temperature	70
3.4	Probability densities $ v_{nlm}(r) ^2$ of two fermion pairs at the bottom of the Fermi sea with angular momentum $l = 0$	71
3.5	The average radius of the Bose cloud and the standard deviation versus boson-fermion coupling constant.	72
3.6	Self-localisation of ^{23}Na atoms in a mixture of ^{40}K atoms at non-zero temperature.	75
3.7	Self-localisation as a probe of fermionic superfluidity?	77
3.8	Changes in the self-localisation by inclusion of the boson-boson interaction.	78
3.9	Self-localisation of a single boson in a superfluid mixture of fermions in 1D space.	83

3.10	Bogoliubov modes $v_k(z)$ corresponding to fermion pairs located close to the bottom of the Fermi sea.	84
3.11	Width of the boson density distribution versus boson-fermion coupling constant g_{bf}	87
3.12	Width of the boson density versus boson-fermion coupling constant g_{bf} for different boson-boson interactions	88
B.1	The one dimensional regularised pairing function $\Delta(x)$	95
B.2	The 3 dimensional pairing function Δ for different regularisations	98

Abbreviations

BEC	Bose Einstein Condensate
BCS	Bardeen Cooper Schrieffer
LDA	Local Density Approximation
GP	Gross Piteavskii
3D	Three Dimensions
2D	Two Dimensions
1D	One Dimension

Chapter 1

Introduction

1.1 Ultra-cold atoms

The realisation of atomic Bose-Einstein condensates in 1995 [1–3] opened the door to an amazing world of *dilute ultra-cold* atomic gases. These systems are fascinating because they are governed by quantum statistics, and because they are now under great experimental control, with many new ideas and challenges just waiting to be almost constantly discovered.

These gases are *dilute* in the sense that the mean inter-particle distance is much larger than the typical range of two-particle interaction. This implies that most of the time the collisions occur just among two atoms; three or more are unlikely to meet. This makes the gas stable against turning into a solid or liquid (which would require three-body collisions) even at extremely low temperatures, where quantum mechanics becomes important.

Indeed, by the term *ultra-cold* we really mean *quantum*, often simultaneously in two different senses:

First, the thermal de Broglie wavelength is much larger than the range of the two-particle interaction potential. This means that the two-particle interaction is in the quantum regime and (often) limited to s-wave collisions, which cause just

phase-shifts in the quantum wave-function of the particles. Note that the thermal de Broglie wavelength, $\lambda_{\text{dB}} = \sqrt{2\pi\hbar^2/mk_{\text{B}}T}$, depends on the mass of the particle m and the temperature T , and for atomic gases this s-wave regime is typically reached below 1 mK.

Second, at even lower temperatures, typically below 1 μK , the thermal wavelength also becomes larger than the typical inter-particle distance in the gas. This means that the gas becomes quantum-degenerate, i.e. also quantum in a many-body sense. At this point the quantum statistic is important and the macroscopic properties of the gas crucially depend on whether the atoms are bosons or fermions.

It took about 20 years to develop the experimental techniques to bring atoms into this ultra-cold regime [4]. First atoms are trapped and pre-cooled via laser cooling in a magneto-optical trap. With this technique, the kinetic energy of the particles is already reduced to values corresponding to the temperature below 1 mK or even below 100 μK . Further cooling is performed using evaporative cooling in a magnetic or optical trap. In this stage it is possible to reach even temperatures of the order of 1 nK.

Subsequently to cooling methods, many other techniques have been developed for manipulation of ultra-cold gases in the quantum degenerate regime. Today, almost all crucial parameters of these systems can be controlled. These include not just the temperature and number of atoms, but the interactions [5], the dimensionality of the gas [6], and the shape of the trap it is held in [7]. The interactions can be made weak or strong, and repulsive or attractive [5]. The gas can be three-dimensional (3D), two-dimensional (2D) or one-dimensional (1D). The trap the gas is held in can range from a simple parabolic potential or uniform [8] to a complex optical lattice, e.g. a triangular or a hexagonal one [9], which additionally can be put into periodical motion [10].

All this makes these atomic systems a fascinating “playing ground” to study many-body quantum mechanics, and simulate a variety of still poorly understood quantum phenomena that are also relevant to other many-body systems, most commonly in condensed-matter physics [11]. Crucially, in the world of ultra-cold atoms

it is possible to start with a simple system, e.g. a weakly-interacting gas in a simple trap, that can be fully understood, and then controllably make it more complicated, e.g. by increasing interaction strength and making the trap more complex. In this way the researchers gradually approach the truly fascinating complex physics, such as the quantum phase transition between a superfluid and a Mott-insulator [12], or the transition between the “conventional” low-temperature Bardeen-Cooper-Schrieffer (BCS) superfluidity and Bose-Einstein condensation in a Fermi gas [13].

1.2 Indistinguishable particles

The many-body wave function describing many identical particles must be either symmetric or antisymmetric under exchange of two such particles:

$$\Psi(\dots x_i \dots x_j \dots, t) = \pm \Psi(\dots x_j \dots x_i \dots, t) \quad (1.1)$$

where t is the time, and the quantity x_i denotes all the relevant coordinates of the i -th particle, including the spatial coordinate \mathbf{x}_i and any discrete variables such as the spin component. The basic reason for this (anti)symmetry requirement is that if we exchange the same two particles twice, the wavefunction must return to its original value. The wavefunction is symmetric under exchange for identical *bosons* and antisymmetric for identical *fermions* [14].

1.2.1 Bosons

Bosons have an integer spin. Mean number of particles that occupies the same energy level E_i is given by the Bose-Einstein statistics:

$$\langle n_i \rangle = \frac{1}{e^{(E_i - \mu)/(k_B T)} - 1} \quad (1.2)$$

where μ is the chemical potential which (in a non-interacting gas) must be lower than the ground state energy E_0 .

For a fixed averaged number of particles, if the gas is cooled μ grows. If it reaches E_0 from below, the ground state becomes macroscopically occupied. This phenomenon is called Bose-Einstein condensation and occurs at a non-zero critical temperature.

Qualitatively, condensation occurs if the number of thermally available states becomes comparable to the total number of particles in the gas, or equivalently if the thermal de Broglie wavelength λ_{dB} becomes equal to the typical distance between the particles. At this point the gas becomes quantum degenerate. The particles start to "meet" in the same energy levels, or in the same space (associating λ_{dB} with the quantum mechanical "size" of the particles), and quantum statistics becomes important.

More quantitatively, for N bosons in a 3D cubic box with a side of length L , the condition for condensation can be written as

$$\frac{N\lambda_{\text{dB}}^3}{L^3} = \zeta(3/2), \quad (1.3)$$

where $\zeta(3/2) \approx 2.612$ is the Riemann function. The left hand side of this equation is known as the phase space density and essentially measures the ratio of λ_{dB} and the average distance between the particles. Up to the numerical factor of 2.612 we see that this quantitative condition agrees with our qualitative picture of particles "meeting each other".

Equivalently, the critical temperature for condensation is given by

$$k_{\text{B}}T_c = \frac{2\pi\hbar^2}{m} \left(\frac{N}{L^3\zeta(3/2)} \right)^{2/3}. \quad (1.4)$$

The above analysis applies to an ideal, non-interacting gas. If the gas is interacting, in the condensed state it will also be superfluid, i.e. have the ability to

flow without any friction¹. Of course, interactions will in general also complicate the above analysis of the conditions for which the gas becomes condensed and superfluid. However, in the weakly interacting atomic gases, the above analysis can be surprisingly accurate for estimating T_c , while the condensate still displays the interaction-driven phenomenon of superfluidity [15]. This is an example of what we mentioned in the previous section - how in their simplest form atomic gases can be really extremely simple. Yet, by increasing interactions (see Sec. 1.3) we can also reach more complicated many-body states.

1.2.2 Fermions

Fermions have half-integer spin and obey Fermi-Dirac statistics [16]. In a non-interacting gas the mean occupation of a state of energy E_i is given by

$$\langle n_i \rangle = \frac{1}{e^{(E_i - \mu)/(k_B T)} + 1} \quad (1.5)$$

and, crucially, cannot be larger than 1. This constraint is just the well known Pauli exclusion principle.

At high enough temperature (where $-\mu \gg k_B T$) there is no important distinction between fermions and bosons, at least as far as (quantum) statistical physics are concerned. The only difference between Eqs. (1.2) and (1.5) is in the sign of the “1” in the denominator. If this term is negligible compared to $\exp[(E_i - \mu)/(k_B T)]$, both kinds of particles obey classical Boltzmann statistics.

The condition for fermions to become quantum degenerate is also qualitatively the same as for bosons, i.e. that λ_{dB} becomes comparable to the average inter-particle distance in the gas. At this point (below the degeneracy temperature) the difference between the two types of particles becomes pronounced. While bosons like to occupy the same (ground) state and form a BEC, fermions are still limited to one particle per state.

¹Note that this is just a common qualitative definition of superfluidity. Later in the thesis we will discuss the concept of superfluidity in greater detail.

Generally, the value of the chemical potential μ is found by fixing total number of particles:

$$N = \sum_{i=0}^{\infty} \langle n_i \rangle. \quad (1.6)$$

(Note that we assume that the system is large enough that grand-canonical fluctuations in total N can be neglected and make no distinction between N and $\langle N \rangle$.) At $T = 0$ the value of the chemical potential is called the Fermi energy, E_F . Note that in a non-interacting gas at $T = 0$ the occupation of all states with $E_i < \mu$ is exactly 1 and for all the states with $E_i > \mu$ it is exactly 0. In other words fermions uniformly occupy all the states up to energy $\mu = E_F$. At E_F the occupation probability drops like a step function. At non-zero T particles from the highest occupied levels get thermally excited above E_F and the sharp edge of the occupation function softens. In presence of interactions such softening occurs even at $T = 0$.

Again considering a gas of N identical particles in a box with a side L , we can write $E_F = \hbar^2 k_F^2 / (2m)$, where k_F is the Fermi wavevector given by:

$$k_F = (6\pi^2 N / L^3)^{1/3}, \quad (1.7)$$

and again note that up to a numerical constant k_F is simply the inverse of the typical inter-particle spacing. In momentum space the sphere defined by $|k| = k_F$ is called the Fermi surface.

An interacting Fermi gas can also become superfluid at sufficiently low temperature. This was in fact first discovered for an electron gas in a metal, which becomes superconducting below some non-zero critical temperature. (The only difference between superconductivity and superfluidity is that in case of charged particles superfluid flow also carries electrical current.) At first sight, this seems to contradict our qualitative association of superfluidity with Bose-Einstein condensation, since we have said that fermions can not condense into the same state. However, two fermions can form a pair which in many ways behaves like a boson - adding the half-integer spins of two fermions gives a total integer spin. Qualitatively, even if

all individual fermions remain in different single-particle states, the states describing the centre-of-mass motion of pairs of fermions can have Bose-like occupation numbers.

In the simplest scenario (and the only one we will consider in this thesis) pairing occurs between fermions of different spin in a mixture of two spin states. Within this case, conceptually the simplest type of pairing is if two fermions form a tightly bound molecule. In this case it is obvious that such a molecule is a boson and transition to superfluidity can qualitatively be understood as simple Bose-Einstein condensation. Historically, however, superfluidity (or rather superconductivity) was first discovered in the opposite limit of very loosely bound pairs which are actually correlated in momentum space.

These pairs are known as Cooper pairs, and are at the heart of the BCS theory of "conventional" low-temperature superconductivity. Cooper discovered that at sufficiently low T any arbitrarily weak attraction between degenerate electrons leads to their pairing. The key ideas of Cooper's theory can actually be qualitatively understood as a combination of our above discussion of non-interacting degenerate fermions, and simple single-particle physics. In single-particle quantum mechanics it is well known that in 2D a particle can be bound by an arbitrarily weak attractive potential. Now considering two particles and going into the centre-of-mass frame, this means that in 2D two particles are bound to each other by an arbitrarily weak attraction. Now, in a (very) degenerate two-component Fermi gas, in momentum space particles can move only along the Fermi surface, which is a 2D space. Hence, the system is unstable against pairing in momentum space. If we consider pairs of particles with exactly opposite momenta, $\pm\hbar\mathbf{k}$, their centre-of-mass momentum is zero, no matter what \mathbf{k} is. Therefore, in a collection of such pairs each particle occupies a different \mathbf{k} state (thus not violating Pauli principle), but all pairs are in the zero (centre-of-mass) momentum state, which is indeed reminiscent of a BEC.

It is important to keep in mind that the system is 3D but Pauli exclusion makes it effectively 2D at low temperatures. Cooper pairing is fundamentally a many-body

effect, but conceptually many-body physics is in this effective reduction of the dimensionality of space, while pairing itself can then be understood as a two-body 2D effect. Indeed, one can show that the existence of a two-body bound state in 1D and 2D is both a necessary and a sufficient condition for a BCS instability [17].

In ultra-cold atomic gases, by tuning the strength of interactions (see Sec. 1.3) it is possible to study the continuous transition from BCS physics (pairing in momentum space) to molecular-BEC physics, where pairing is a two-body phenomenon, only the condensation of molecules is a many-body effect. This BEC-BCS crossover has been a topic of intense study over the last decade [18].

1.3 Interactions

Interactions are at the heart of all the most interesting many-body physics.

In ultra-cold atoms most of the many-body effects can be deduced starting from the two-body interaction potential [11]. At large distances atoms interact with each other by the Van der Waals potential that scales as $-C_6/r^6$. The source of this interaction are fluctuations of electric dipoles of the atoms. At very short distances, when particles are separated by a few Bohr radii a_0 , the valence electrons strongly repel each other, which leads to a "hard core" repulsion. In this work we restrict ourselves to the dilute and ultra-cold regime, in which de Broglie wavelength λ_{dB} and the average distance between the atoms $n^{-1/3} \sim 10^5 a_0$ (where n is the gas density) are much greater than the range of the interaction potential $r_0 \sim 100 a_0$. As a consequence it is enough to describe the collisions by just one quantity, the s-wave scattering length.

We consider the Schrödinger equation for two particles in the centre-of-mass frame:

$$(\nabla^2 + k^2)\Psi(\mathbf{r}) = \frac{mV(\mathbf{r})}{\hbar^2}\Psi(\mathbf{r}) \quad \text{where} \quad k^2 = mE/\hbar^2 \quad (1.8)$$

where $m/2$ is the reduced mass, the relative distance between atoms is $|\mathbf{r}|$ and the initial wavevector is \mathbf{k} . For the finite-range potential the wave function $\Psi(\mathbf{r})$

is asymptotically given by the superposition of an incident plane wave: $e^{i\mathbf{k}\mathbf{r}}$ and a scattered wave:

$$\Psi \sim e^{i\mathbf{k}\mathbf{r}} + f(\mathbf{k}', \mathbf{k}) \frac{e^{ikr}}{r} \quad (1.9)$$

where $f(\mathbf{k}', \mathbf{k}) = -\frac{2m}{4\pi\hbar^2} \int d^3r' e^{-i\mathbf{k}'\mathbf{r}'} V(\mathbf{r}') \Psi(\mathbf{r}')$ is the scattering amplitude and $\mathbf{k}' = k\mathbf{r}/r$ gives the direction of the scattering.

For small enough energies $kr_0 \ll 1$, the scattering process is isotropic, i.e. $f(\mathbf{k}', \mathbf{k})$ is independent of \mathbf{k}' :

$$f_{k \rightarrow 0} = -\frac{2m}{4\pi\hbar^2} \int d^3r' V(\mathbf{r}') \Psi(\mathbf{r}') = -a \quad (1.10)$$

The scattered wave (considered far from the origin of the potential) is spherically symmetric, meaning that the collisions occur in the s-wave regime.

If we assume a zero range potential $V(\mathbf{r}) = g_0\delta(\mathbf{r})$, and use the Born approximation ² $\Psi = e^{i\mathbf{k}\mathbf{r}}$ in equation (1.10):

$$f_{k \rightarrow 0} = -\frac{2m}{4\pi\hbar^2} g_0 = -a, \quad (1.11)$$

where a is the s-wave scattering length.

The strength of the potential is

$$g_0 = \frac{4\pi\hbar^2 a}{m}. \quad (1.12)$$

The positive (negative) scattering length corresponds to an effective repulsive (attractive) interaction.

Let us notice that formally in 3D the $V(\mathbf{r})$ requires a regularisation. Indeed, the δ potential does not lead to scattering (it effectively leads to $a = 0$), while the Born approximation gives a finite value (Eq. 1.11). To avoid this unphysical behaviour

²We replace the unknown $\Psi(\mathbf{r}')$ by a wave function at order zero in $V(\mathbf{r})$

the *pseudo-potential* is introduced [16]:

$$V(\mathbf{r})\Psi(\mathbf{r}) = V_0\delta(\mathbf{r})\frac{\partial}{\partial r}(r\Psi(\mathbf{r})) \quad (1.13)$$

Inserting the pseudo-potential with spherically symmetric wave function $\Psi(\mathbf{r}) = u(\mathbf{r})/r$ in Eq. 1.8 we deduce that the scattering amplitude is:

$$f_k = -\frac{a}{1 + ika} \quad (1.14)$$

To sum up, if the de Broglie wavelength $2\pi/k$ of colliding atoms is much greater than the details of the inter-atomic potential, $1/k \gg r_0$, it is possible to use the above simple zero-range model.

Let us also stress that the above discussion applies to bosons and to fermions in two different internal states. By symmetry two fermions in the same spin state can not have s-wave interactions. They can scatter only through waves with angular momentum $l = 1, 3, \dots$ and such scattering is usually negligible below temperature $k_B T \sim \hbar^2/mr_0^2$, which is typically ~ 1 mK.

1.3.1 Feshbach Resonances

One of the most important experimental tools in the research with ultra-cold atoms is the Feshbach scattering resonance [5, 19], which allows the scattering length a to be tuned to be positive or negative, small or large. Here we qualitatively outline the idea of how scattering resonances can occur in general, and how they are controllably induced in ultra-cold atomic gases.

All two-particle scattering properties (which in our case of s-wave scattering are really captured just by a) depend on the two-particle interaction potential, which is basically the molecular potential for a diatomic molecule formed by the two colliding particles. If the potential is very shallow there are no bound molecular states and the interaction between the particles is attractive ($a < 0$). Now suppose

we could somehow gradually increase the potential depth. Bound states will then appear one at a time.

As the potential depth is increased, before the first bound state appears, a grows more negative (the attraction is stronger). At the point when the first bound state appears a scattering resonance occurs: a diverges and flips sign to positive. Qualitatively, once we have a bound state just below the continuum, i.e. just below the zero-energy scattering state³, we can intuitively understand from second-order perturbation theory that the two states repel each other, so the energy of the scattering state is shifted up. This corresponds to an effective repulsion between the two particles, even though the underlying molecular potential is always attractive.

Then, as the molecular state becomes more bound, moving away from the continuum, the repulsion weakens and eventually the interaction becomes attractive again. This whole process repeats every time a new bound state appears. Real inter-atomic potentials have many bound states, but resonant behaviour of the scattering length is dominated by the bound state that has just appeared (giving a large positive a) or a virtual state (above the scattering state) that is just about to become bound (giving a large negative a).

The above qualitative picture corresponds to a "single channel" model, in which we have not explained how one could experimentally vary the depth of the molecular potential. The proper microscopic description of how scattering resonances are controllably induced requires us to consider the "two channel model". The "channels" we refer to here correspond to the different two-particle spin states of the colliding particles. It is intuitive that the molecular potential depends on the spins of the two atoms. At large distances these two channels are decoupled, i.e. after particles meet and separate they still have their original spins. However, at short distances, where the interaction of the valence electrons from two different atoms becomes comparable to their interaction with their own nuclei, the channels are weakly coupled. We call the channel in which particles enter and can leave

³The kinetic energy of two colliding ultra-cold atoms is negligible compared to typical molecular-binding energies, except right at the scattering resonance.

the collision process “open” and the other channel in which they might just spend some time during the collision process “closed”.

The possibility to experimentally induce scattering resonances comes from the fact that the two different spin channels have different magnetic moments and hence the relative position of their bound states can be tuned with an external magnetic field. So, microscopically, a Feshbach resonance actually occurs when the bound molecular state in the closed channel energetically approaches the scattering state in the open channel.

Now, for concreteness, let us focus on the case of $a > 0$, where a real bound molecular states exists in the closed channel⁴. In many cases, we can still “integrate out” this closed-channel state and understand all the many-body physics within the single-channel picture. This corresponds to the experimental situation in which at any one time the number of molecules in the gas is negligible and we have only strongly interacting atoms. The closed channel is microscopically relevant for understanding where the strong atomic interactions come from, but in our many-body Hamiltonian we can still have just binary interactions between the atoms [20]. In the opposite case of two-channel description, in the many-body Hamiltonian we explicitly include the microscopic formation and dissociation of molecules in the Feshbach resonance state. This is a better description if at all times there is a significant number of molecules present in the gas. This scenario will be relevant for us when we consider mixtures of Bose and Fermi gases with our bosons actually being formed by pairing of fermions.

In general, the microscopic justification for the applicability of single- or two-channel model is related to atomic-physics details of specific Feshbach resonances [20], which are not directly relevant for our phenomenological many-body Hamiltonians, and are beyond the scope of this thesis. We just briefly mention that in our scenario we will use photo-association to actively convert pairs of atoms into molecules (and vice-versa) and control their relative populations.

⁴Again, we stress that there are always many deeply bound molecular states, but what primarily matters is whether the energetically closest state is a real “just bound” state or a virtual “just unbound” one.

1.4 Theoretical many-body methods

In this section we outline two very commonly used theoretical tools for describing interacting many-body systems, which we will be referring to throughout the thesis.

1.4.1 Gross–Pitaevskii equation

We first consider the simpler case of a weakly interacting Bose gas at $T = 0$. Atoms interacting with the zero range potential with a mass m placed in the potential $U(\mathbf{r})$ can be described by the Hamiltonian in the second-quantisation formalism:

$$\hat{H} = \int d^3r \hat{\psi}^\dagger(\mathbf{r}) \left[-\frac{\hbar^2}{2m} \nabla^2 + U(\mathbf{r}) + \frac{g_{bb}}{2} \hat{\psi}^\dagger(\mathbf{r}) \hat{\psi}(\mathbf{r}) \right] \hat{\psi}(\mathbf{r}) \quad (1.15)$$

where $\hat{\psi}(\mathbf{r})$ is the boson field operator, and g_{bb} is the boson-boson interaction strength. If the system undergoes BEC, one state is macroscopically occupied. The ideal condensate is then a product state of all the single-particle functions $\psi(\mathbf{r}_1 \dots \mathbf{r}_N)$:

$$\psi(\mathbf{r}_1 \dots \mathbf{r}_N) = \phi(\mathbf{r}_1) \dots \phi(\mathbf{r}_N), \quad (1.16)$$

where $\phi(\mathbf{r})$ is the solution of the Gross–Pitaevskii (GP) equation:

$$-\frac{\hbar^2}{2m} \nabla^2 \phi(\mathbf{r}) + U(\mathbf{r}) + g_{bb} N |\phi(\mathbf{r})|^2 \phi(\mathbf{r}) = \mu \phi(\mathbf{r}), \quad (1.17)$$

The GP equation is obtained by minimisation of the energy functional in Eq. (1.15), assuming that the many-body function is the product state as in Eq. (1.16).

1.4.2 Bogoliubov transformation

Now let us consider a mixture of Fermions of equal mass m in a balanced mixture of two different internal states denoted as $s = \{\uparrow, \downarrow\}$, interacting via $V(\mathbf{r}_1 - \mathbf{r}_2) = -|g_{ff}| \delta(\mathbf{r}_1 - \mathbf{r}_2)$ in an arbitrary external potential $U(\mathbf{r})$.

We use the grand canonical ensemble to write the Hamiltonian in the language of second quantisation:

$$\hat{K} = \hat{H} - \mu \sum_s N_s = \sum_s \int d^3r \left[\hat{\psi}_s^\dagger(\mathbf{r}) H_0 \hat{\psi}_s(\mathbf{r}) - \frac{|g_{ff}|}{2} \hat{\psi}_s^\dagger(\mathbf{r}) \hat{\psi}_{-s}^\dagger(\mathbf{r}) \hat{\psi}_{-s}(\mathbf{r}) \hat{\psi}_s(\mathbf{r}) \right] \quad (1.18)$$

where $H_0 = -\frac{\hbar^2}{2m} \nabla^2 + U(\mathbf{r}) - \mu$.

The terms describing the interaction can be replaced by an average potential acting on a single particle. This is a generalisation of the Hartree–Fock theory, which assumes that each particle is moving in the field created by averaging over its interactions with all the other particles [14]. Due to the huge number of particles involved in the field we neglect the fluctuations of its expectation value. The effective Hamiltonian is:

$$\begin{aligned} \hat{K}_{eff} = & \int d^3r [\hat{\psi}_\uparrow^\dagger(\mathbf{r}) H_0 \hat{\psi}_\uparrow(\mathbf{r}) + \hat{\psi}_\downarrow^\dagger(\mathbf{r}) H_0 \hat{\psi}_\downarrow(\mathbf{r}) \\ & + W(\mathbf{r}) \hat{\psi}_\uparrow^\dagger(\mathbf{r}) \hat{\psi}_\uparrow(\mathbf{r}) + W(\mathbf{r}) \hat{\psi}_\downarrow^\dagger(\mathbf{r}) \hat{\psi}_\downarrow(\mathbf{r}) \\ & + \Delta(\mathbf{r}) \hat{\psi}_\uparrow^\dagger(\mathbf{r}) \hat{\psi}_\downarrow^\dagger(\mathbf{r}) + \Delta^\dagger(\mathbf{r}) \hat{\psi}_\downarrow(\mathbf{r}) \hat{\psi}_\uparrow(\mathbf{r})]. \end{aligned} \quad (1.19)$$

We now want to determine unknown fields $W(\mathbf{r})$ and $\Delta(\mathbf{r})$ (which may be complex) by requiring that the free energy F is stationary for the states that diagonalised K_{eff} . To find those eigenvectors for K_{eff} we use unitary Bogoliubov transformations:

$$\begin{pmatrix} \hat{\psi}_\uparrow(\mathbf{r}) \\ \hat{\psi}_\downarrow^\dagger(\mathbf{r}) \end{pmatrix} = \sum_{n, E_n \geq 0} \hat{\gamma}_{n,\uparrow} \begin{pmatrix} u_n(\mathbf{r}) \\ v_n(\mathbf{r}) \end{pmatrix} + \hat{\gamma}_{n,\downarrow}^\dagger \begin{pmatrix} -v_n^*(\mathbf{r}) \\ u_n^*(\mathbf{r}) \end{pmatrix} \quad (1.20)$$

where $\hat{\gamma}_{n,\uparrow}$ and $\hat{\gamma}_{n,\downarrow}^\dagger$ creates excitations designated as *quasiparticles*

$$\hat{\gamma}_{n,\uparrow} = \langle u_n | \hat{\psi}_\uparrow \rangle + \langle v_n | \hat{\psi}_\downarrow^\dagger \rangle, \quad \hat{\gamma}_{n,\downarrow}^\dagger = -\langle v_n^* | \hat{\psi}_\uparrow \rangle + \langle u_n^* | \hat{\psi}_\downarrow^\dagger \rangle$$

The effective Hamiltonian is expressed in the matrix form⁵:

$$K_{ef} = \int d^3r \begin{pmatrix} \hat{\psi}_\uparrow^\dagger & \hat{\psi}_\downarrow \end{pmatrix} \Omega \begin{pmatrix} \hat{\psi}_\uparrow \\ \hat{\psi}_\downarrow^\dagger \end{pmatrix} \quad (1.21)$$

$$\Omega = \begin{pmatrix} H_0 + W(\mathbf{r}) & \Delta(\mathbf{r}) \\ \Delta^\dagger(\mathbf{r}) & -H_0^\dagger - W(\mathbf{r}) \end{pmatrix} \quad (1.22)$$

The form of the transformations (Eq. 1.20) and the sum over restricted to positive eigenvalues are consequences of the symmetries of the Hamiltonian \hat{K}_{eff} (Eq. 1.19). The functions u_n and v_n are the eigenvectors for the Bogoliubov de Gennes equation (1.23).

$$\Omega \begin{pmatrix} u_n \\ v_n \end{pmatrix} = E_n \begin{pmatrix} u_n \\ v_n \end{pmatrix} \quad (1.23)$$

By the definition of the free energy in equilibrium is:

$$F = \langle \hat{K} \rangle - TS \quad (1.24)$$

where the average $\langle \hat{K} \rangle$ is given by

$$\langle \hat{K} \rangle = \frac{\sum_n \langle \Psi_n | \hat{K} | \Psi_n \rangle e^{-E_n/(k_B T)}}{\sum_n e^{-E_n/(k_B T)}} \quad (1.25)$$

Using Wick's theorem we simplify the interactions terms from the Eq. (1.18) into a quadratic form with respect to the fermionic operators. We vary the free energy in respect of eigenfunctions and eigenvalues of \hat{K}_{eff} , we then get

$$\begin{aligned} \delta F = & \sum_s \int d^3r \left[\delta \langle \hat{\psi}_s^\dagger H_0 \hat{\psi}_s \rangle - |g_{ff}| \delta \langle \hat{\psi}_s^\dagger \hat{\psi}_s \rangle \langle \hat{\psi}_{-s}^\dagger \hat{\psi}_{-s} \rangle \right. \\ & - |g_{ff}| \langle \hat{\psi}_s^\dagger \hat{\psi}_s \rangle \delta \langle \hat{\psi}_{-s}^\dagger \hat{\psi}_{-s} \rangle - |g_{ff}| \delta \langle \hat{\psi}_s^\dagger \hat{\psi}_{-s}^\dagger \rangle \langle \hat{\psi}_{-s} \hat{\psi}_s \rangle \\ & \left. - |g_{ff}| \langle \hat{\psi}_s \hat{\psi}_{-s}^\dagger \rangle \delta \langle \hat{\psi}_{-s}^\dagger \hat{\psi}_s \rangle \right] - T \delta S. \end{aligned} \quad (1.26)$$

⁵Here the constant terms are omitted.

When we compare the equation above with a variation of the effective free energy $F_{eff} = \langle \hat{K}_{eff} \rangle$ for which from a definition $\delta F_{eff} = 0$:

$$\begin{aligned} \delta F_{eff} = & \sum_s \int d^3r [\delta \langle \hat{\psi}_s^\dagger H_0 \hat{\psi}_s \rangle + W(\mathbf{r}) \delta \langle \hat{\psi}_s^\dagger \hat{\psi}_s \rangle \\ & + W(\mathbf{r}) \delta \langle \hat{\psi}_{-s}^\dagger \hat{\psi}_{-s} \rangle + \Delta(\mathbf{r}) \delta \langle \hat{\psi}_s^\dagger \hat{\psi}_{-s}^\dagger \rangle \\ & + \Delta^* \delta \langle \hat{\psi}_{-s} \hat{\psi}_s \rangle] - T \delta S = 0, \end{aligned} \quad (1.27)$$

we can deduce $W(\mathbf{r})$ and $\Delta(\mathbf{r})$. Thus, the values of the fields $W(\mathbf{r})$ and $\Delta(\mathbf{r})$, that ensure the extremum of the free energy (Eq. 1.24) for states of the effective Hamiltonian (Eq. 1.19) reads :

$$\begin{aligned} W(\mathbf{r}) = -|g_{ff}| \langle \hat{\psi}_{-s}^\dagger \hat{\psi}_{-s} \rangle &= -|g_{ff}| \langle \hat{\psi}_s^\dagger \hat{\psi}_s \rangle \\ \Delta(\mathbf{r}) = -|g_{ff}| \langle \hat{\psi}_{-s} \hat{\psi}_s \rangle &= -|g_{ff}| \langle \hat{\psi}_s^\dagger \hat{\psi}_{-s}^\dagger \rangle. \end{aligned} \quad (1.28)$$

$W(\mathbf{r})$ is the standard Hartree-Fock term, proportional to the density of fermions. $\Delta(\mathbf{r})$ is the *paring function*.

By substituting Eq. (1.20) and using the average values of the operators:

$$\begin{aligned} \langle \hat{\gamma}_{n,s}^\dagger \hat{\gamma}_{n',s'} \rangle &= \delta_{n,n'} \delta_{s,s'} f(E_n) \\ \langle \hat{\gamma}_{n,s} \hat{\gamma}_{n',s'} \rangle &= 0, \end{aligned}$$

where $f(E_n)$ is the Fermi distribution $f(E_n) = 1 / (e^{E_n / (k_B T)} + 1)$, the equation for the paring function and Hartree Fock term can be written:

$$W(\mathbf{r}) = -|g_{ff}| \sum_n [|u_n(\mathbf{r})|^2 f(E_n) + |v_n(\mathbf{r})|^2 (1 - f(E_n))] \quad (1.29)$$

$$\Delta(\mathbf{r}) = |g_{ff}| \sum_n u_n(\mathbf{r}) v_n^*(\mathbf{r}) [1 - 2f(E_n)]. \quad (1.30)$$

The equations 1.29, 1.30 and 1.23 are a consistent set of equation, solve usually in the self-consistent matter. For 3D $\Delta(\mathbf{r})$ requires a regularisation, a possible procedure is described in App. B.2

1.4.2.1 Homogeneous BCS system

If we replace Ψ by the Bogoliubov transformation (Eq. (1.20)) in the effective Hamiltonian

$$\hat{K}_{eff} = \sum_k E_k \left(\hat{\gamma}_{\mathbf{k},\uparrow}^\dagger \hat{\gamma}_{\mathbf{k},\uparrow} + \hat{\gamma}_{\mathbf{k},\downarrow}^\dagger \hat{\gamma}_{\mathbf{k},\downarrow} \right) \quad (1.31)$$

The sum is over \mathbf{k} , because we are allowed to express the fermionic operators in the momentum space. In addition, we assume the translational symmetry, because the momentum of the system is conserved. It corresponds to the fact that the Cooper pairs have zero relative momentum.

The values of the excitation energies E_k are calculated using the normalisation condition $u_{\mathbf{k}} + v_{\mathbf{k}} = 1$ and Eq. (1.23):

$$E_k = \sqrt{\epsilon_k^2 + \Delta^2}, \quad \text{where} \quad \epsilon_k = \frac{\hbar^2 k^2}{2m} - \mu. \quad (1.32)$$

This dispersion relation is sketched in Fig. 1.1. Due to the fact that $W(\mathbf{r}) = \text{const.}$ for homogeneous system, it can be included in the definition of μ .

The amplitudes v_k and u_k can be expressed as:

$$v_k^2 = \frac{1}{2} \left(1 - \frac{\epsilon_k}{E_k} \right) \quad u_k^2 = \frac{1}{2} \left(1 + \frac{\epsilon_k}{E_k} \right) \quad (1.33)$$

The equation for the pairing function:

$$\Delta = |g_{ff}| \sum_{\mathbf{k}} \frac{\Delta}{2\sqrt{\epsilon_k^2 + \Delta^2}} \quad (1.34)$$

For a homogeneous system we can derive the Bogoliubov de Gennes equations [Eqs. (1.23) and (1.30)] and the pairing function alternatively. It is done by a variational method that allows us to find v_n, u_n using the ansatz:

$$|\Psi_{\text{BCS}}\rangle = \prod_k \left(u_k + v_k \hat{a}_{\mathbf{k},\uparrow}^\dagger \hat{a}_{\mathbf{k},\downarrow}^\dagger \right) \quad (1.35)$$

where \hat{a} comes from expression the fermionic field in the one particle momentum base $\psi_s(\mathbf{r}) = \frac{1}{(2\pi)^{3/2}} \sum_k e^{i\mathbf{k}\mathbf{r}} \hat{a}_{ks}$ ([20])

For $\Delta = 0$ the system is in the *normal* state with the Fermi sea filled $u_k = 0, v_k = 1$ below the Fermi energy $E_f = \mu$. Above that level $u_k = 1, v_k = 0$.

If $\Delta \neq 0$ there are Cooper pairs present in the system. The mixture of fermions is in the superfluid regime described by the function Eq.(1.35), in which the elementary excitation is realised by excitation of two quasiparticles with energy equal 2Δ :

$$\hat{\gamma}_{\mathbf{k},s}^\dagger \hat{\gamma}_{\mathbf{k}',s'}^\dagger |\Psi_{BCS}\rangle = \hat{a}_{k,s}^\dagger \hat{a}_{k',s'}^\dagger \prod_{\mathbf{q} \neq \mathbf{k}, \mathbf{k}'} \left(u_q + v_q \hat{a}_{-\mathbf{q}\downarrow}^\dagger \hat{a}_{\mathbf{q}\uparrow}^\dagger \right) |0\rangle. \quad (1.36)$$

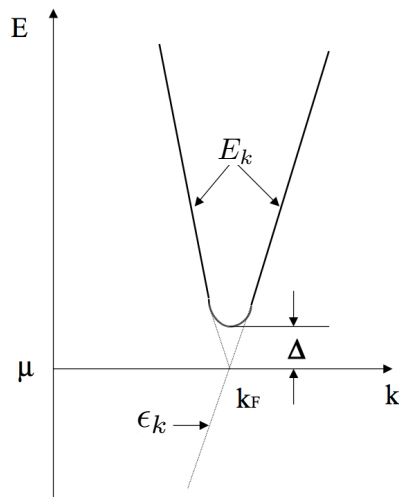


FIGURE 1.1: Excitation spectrum in a homogeneous BCS superfluid. Adopted from [21].

1.4.2.2 Critical temperature

For a homogeneous mixture at non-zero temperature the non-interacting quasiparticles are governed by the Hamiltonian in Eq. (1.31) and the distribution function is $f(E_k) = 1/(e^{E_k/(k_B T)} + 1)$. The equation for a pairing function can be

written as:

$$\begin{aligned}\Delta(\mathbf{r}) &= |g_{ff}| \sum_k u_k v_k^* [1 - 2f(E_k)] = |g_{ff}| \sum_k u_k v_k^* \tanh\left(\frac{E_k}{2k_B T}\right) \\ &= |g_{ff}| \int_0^{k_c} \frac{d^3k}{(2\pi)^2} \frac{\Delta}{2\sqrt{\epsilon_k^2 + \Delta^2}} \tanh\left(\frac{\sqrt{\epsilon_k^2 + \Delta^2}}{2k_B T}\right).\end{aligned}\quad (1.37)$$

When $\mu \gg k_B T$ and $\mu = E_f$ we can calculate the critical temperature for the BCS transition to superfluidity:

$$T_{c,\text{BCS}} = \frac{e^\gamma}{\pi e^2} e^{-\pi/2k_f|a|} = \frac{e^\gamma}{\pi} \Delta_{T=0}, \quad (1.38)$$

where γ is Euler constant, $e^\gamma = 1.78$.

1.5 Bosonic vs. fermionic superfluidity

The BEC and BCS regime both reveal the phenomenon of superfluidity. However, one should not forget that the underlining system are bosonic and fermionic, respectively, and their characteristic features will still be revealed in some processes. Here we point out some differences between the two regimes and in particular stress one that is relevant for this thesis, the possibility of “gapless superfluidity” in a fermionic system. For this purpose we will (as commonly) associate superfluidity with the dissipationless flow below some critical velocity (*the Landau velocity*).

One obvious difference we have already introduced is that fermions, unlike bosons, have to pair up in order to condense and become superfluid. This is first seen in the way we define long-range order, characterising the superfluid state, in the two cases.

For bosons long-range order is seen in the correlations between two single-particle operators at different positions. In the condensed/superfluid state we have:

$$\langle \Psi_o^\dagger(\mathbf{r}) \Psi_o(\mathbf{r}') \rangle \neq 0 \quad (1.39)$$

for $|\mathbf{r} - \mathbf{r}'| \rightarrow \infty$. This is equivalent to saying that the system is coherent across the whole sample, or that there is a macroscopic wavefunction which contains a macroscopic fraction of the particles. We can then define a local order parameter $\Psi(\mathbf{r}) = \sqrt{n}e^{i\alpha(\mathbf{r},t)}$, where n is the density, and the velocity of the frictionless flow is $\mathbf{v}_{s,\text{BEC}} = (\hbar/m)\nabla\alpha(\mathbf{r})$.

In case of a fermionic system one has to consider a two body density matrix. The appearance of the condensate of pairs is seen in the fact that:

$$\langle \Psi_{\uparrow}^{\dagger}(\mathbf{r}')\Psi_{\downarrow}^{\dagger}(\mathbf{r}')\Psi_{\uparrow}(\mathbf{r})\Psi_{\downarrow}(\mathbf{r}) \rangle = \Delta(\mathbf{r})\Delta(\mathbf{r}') \neq 0 \quad (1.40)$$

for $|\mathbf{r} - \mathbf{r}'| \rightarrow \infty$. Now $\Delta(\mathbf{r})$ (containing two single-particle operators) plays the role of the order parameter [22], we can write $\Delta(\mathbf{r}) = |\Delta(\mathbf{r})|e^{i\alpha(\mathbf{r},t)}$, and the velocity of pair-movement is $\mathbf{v}_{s,\text{BCS}} = [\hbar/(2m)]\nabla\alpha(\mathbf{r})$.

The second related point is that single-particle excitations⁶ are still bosonic and fermionic in the two regimes. This is in some sense obvious, but it is important to stress because it has some profound implications. For example in a BEC the lowest-energy excitations are at momentum $k \rightarrow 0$. In the BCS state, even though pairs are condensed in the $k = 0$ state, lowest-energy single-particle excitations are still close to k_F (see Fig. 1.1). This reinforces the point that Pauli exclusion and the underlying Fermi surface play a crucial role in this system.

Now let us turn to the issue of the critical velocity. The Landau criterion for superfluidity defines a critical velocity v_c up to which frictionless superflow (past a wall or some object) is stable against the creation of excitations [23]. Above v_c it becomes energetically favourable to transfer momentum from the superflow to the excitations, so the flow is damped.

The basic idea can be understood as follows. If the lab is stationary then the lowest energy state for the superfluid is to also be stationary - any movement costs kinetic energy. However, for the (quasi-)particles to break away from the superflow and reduce their kinetic energy in the lab frame they must also pay the price of creating

⁶Here, in the BEC limit we consider a tightly bound molecule a single bosonic particle, even if we know that it is made up of two fermions.

an excitation in the superfluid, in its own moving frame. This cost is simply given by the dispersion relation E_k , calculated for a stationary superfluid (i.e. in its own frame). For low enough v_s this cost is higher than the benefit of reducing kinetic energy in the lab frame, so the constant flow of the whole superfluid is a metastable state even though it is not the absolute ground state.

Mathematically, in the lab frame the cost of creating an excitation in the superfluid is $E_k + \hbar \mathbf{k} \cdot \mathbf{v}_s$, where the second term is essentially a Doppler shift. Naturally it is most favourable to create an excitation with \mathbf{k} antiparallel to \mathbf{v}_s . This is energetically favoured if $E_k - \hbar k v_s < 0$. We thus get Landau's critical velocity:

$$v_c = \min_k \frac{E_k}{\hbar k} \quad (1.41)$$

Here the minimum has to be taken over all possible excitations. These include single-particle excitations, but also various collective excitations such as phonons or vortex pairs (with different excitations being most favourable in different geometries).

In the (weakly interacting) BEC regime critical velocity is set by the speed of sound, i.e. the relevant excitations are phonons with $k \rightarrow 0$:

$$v_{c,\text{BEC}} = \sqrt{\frac{\mu}{m}}. \quad (1.42)$$

In the (weakly interacting) BCS regime, pair-breaking excitations near $k = k_F$ give the critical velocity:

$$v_{c,\text{BCS}} = \sqrt{\left(\sqrt{\mu^2 + \Delta^2} - \mu\right) / m} \approx \frac{\Delta}{\hbar k_F}, \quad (1.43)$$

where the second (approximate) equality assumes $\Delta \ll \mu$ (see Fig. 1.1).

Finally, we come to our conceptual point about gapless fermionic superfluidity. As we tried to convey, the condition $v_s > v_c$ is equivalent to the gap in the excitation spectrum disappearing, once we include the Doppler shift to transpose the excitation spectrum from the frame of a moving superfluid to the lab rest

frame. At this point the energy of some pair-breaking excitations with momenta close to k_F become negative and it becomes favourable for them to be occupied. But now remember that these excitations are fermions and must obey the Pauli exclusion principle, so the occupation of each such excitation mode can be at most 1, limiting the total density of excitations. If v_s is just above v_c the number of such excitation states is small. Hence, once all such excitation modes are fully occupied, any remaining superfluid fraction is still protected against further excitations.

We can thus simultaneously have no gap and a non-zero superfluid fraction which still exhibits dissipationless flow. This is qualitatively different from the BEC case, where there is no limit on the occupation of excited states, so once v_s exceeds v_c this inevitably leads to dissipation and complete suppression of the superflow.

Chapter 2

Effects of time reveals symmetry breaking for fermions and Bose-Fermi mixtures in a triangular lattice

2.1 Introduction

Cold atoms in optical lattices provide a unique medium for mimicking effects known from other areas of physics. This is primarily due to the great flexibility and precise manipulation of the cold atomic system [11, 24, 25]. Atoms of a fermionic or bosonic character may be placed in an optical lattice potential whose geometry may be easily controlled by changing directions and/or polarisations of laser beams. Interactions between atoms may be controlled via magnetic, optical or microwave Feshbach resonances [5, 26]. The change in the depth of the optical lattice modifies primarily the tunnelling between lattice sites (with a lesser effect on the effective interaction strength), enabling, e.g., the superfluid-Mott insulator quantum phase transition, as proposed by Jaksch *et al.* [27] and subsequently demonstrated in Ref. [28]. Another spectacular way of controlling the tunnelling

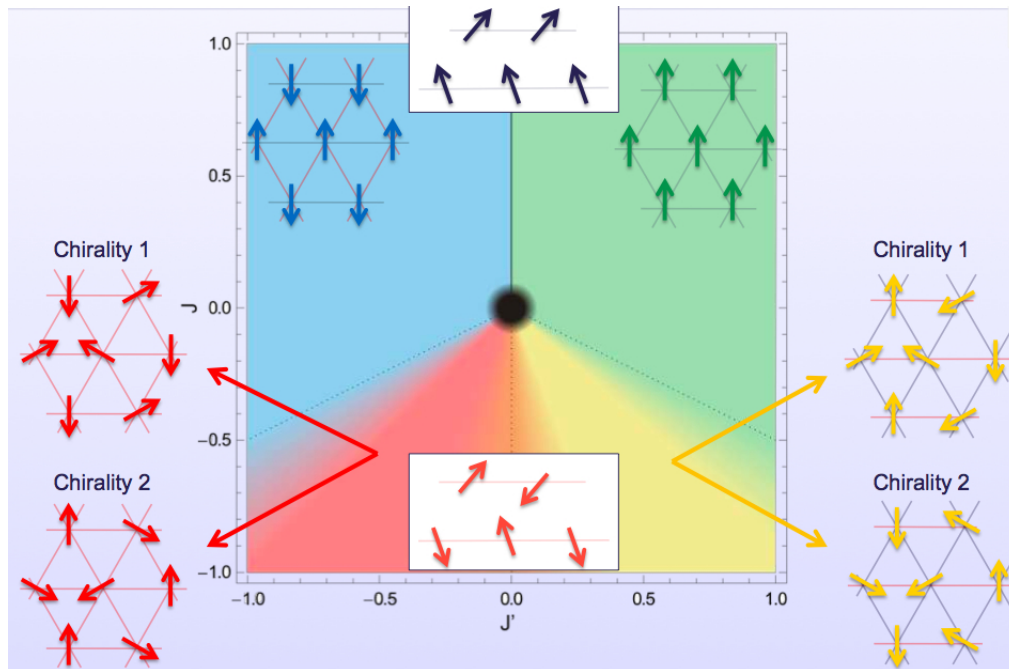


FIGURE 2.1: Experimentally observed phase diagram showing various orderings of the local phases of the BEC, mapped onto spin orders. The J , J' on the axes are the tunnelling amplitudes. Adopted from [10].

has been proposed by Eckardt, Weiss and Holthaus [29]. Fast periodic modulations of the optical lattice allow for an effective, time-averaged tunnelling to be dramatically altered while keeping the depth of the lattice potential unchanged. For example, by varying the strength of the modulation one can induce the Mott transition [29–31]. Importantly, not only the magnitude, but also the phase, φ , of the tunnelling amplitudes can be altered using this approach. So far most experiments exploited only the special case $\varphi = \pi$, corresponding to a negative tunnelling matrix element. This is enough to create frustrated magnetism with cold bosons in a triangular lattice in 2D [32] and in 3D [33]. This idea was incorporated in the fascinating experiments of the Hamburg group [10], where the authors independently tune the tunnel-couplings in different lattice directions and are able to reproduce a phase diagram corresponding to the classical XY spin model with a magnetic field (see Fig. 2.1).

By extending similar methods to realise complex hopping parameters [34–36], even richer physics becomes accessible in the driven optical lattice, with realisation of artificial gauge fields being a particularly promising research direction [36].

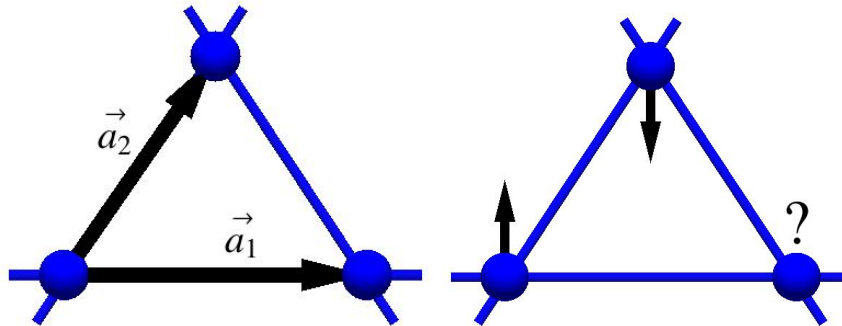


FIGURE 2.2: The schematic picture of a triangular plaquette. In panel (a) the lattice vectors are shown. In panel (b) the idea of geometrical frustration is illustrated for Ising spins with antiferromagnetic interactions. The question mark indicates that the spin cannot simultaneously minimise the energy of its interaction with both of its neighbours.

In this chapter we present a method involving periodic lattice modulations that break the time-reversal invariance (TRI) in order to induce complex values of the tunnelling amplitudes. We discuss implications of the broken TRI for fermions and for Bose-Fermi mixtures [34]. The content of this part of thesis is organised as follows. We start with a general introduction to the particles on the optical triangular lattice. Then, we introduce the periodically time-dependent Hamiltonians in the framework of the Floquet theory. Finally, in the last part we present our results on superfluid fermions in the Bardeen-Cooper-Schriffer (BCS) regime and on Bose-Fermi mixtures.

2.2 Background

2.2.1 Triangular lattice

2.2.1.1 The triangular lattice and frustration

In the quest to simulate condensed matter systems with ultra cold atoms, realisation of triangular structures is an important step, mainly due to the effect of geometrical frustration. In order to explain what we mean by this term let us first define some basics concepts. To describe a lattice, we need to construct lattice

vectors which enable us to reach all (and only those) points with position vectors:

$$\mathbf{R} = \{n\mathbf{a}_i + m\mathbf{a}_j, m, n \in \mathbb{Z}, i \neq j\} \quad (2.1)$$

The primitive vectors of the triangular lattice in the x, y basis have following coordinates :

$$\mathbf{a}_1 = a \begin{pmatrix} 0 \\ 1 \end{pmatrix} \quad \mathbf{a}_2 = \frac{a}{2} \begin{pmatrix} 1 \\ \sqrt{3} \end{pmatrix}, \quad (2.2)$$

where a is the lattice constant. These vectors are presented in Fig. 2.2(a). The third fundamental vector is given by $\mathbf{a}_3 = \mathbf{a}_1 - \mathbf{a}_2$.

One can immediately see how this geometry leads to intriguing many-body physics. For instance, let us consider Ising spins with antiferromagnetic interactions. As shown in Fig.2.2(b), we cannot find a spin configuration to fully satisfy the interaction between every pair of spins.

2.2.1.2 Triangular optical lattice

In experiments with neutral cold atoms, triangular lattice is realised by the interference pattern created by overlapping laser beams. Off-resonant light shifts the (internal) ground state energy of the particles due to the second order Stark effect. According to perturbation theory it produces a potential:

$$\mathbf{V}(\mathbf{r}) \approx -\alpha(\omega_L)|\mathbf{E}(\mathbf{r})|^2 \quad (2.3)$$

where $|\mathbf{E}(\mathbf{r})|$ is the electric field amplitude¹, and $\alpha(\omega_L)$ stands for atomic polarisability. The sign of the polarisability depends on the detuning of the laser light from the dominant dipole transition between two internal atomic states. The potential defined by the Eq. (2.3) is thus either attractive or repulsive, depending on the sign of the detuning. The optical traps rely on a *spatially varying* Stark shift

¹Let us notice that the time dependence of the electric field is averaged out due to the assumption that the centre-of-mass motion of atoms is much slower than the oscillation of the electric field.

[7]. By interfering laser beams, periodically varying laser intensity, and therefore periodically varying potential for the atoms, is produced:

$$V(\mathbf{r}) = - \sum_{i,j} \mathbf{E}_i \cdot \mathbf{E}_j \cos((\mathbf{k}_i - \mathbf{k}_j) \cdot \mathbf{r} + \varphi_i - \varphi_j) \quad (2.4)$$

where \mathbf{k}_i denotes the wave vector of a laser beam, and φ_i its phase. The vectors $\mathbf{b}_l = \varepsilon_{lij}(\mathbf{k}_i - \mathbf{k}_j)$ are the reciprocal lattice vectors, satisfying $\mathbf{a}_i \cdot \mathbf{b}_j = 2\pi\delta_{ij}$.

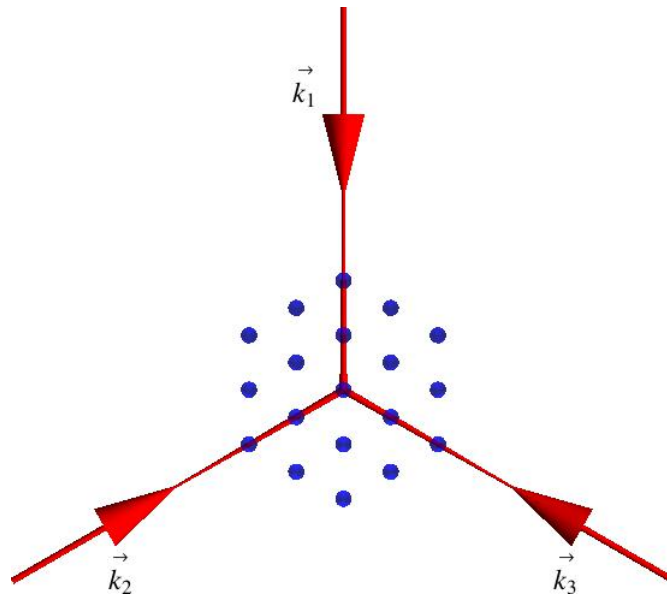


FIGURE 2.3: Schematic image of a 2D triangular array of 1D tubes. The red arrows are indicating the laser wave vectors \mathbf{k}_i . All three polarisation vectors are perpendicular to the plane of the drawing.

A triangular two dimensional optical lattice can be created using a configuration of laser beams shown in Fig. 2.7. The angle at which the beams intersect is $2\pi/3$. Let us notice the importance of the beam polarisations. For a triangular lattice all three polarisations are orthogonal to the plane spanned by the laser wave vectors. In-plane polarisations enable creation of a hexagonal lattice [9]. The control over the laser phases is also possible, allowing motion of the lattice to be introduced.

2.2.1.3 Layered two-dimensional system

A two-dimensional triangular lattice is suitable for study of long- or quasi-long-range order. The three-beam configuration presented in Fig. 2.7 creates an array of

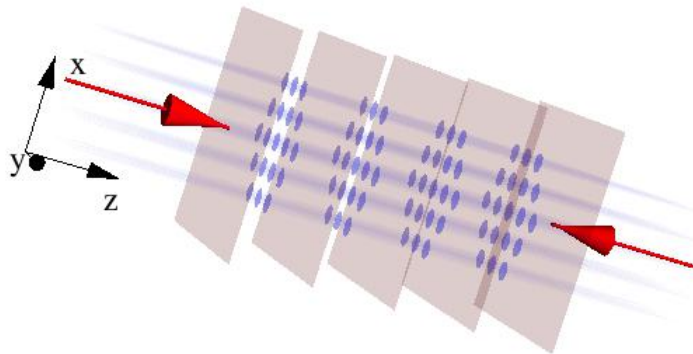


FIGURE 2.4: Schematic picture of a stack of two-dimensional systems. It is created by adding an optical lattice along the z direction, which can completely suppress the tunnelling between the different $x - y$ planes.

one-dimensional tubes. By adding a standing wave in the z direction it is possible to reduce the system to a stack of independent $x - y$ planes (Fig. 2.4). According to Mermin-Wagner theorem [37], for dimensions $d \leq 2$ true long-range order is impossible at non-zero temperatures². However, ultracold-atom systems created in the lab are finite in size, and so can appear fully ordered at low but non-zero T , displaying phenomena such as ferromagnetism, Bose-Einstein condensation and BCS superfluidity. In this regime they are also well described by zero-temperature theories, which allow true long-range order even in the thermodynamic limit. In our theoretical study we are therefore justified to use infinite-system $T = 0$ calculations to describe finite-size $T \neq 0$ experimental systems.

2.2.2 Fermion and Bosons on a lattice

2.2.2.1 The single particle states

The single particle eigenstates of the lattice potential in Eq. (2.4) are the Bloch waves

$$\phi_{n,\mathbf{q}}(\mathbf{r}) = e^{i\mathbf{q}\cdot\mathbf{r}} u_{n,\mathbf{q}}(\mathbf{r}) \quad (2.5)$$

²This conclusion holds for systems with continuous Hamiltonian symmetry and short-range interactions, which we are considering in this thesis.

where n is the band index and \mathbf{q} the quasi-momentum, which takes values in the first Brillouin Zone (BZ). The function $u_{n,\mathbf{q}}(\mathbf{r})$ is periodic with the period of the fundamental lattice vectors \mathbf{a}_i . The energy eigenvalues $\epsilon_n(\mathbf{q})$ for the Bloch waves form bands for varying \mathbf{q} inside the first Brillouin zone [38].

Throughout our work we will follow common approximations for deep lattices, such as tight binding approximation with nearest neighbour tunnelling and the restriction to the lowest band only.

In this description the starting single-particle basis is provided by Wannier functions $W(\mathbf{r} - \mathbf{R}_i)$. The Wannier functions are localised on the lattice sites and depend only on the relative distance $\mathbf{r} - \mathbf{R}_i$. The Bloch states of a given band are then constructed as linear combinations of the same Wannier function localised on different sites. We assume that the Wannier function decays significantly within a single lattice spacing, so only nearest-neighbour hopping is relevant. Later on, when we introduce interactions between particles, we will also assume that the mean interaction energies at a single site are much smaller than the separation between the lowest and the first excited band.

As an illustration, let us consider a simple 1D lattice with lattice period a . The dispersion relation for the lowest band is then simply

$$\epsilon(q) = -2J \cos(qa), \quad (2.6)$$

where the nearest-neighbour tunnelling matrix element J is real and defined to be positive.

2.2.2.2 Many-body Hamiltonian

The simplest many-body Hamiltonian involves the competition between the kinetic energy (i.e. tunnelling) and the on-site interactions between the particles. The schematic idea is presented in the Fig 2.5. This leads to a Hubbard Hamiltonian, derived for balanced mixture of fermions in two different spin states $\sigma = \uparrow, \downarrow$ in

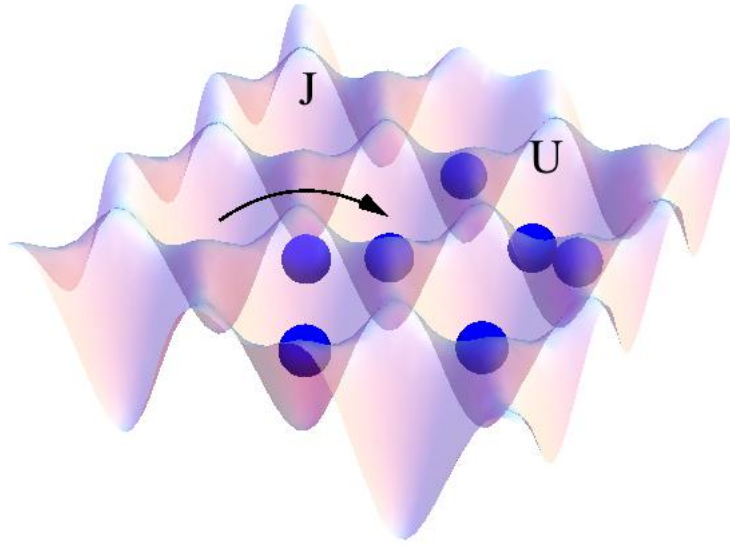


FIGURE 2.5: Schematic image of the tunnelling and the on-site interaction in the Hubbard Hamiltonian.

the form [39]:

$$\begin{aligned} \hat{H}_F = & - \sum_{\langle ij \rangle} J_{ij} \left(\hat{a}_{i\uparrow}^\dagger \hat{a}_{j\uparrow} + \hat{a}_{i\downarrow}^\dagger \hat{a}_{j\downarrow} \right) - \mu \sum_i (\hat{n}_{i\uparrow} + \hat{n}_{i\downarrow}) \\ & + \frac{U}{2} \sum_i \hat{a}_{i\downarrow}^\dagger \hat{a}_{i\uparrow}^\dagger \hat{a}_{i\uparrow} \hat{a}_{i\downarrow}, \end{aligned} \quad (2.7)$$

where operators $\hat{a}_{i,\sigma}$ have anti-commutation relations and μ stands for the chemical potential.

The term that describes the quantum tunnelling between nearest neighbour sites is:

$$J_{i,j} = - \int d^2r W_\sigma(r - R_i)^* (\mathbf{p}^2/2m + V(\mathbf{r})) W_\sigma(r - R_j). \quad (2.8)$$

Interactions are restricted only to the atoms on the same site, that interact by short-range s-wave scattering potential $V(\mathbf{r}_1, \mathbf{r}_2) \propto \delta(\mathbf{r}_1 - \mathbf{r}_2)$:

$$U = \int dr_1 dr_2 W_{\sigma_1}(\mathbf{r}_1)^* W_{\sigma_2}(\mathbf{r}_2)^* V(\mathbf{r}_1, \mathbf{r}_2) W_{\sigma_1}(\mathbf{r}_1) W_{\sigma_2}(\mathbf{r}_2). \quad (2.9)$$

Let us notice that for fermions only two particles of different spin states are allowed to occupy the same lattice site. We then refer to the situation where the filling is

one fermion per site as “half-filling” since the lattice contains half as many particles as the maximum number.

Bose Hubbard Hamiltonian for spineless bosons can be expressed as :

$$\hat{H}_B = - \sum_{\langle ij \rangle} J_{ij} \hat{b}_i^\dagger \hat{b}_j + \frac{U}{2} \sum_i \hat{b}_i^\dagger \hat{b}_i^\dagger \hat{b}_i \hat{b}_i - \mu \sum_i \hat{b}_i^\dagger \hat{b}_i, \quad (2.10)$$

with bosonic \hat{b}_i operators, which fulfil commutation relations.

2.2.2.3 Local order parameter and long-range order

We are interested in studying the relationships between the local phases, θ_i , of the wave function of a many-body system on different lattice sites. Below some critical temperature the system develops long-range order, meaning that the relative phase between any two points in the lattice is fixed - in such a state, by looking at one part of the system we can predict the phase θ at arbitrary distances. The simplest, and most common, example of this is a constant phase, corresponding to a “uniform order parameter”.

This language is quite generic and applies to many different physical systems. Let us give a few examples relevant to our considerations. In the XY spin model, classical spins of unit length can rotate in two dimensions and are described by the vector $\mathbf{s}_i = (\cos \theta_i, \sin \theta_i)$. A constant value of this vector throughout the lattice corresponds to ferromagnetic ordering with all the spins pointing in the same direction. N atoms in the $q = 0$ minimum of the lowest Bloch band correspond to an ideal Bose Einstein condensate with a constant phase; this picture also holds in presence of weak repulsive interactions between bosons [15]. In case of a balanced and stationary mixture of fermions in the BCS regime a similar picture also holds, but θ is now the phase of the pairing wave function of the Cooper pairs.

In all the above systems the choice of the constant global phase is arbitrary. At the critical temperature the system is expected to randomly choose the value of the phase, exhibiting spontaneous symmetry breaking.

In this work we are interested in engineering a more general class of Hamiltonians, which have ground states corresponding to condensation (in the general sense discussed above, i.e. the same language can apply to spin-ordering) into non-zero quasi-momentum states. It is precisely such Hamiltonians that are created by introducing complex single-particle tunnelling matrix elements into the Hubbard Hamiltonian. In this case the ground-state BEC wave function has a phase $\theta_i = \mathbf{q} \cdot \mathbf{r}_i$ that varies at each point of the lattice, according to the quasi-momentum vector \mathbf{q} .

It is important to stress that if this is truly the ground state of the system, then we do not expect it to have any global current. Indeed, if (by making J complex) we shift the minimum of the single-particle dispersion relation to a non-zero \mathbf{q} , it is still true that at that \mathbf{q} the group velocity, $\mathbf{v}_g = (1/\hbar)\partial\epsilon(\mathbf{q})/\partial\mathbf{q}$, is zero [38]. This is just another example of the difference between the canonical and mechanical momentum - the system condenses into a state of non-zero canonical momentum, but the mechanical momentum in the ground-state is still zero. As a final remark, the ground-state may involve local currents circulating the lattice plaquettes, but those currents cancel out on the global scale.

2.3 Periodically driven lattices

In the previous section we discussed the concept of the local order parameter (Sec. 2.2.2.3), common to different many-body systems. We can study the phase of a Bose or a Fermi-pair condensate, $\theta_i = \mathbf{q} \cdot \mathbf{r}_i$, and then map it onto the classical vector \mathbf{s}_i representing a direction of a spin on the i -th lattice site. This is especially interesting in the case of triangular lattice where the consequences of frustration can be observed.

The *interaction* energy per spin can be associated with the dispersion relation of an atom in a *non-interacting* gas. Again, for illustration let us consider a 1D lattice of spins, with lattice constant a . The energy of nearest-neighbour spin-spin

interactions can be written as:

$$E = -J \sum_i (\mathbf{s}_i \cdot \mathbf{s}_{i-1} + \mathbf{s}_i \cdot \mathbf{s}_{i+1}) = -J \sum_i (\cos(\theta_i - \theta_{i-1}) + \cos(\theta_i - \theta_{i+1})), \quad (2.11)$$

where $J > 0$ corresponds to ferromagnetic interactions, favouring alignment of the spins. Now we easily see that a spin-wave of wave vector $-\pi/a < q < \pi/a$, such that $\theta_i - \theta_{i-1} = qa$, has energy per particle of $-2J \cos(qa)$, which is identical to the dispersion relation in Eq. (2.6).

A key to the simulation of exotic magnetism is the possibility to experimentally manipulate the value of J , and specifically make it complex, $J_{eff} = |J_{eff}|e^{i\varphi_J}$. By expressing the XY spins as complex numbers, $s_i = \cos(\theta_i) + i \sin(\theta_i)$, and replacing $\mathbf{s}_i \cdot \mathbf{s}_{i+1} \rightarrow s_i^* s_{i+1}$, it is straightforward to repeat the above calculation and get $E(q) = -2|J_{eff}| \cos(qa - \varphi_J)$. We see that the minimum of the dispersion relation is now shifted to a non-zero $q = \varphi_J/a$, as discussed in Sec. 2.2.2.3.

Below, in Sec. 2.3.1, we will explain how complex J values are experimentally realised by periodic modulations of the optical lattice. Specifically, we will introduce periodic modulations that break time reversal symmetry. With that tool introduced, all the work that follows is based on extending the above 1D ideas to a triangular 2D lattice, with different tunnelling matrix elements along different lattice directions.

2.3.0.4 Is a driven lattice in equilibrium?

Before proceeding we briefly address one important conceptual issue. Our goal is to study equilibrium physics (specifically many-body ground states) of a lattice Hamiltonian with complex J values. However, to create such a Hamiltonian we will employ time-dependent modulations of the optical lattice. This means that our Hamiltonian is actually time-dependant, and so we do not really expect the energy (ground state or otherwise) to be a well defined conserved quantity.

While this concern is in general valid, it turns out that there is still a well defined way to think about equilibrium physics for the specific case of periodic time-dependence of the Hamiltonian. This problem is addressed by the Floquet theory. Moreover, further simplifications arise if the rate at which the Hamiltonian is modulated is large compared to any other relevant energy scale in the problem. Qualitatively, in a sense we can “integrate out” the fast modulation and work with a time-averaged stationary effective Hamiltonian. Generally, here we will just qualitatively outline the basic ideas of Floquet theory without formal details. More formal discussions can be found in Refs. [40–43].

According to the Floquet theorem, the solution of the time dependent Schrödinger equation can be expanded into the time-dependent Floquet states $\phi(\mathbf{r}, t)$. The first key point is that at any point in time the set of these states is complete and orthonormal, so we can expand any function as a superposition of these states. At the next moment in time all the individual Floquet states change (since the Hamiltonian changes) but there is a unique mapping of “which state transforms into which”. What this essentially means is that if we write an arbitrary wave function as $\psi = \sum c_n \phi_n(\mathbf{r}, t)$ then under unitary evolution the coefficients c_n are still constant, as with the standard time-independent Hamiltonians. We therefore still have a valid definition of effective eigenstates and their (conserved) occupations $|c_n|^2$.

The second question is what are the energies of these eigenstates, which need to be defined in order to, for example, study the scattering between different states and have the values of the occupation numbers defined in some equilibrium thermodynamic sense. This is where the fact that our Hamiltonian modulation is periodic is particularly important. While in general eigenenergy of a time-varying Hamiltonian is not defined, here it is defined up to modulo $\hbar\omega$, where ω is the driving frequency:

$$\epsilon_{n,m} = \epsilon_n + m\hbar\omega \quad \text{for which} \quad |\phi_{n,m}(\mathbf{r}, t)\rangle = |\phi_n(\mathbf{r}, t)\rangle \exp(-im\omega) \quad (2.12)$$

These are called quasi-energies, in analogy with the quasi-momentum of a particle

in a spatially periodic potential (see Sec. 2.2.2.1). We still need energies that will stay constant during the time evolution, and can be used to define time-independent probability for a given Floquet state to be occupied. For this, the so-called mean energy has to be introduced [44], which is determined by additionally averaging over the modulation period $T = 2\pi/\omega$.

Similarly, when calculating matrix elements involving Floquet states, inner products involve integration over both space and time, which is effectively introduced as an additional coordinate. For example, the orthogonality of two states is given by:

$$\langle\langle\phi_{n',m'}|\phi_{n,m}\rangle\rangle = \frac{\omega}{2\pi} \int_0^{2\pi/\omega} dt \int dx \phi_{n',m'}^* \phi_{n,m} = \delta_{n',n} \delta_{m',m}. \quad (2.13)$$

2.3.1 Realisation of complex tunnellings

In this section we will show that using a specific type of periodic lattice modulations, which break time-reversal invariance (TRI), we can change not only the sign of the tunnelling amplitudes, but may also induce their complex values. Before introducing our specific scheme, we briefly make some intuitive and some formal remarks considering the connection between TRI-breaking and complex tunnelling amplitudes.

As we explained earlier, by creating complex J values, ultimately our goal is to create a system with a minimum of the single-particle dispersion relation at a non-zero (canonical) momentum p . This clearly breaks the symmetry between \mathbf{p} and $-\mathbf{p}$ states. It is then rather intuitive that breaking TRI would be an effective way to achieve this. Specifically, we will achieve it using an external driving of the lattice with a double harmonic modulation, which indeed breaks *general* time-reversal symmetry³ [45].

³Time inversion is just one example of an anti-unitary operator, $T = UK$, where U is unitary and K stands for complex conjugation, $K\phi = \phi^*$. A system breaks *general* time-reversal symmetry if it is impossible to find *any* anti-unitary operator that commutes with the Hamiltonian. If a general time-reversal symmetry exists, then it is easy to construct a basis (without

While this sort of intuition provided the original motivation for our proposal, we note that it has more recently been shown that breaking TRI is formally neither necessary nor in general sufficient to obtain an effective Bose-Hubbard Hamiltonian with complex tunnelling amplitude [33]. Nevertheless, for our analysis, and for experimental implementations, it is only important that we can find a specific relatively simple TRI-breaking lattice modulation scheme which achieves our goal of making the tunnelling amplitude complex.

2.3.1.1 A shaken one-dimensional optical lattice

For simplicity, let us again begin with a single particle in a 1D optical lattice potential. The Hamiltonian for atoms in the laboratory frame of reference can be written as:

$$H_0 = \frac{p^2}{2m} + \cos(2k_L [x - x_o(t)]), \quad (2.14)$$

where $x_o(t)$ is the effective origin of the lattice and we allow for the possibility that it is time dependent. The shaking of the lattice is achieved by periodically varying $x_o(t)$. In practice it is introduced by changing the phases φ_i of the laser beams in Eq. (2.4).

For further calculations it is convenient to switch to the frame co-moving with the shaking lattice. This requires to use unitary gauge transformations including the shift of the position (by $x_o(t)$) and momentum (by $-M\dot{x}_o(t)$). The lattice becomes a stationary one and an additional term, which reflects the inertial force $-M\ddot{x}_o(t)$, emerges in the Hamiltonian:

$$H_0 = \frac{p^2}{2m} + V(x) - M\ddot{x}_o(t)x. \quad (2.15)$$

We consider a case where $\ddot{x}_o(t)$ has a form of double harmonic perturbation expressed as:

$$\ddot{x}_o(t) = -\frac{1}{M} (K_1 \cos(\omega t) + K_2 \cos(2\omega t + \varphi)). \quad (2.16)$$

diagonalisation of the Hamiltonian) in which the Hamiltonian is represented by a real symmetric matrix.

Here $K_{1,2}$ stand for the strengths of the driving at the fundamental frequency ω and its second harmonic, respectively. The Hamiltonian is time-periodic, i.e. $H_0(t + 2\pi/\omega) = H_0(t)$, and the Floquet theorem [40–42] guarantees that the Floquet Hamiltonian:

$$\mathcal{H} = H_0 - i\hbar\partial_t \quad (2.17)$$

is diagonalised by periodic functions with (temporal) Fourier components at frequencies $m\omega$. As we mentioned earlier, the eigenvalues of the \mathcal{H} are referred to as quasi-energies of the system [Eq. (2.12)] and are defined up to modulo $\hbar\omega$.

For our basis states, we are interested in Floquet analogues of Wannier states, i.e. states which are localised on individual lattice sites, and between which our hopping matrix element is defined. These now have the form:

$$\phi_{j,m}(x, t) = \exp \left\{ -ix \left[\frac{K_1}{\omega} \sin(\omega t) + \frac{K_2}{2\omega} \sin(2\omega t + \varphi) \right] \right\} \times \exp(im\omega t) W_j(x), \quad (2.18)$$

and fulfil

$$\langle\langle \phi_{j',m'} | \phi_{j,m} \rangle\rangle = \frac{\omega}{2\pi} \int_0^{2\pi/\omega} dt \int dx \phi_{j',m'}^* \phi_{j,m} = \delta_{j',j} \delta_{m',m}, \quad (2.19)$$

where m denotes a Fourier component and $W_j(x) = W(x - x_j)$ is a Wannier function of the lowest energy band localised on the j -th lattice site.

Note that these states can be viewed in the dressed atom picture, with W being the atomic state and m the number of “photons” present in the system.

In analogy to Eq. (2.8), let us first define the effective tunnelling as:

$$J_{eff} = -\langle\langle \phi_{j+1,m} | \mathcal{H} | \phi_{j,m} \rangle\rangle \quad (2.20)$$

It describes the process of hopping to the nearest lattice site, while m stays the same. Employing the identity $e^{iz \sin \theta} = \sum_{k=-\infty}^{\infty} e^{ik\theta} J_k(z)$, one can obtain:

$$J_{eff} = J \sum_{k=-\infty}^{\infty} \mathcal{J}_{2k}(s_1) \mathcal{J}_k(s_2) e^{ik\varphi}, \quad (2.21)$$

where

$$s_i = \frac{aK_i}{\omega_i}, \quad (2.22)$$

are dimensionless strengths of the first ($i = 1$) and the second ($i = 2$) harmonic, J is the bare tunnelling matrix element and \mathcal{J}_n is the ordinary Bessel function.

One could also consider a tunnelling matrix element that involves a change in m . However, recalling the dressed atom picture, such a process corresponds to absorption or emission of a photon. If $\hbar\omega \gg J$ this process is "off-resonant" and thus strongly suppressed. Usually, when considering the rate of some process we separately consider the size of the relevant matrix element and the issue whether the process is resonant. Here, since the Floquet matrix element already involves the averaging over time, the off-resonance of the m -changing process explicitly appears as the suppression of the matrix element.

More generally, if $\hbar\omega$ is greater than any other relevant energy scale in the problem, the matrix of the Floquet Hamiltonian consists of diagonal m -blocks, in our case in the basis (2.18), which are very weakly coupled to each other⁴.

The diagonal blocks of the Floquet Hamiltonian in the tight-binding approximation and taking into account only nearest-neighbour tunnelling becomes:

$$\langle\langle \phi_{j',m} | \mathcal{H} | \phi_{j,m} \rangle\rangle = -J_{eff} \delta_{j',j+1} - J_{eff}^* \delta_{j',j-1} + (m\omega + E_0) \delta_{j',j}, \quad (2.23)$$

where $E_0 = \langle W_j | (p^2/2m + V) | W_j \rangle$. Let us stress again that there will not be any tunnelling between different m for different lattice sites due to the fact that

⁴In our lattice problem, this criterion concerns just the energies within the lowest energy band. The gap energy between the two different lattice bands should still be greater than the driving frequency. The latter criterion is important to avoid inter-band transitions occurring due to the shaking of the lattice [46].

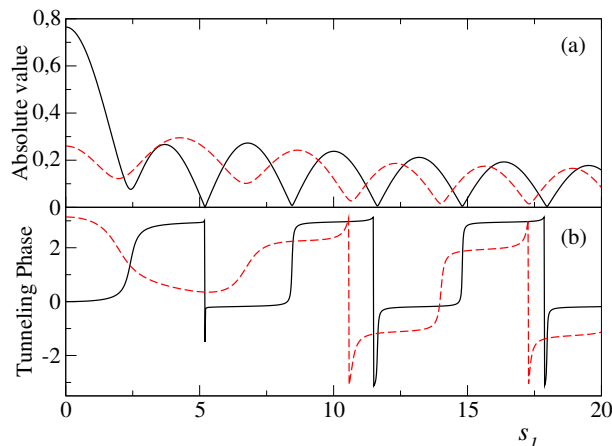


FIGURE 2.6: The absolute value (top), A , and the complex phase φ_J (bottom) of the effective tunnelling amplitude, $J_{eff}/J = A \exp(i\varphi_J)$, Eq. (2.21), for a double harmonic modulation of the optical lattice potential, as a function of the dimensionless strength s_1 of the ω component for $s_2 = 1$ [see Eq. (2.22)], $\varphi = 0.2$ (black solid lines) and $s_2 = 3$, $\varphi = 0.5$ (red dashed lines).

$\hbar\omega \gg J$ (blocks for different m are independent), nor any transfer of probabilities between different m values on the same lattice site if $\hbar\omega \gg E_o$ (elements of a block with given m are decoupled among themselves). The description of a single particle system may then be restricted to a single diagonal block:

$$H_{eff} = \langle\langle \phi_{j',0} | \mathcal{H} | \phi_{j,0} \rangle\rangle = -J_{eff} \delta_{j',j+1} - J_{eff}^* \delta_{j',j-1}, \quad (2.24)$$

where the constant term E_0 has been omitted. If there is only the fundamental frequency present in Eq. (2.16), i.e. $K_2 = 0$, or one of the phase $\varphi = 0$ or $\varphi = \pi$, the Floquet Hamiltonian is time-reversal invariant. (Formally, \mathcal{H} is represented by a real symmetric matrix in a generic basis [45].) In this case the effective tunnelling amplitude J_{eff} in Eq. (2.21) is real.

By breaking TRI we are able to realise nearly arbitrary complex values of the tunnelling amplitude $J_{eff} = |J_{eff}| e^{i\varphi_J}$. In Fig. 2.6 we present the absolute value $|J_{eff}|$ and the phase φ_J as a function of the parameter s_1 , for different fixed values of s_2 and φ .

The eigenstates of the Hamiltonian in Eq. (2.24) are the Bloch waves $\psi_j =$

$e^{iqx_j}/\sqrt{N_s}$, where N_s is the number of lattice sites, with the dispersion relation $E(k) = -2|J_{eff}|\cos(qa - \varphi_J)$. Single harmonic driving allows for $\varphi_J = 0$ or π and thus for the ground state with $q = 0$ or with q at the edge of the first Brillouin zone. The ground state of the system with broken TRI may correspond to any value of q .

So far we have concentrated on a 1D problem. However, similar control of the phases of the tunnelling amplitudes can also be realised in higher dimensions. Indeed, modulations applied to the lattice along orthogonal axes make it possible to engineer arbitrary tunnelling matrix elements along the corresponding directions [32]. In the following we will focus on a 2D triangular lattice.

2.3.2 Triangular optical lattice with complex tunnelings - simulating classical magnetism

With the help of the double harmonic modulations we are able to realise any phase of the tunnelling amplitudes

$$J_\alpha = |J_\alpha|e^{i\varphi_\alpha}, \quad J_\beta = |J_\beta|e^{i\varphi_\beta}; \quad (2.25)$$

see Fig. 2.7. Eigenstates of a single particle in such a lattice are Bloch waves with the dispersion relation

$$E(\mathbf{k}) = -2|J_\alpha|\cos(k_x a - \varphi_\alpha) - 2|J_\beta|\left\{ \cos\left[\left(\sqrt{3}k_y + k_x\right)\frac{a}{2} - \varphi_\beta\right] + \cos\left[\left(\sqrt{3}k_y - k_x\right)\frac{a}{2} - \varphi_\beta\right] \right\}. \quad (2.26)$$

We induce a shift of the dispersion relation along the k_y direction in the reciprocal space by changing the value of φ_β (with the other parameters fixed). The modification of φ_α alters the structure of the dispersion relation. It can reveal a doubly degenerate ground state for $\varphi_\alpha = \pi$. The presence of such a degeneracy has been observed experimentally in a Bose system [10]. For example, for $J_\alpha = J_\beta = -|J_\beta|$ the system in most experimental realisations chooses spontaneously one of the two

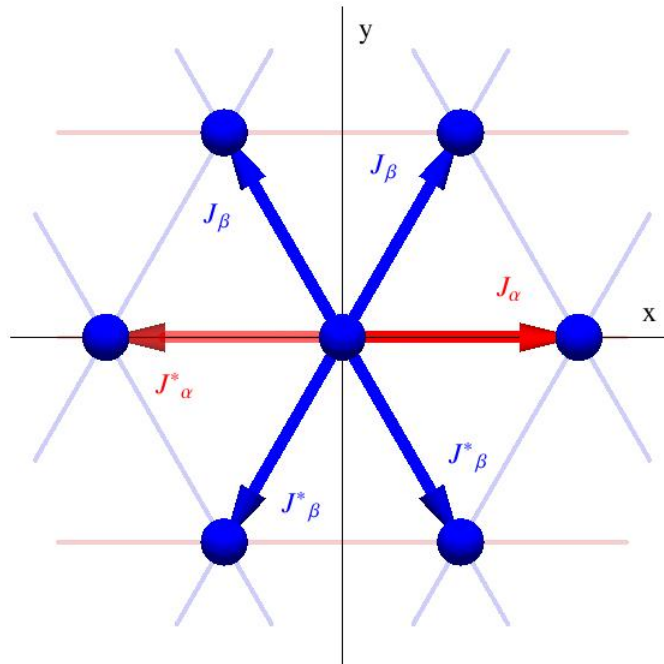


FIGURE 2.7: Triangular Bravais lattice points and amplitudes $J_{\alpha,\beta}$ corresponding to tunnelling from a lattice point to the nearest neighbours.

ground states. With the double harmonic modulation breaking the TRI, the two degenerate minima for $\varphi_\alpha = \pi$ can be moved arbitrarily along the k_y direction with a change of φ_β , see Fig. 2.8.

In the Hamburg experiment a Bose-Einstein condensate has been prepared in a triangular lattice. Although, in that case particle interactions are present, the ground state is still determined by the single particle dispersion relation [Eq. (2.26)]. Indeed, assuming a homogeneous system (which is a good approximation of the experimental situation) the solution of the Gross-Pitaevskii equation has the chemical potential given by $\mu_B = E(\mathbf{k}) + n_B U_B$, where U_B characterises the on-site particle interactions and n_B is the average number of bosons per lattice site. We would like to stress that, in the presence of the interactions, the restriction to a single block of the Floquet Hamiltonian like in Eq. (2.24) is valid provided $\hbar\omega \gg U_B$ [29]. On the other hand, $\hbar\omega$ must be much smaller than the energy separation between bands of the periodic lattice problem for the description limited to the lowest band to be valid.

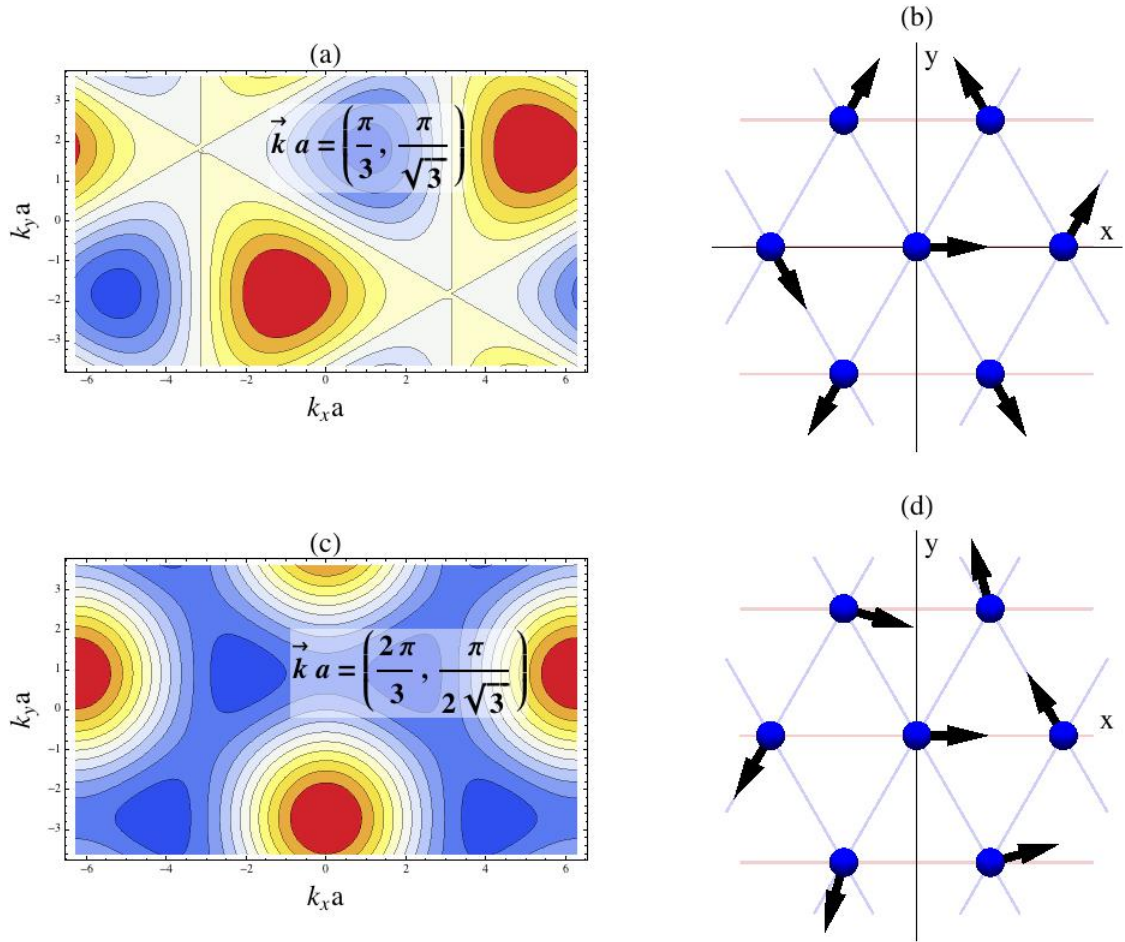


FIGURE 2.8: Contour plots of the dispersion relation Eq. (2.26) for $|J_\alpha| = |J_\beta|$ and $\varphi_\alpha = \varphi_\beta = \pi/2$ (a) and $\varphi_\alpha = \pi$ and $\varphi_\beta = \pi/4$ (c); cool colours indicate regions around energy minima. In right panels directions of arrows indicate phases $e^{i\mathbf{k}\cdot\mathbf{r}_i}$ where \mathbf{k} corresponds to a minimum of the dispersion relation. Specifically $\mathbf{k}a = \left(\frac{\pi}{3}, \frac{\pi}{\sqrt{3}}\right)$ for the minimum in (a) and $\mathbf{k}a = \left(+\frac{2\pi}{3}, \frac{\pi}{2\sqrt{3}}\right)$ for one of the two degenerate, non-equivalent minima in (c). Arrows in panel (b) and (d) are related to (a) and (c), respectively.

2.4 Fermions in the triangular lattice

Consider now a mixture of fermions in two different internal states (say spin up, \uparrow , and down, \downarrow , states) with the attractive contact interactions in a 2D triangular optical lattice. We assume that the tunnelling amplitude can have any complex phase [Eq. (2.25)]. In the tight-binding approximation the Hamiltonian of the Fermi system reads

$$\hat{H}_F = - \sum_{\langle ij \rangle} J_{ij} \left(\hat{a}_{i\uparrow}^\dagger \hat{a}_{j\uparrow} + \hat{a}_{i\downarrow}^\dagger \hat{a}_{j\downarrow} \right) - \mu \sum_i (\hat{n}_{i\uparrow} + \hat{n}_{i\downarrow}) - U \sum_i \hat{a}_{i\downarrow}^\dagger \hat{a}_{i\uparrow}^\dagger \hat{a}_{i\uparrow} \hat{a}_{i\downarrow}, \quad (2.27)$$

where the operator $\hat{a}_{i\uparrow}$ annihilates spin-up fermion at i -site, $\hat{n}_{i,\uparrow} = \hat{a}_{i\uparrow}^\dagger \hat{a}_{i\uparrow}$ and similarly for spin-down fermions. The tunnelling amplitude $J_{ij} = J_{ji}^*$ and it is equal J_α or J_β , Eq. (2.25), depending on a direction of the tunnelling in the triangular lattice, see Fig. 2.7. The parameter $U > 0$ characterises the inter-species, on-site, attractive interactions [Eq. (2.9)] and μ stands for the chemical potential.

The standard BCS approach [21] leads to the effective Hamiltonian:

$$H_{F,eff} = - \sum_{\langle ij \rangle} J_{ij} \left(\hat{a}_{i\uparrow}^\dagger \hat{a}_{j\uparrow} + \hat{a}_{i\downarrow}^\dagger \hat{a}_{j\downarrow} \right) - \mu \sum_i (\hat{n}_{i\uparrow} + \hat{n}_{i\downarrow}) + \sum_i \left(\Delta_i \hat{a}_{i\uparrow}^\dagger \hat{a}_{i\downarrow}^\dagger + \Delta_i^* \hat{a}_{i\downarrow} \hat{a}_{i\uparrow} \right), \quad (2.28)$$

where the pairing function

$$\Delta_i = U \langle \hat{a}_{i,\uparrow} \hat{a}_{i,\downarrow} \rangle. \quad (2.29)$$

If the phases of the tunnelling amplitudes [Eq. (2.25)] are zero the ground state of the system corresponds to a constant pairing function $\Delta = \text{const}$. However, the pairing function can acquire a non-trivial phase when the tunnelling amplitudes become complex. In order to find the ground state of the system let us look for the solutions of the Bogoliubov-de Gennes equations in the form

$$\begin{bmatrix} u_{\mathbf{k}}(\mathbf{r}_i) \\ v_{\mathbf{k}}(\mathbf{r}_i) \end{bmatrix} = \frac{e^{i\mathbf{k}\cdot\mathbf{r}_i}}{\sqrt{N_s}} \begin{bmatrix} U_{\mathbf{k}} e^{i\mathbf{k}_0\cdot\mathbf{r}_i} \\ V_{\mathbf{k}} e^{-i\mathbf{k}_0\cdot\mathbf{r}_i} \end{bmatrix}, \quad (2.30)$$

where $U_{\mathbf{k}}$ and $V_{\mathbf{k}}$ satisfy

$$\begin{bmatrix} E(\mathbf{k} + \mathbf{k}_0) - \mu & \bar{\Delta} \\ \bar{\Delta}^* & -\tilde{E}(\mathbf{k} - \mathbf{k}_0) + \mu \end{bmatrix} \begin{bmatrix} U_{\mathbf{k}} \\ V_{\mathbf{k}} \end{bmatrix} = \varepsilon_{\mathbf{k}} \begin{bmatrix} U_{\mathbf{k}} \\ V_{\mathbf{k}} \end{bmatrix}, \quad (2.31)$$

and $|U_{\mathbf{k}}|^2 + |V_{\mathbf{k}}|^2 = 1$. In Eqs. (2.31), $E(\mathbf{k})$ is the dispersion relation Eq. (2.26) while $\tilde{E}(\mathbf{k}) = E(\mathbf{k}; \varphi_\alpha \rightarrow -\varphi_\alpha, \varphi_\beta \rightarrow -\varphi_\beta)$. Solving (2.31) we obtain the following eigenvalues

$$\varepsilon_{\mathbf{k},\pm} = \frac{E(\mathbf{k} + \mathbf{k}_0) - \tilde{E}(\mathbf{k} - \mathbf{k}_0)}{2} \pm \sqrt{\frac{(E(\mathbf{k} + \mathbf{k}_0) + \tilde{E}(\mathbf{k} - \mathbf{k}_0) - 2\mu)^2}{4} + |\bar{\Delta}|^2}. \quad (2.32)$$

It may happen that the excitation spectrum of the system, i.e. the upper branch $\varepsilon_{\mathbf{k},+}$, is negative for some \mathbf{k} . In such a case, the corresponding quasi-particles are present even at zero temperature. Therefore, at $T = 0$, the proper equation for $\bar{\Delta}$ reads

$$\bar{\Delta} = \frac{U}{N_s} \sum_{\mathbf{k}} \frac{\bar{\Delta}}{2\varepsilon_{\mathbf{k},+}} [1 - 2\theta(-\varepsilon_{\mathbf{k},+})], \quad (2.33)$$

where the Heaviside function $\theta(-\varepsilon_{\mathbf{k},+})$ ensures that quasi-particles corresponding to negative energy spectrum are also included [21]. Finally the desired pairing function becomes

$$\begin{aligned} \Delta_i &= U \sum_{\mathbf{k}} u_{\mathbf{k},+}(\mathbf{r}_i) v_{\mathbf{k},+}^*(\mathbf{r}_i) [1 - 2\theta(-\varepsilon_{\mathbf{k},+})] \\ &= e^{i2\mathbf{k}_0 \cdot \mathbf{r}_i} \bar{\Delta}. \end{aligned} \quad (2.34)$$

When we switch from $\varphi_\alpha = \varphi_\beta = 0$ to $\varphi_\alpha = 0$ and $\varphi_\beta \neq 0$ the minimum of the dispersion relation Eq. (2.26) is shifted from $\mathbf{k} = 0$ to $\mathbf{k} = \mathbf{k}_0 = (0, 2\varphi_\beta)$. In the ground state of the system fermions occupy energy levels starting from the new minimum up to the Fermi level. Thus, all fermions acquire quasi-momentum \mathbf{k}_0 and consequently the pairing function gets the quasi-momentum $2\mathbf{k}_0$, see Eq. (2.34).

For $|J_\alpha| = |J_\beta|$ and $\varphi_\alpha = \pi$ there are two non-equivalent, degenerate minima of $E(\mathbf{k})$. For example, for $\varphi_\beta = \pi/4$ they are located at $\mathbf{k} = \left(\pm \frac{2\pi}{3a}, \frac{\pi}{2a\sqrt{3}}\right)$; see Fig. 2.8(c). In the ground state, fermions occupy energy levels with quasi-momenta around both of the minima. A nonzero pairing function exists for different values of \mathbf{k}_0 . However, for $\mathbf{k}_0 = \left(0, \frac{\pi}{a\sqrt{3}}\right)$ we obtain the lowest energy of the Hamiltonian Eq. (2.28). A slight change of \mathbf{k}_0 causes a rapid decrease of the energy gap in the excitation spectrum Eq. (2.32). In Fig. 2.9 we present the Fourier transform $|\Delta_{\mathbf{k}}|^2$ of the pairing function, where $\Delta_{\mathbf{k}} = \sum_i \Delta_i e^{-i\mathbf{k} \cdot \mathbf{r}_i} / \sqrt{N_s}$, obtained numerically for a finite system. For the chemical potential $\mu = 0$ (which would correspond to the half-filling regime for noninteracting particles), $|J_\alpha| = |J_\beta|$, $U/|J_\alpha| = 2$, we obtain $|\Delta_i|/|J_\alpha| = 0.111$ at the centre of the lattice, which agrees with the analytical

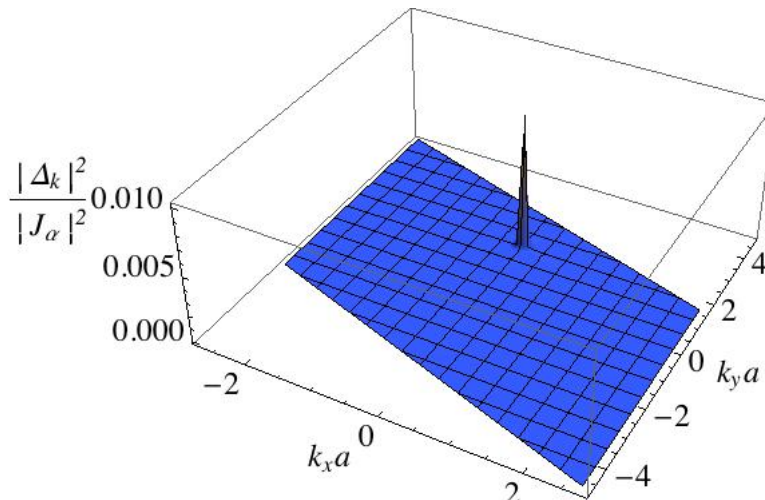


FIGURE 2.9: Modulus squared of the Fourier transform of the BCS pairing function $|\Delta_{\mathbf{k}}|^2$, where $\Delta_{\mathbf{k}} = \sum_i \Delta_i e^{-i\mathbf{k}\cdot\mathbf{r}_i} / \sqrt{N_s}$, obtained numerically for a finite system of 60×60 lattice sites for $|J_\alpha| = |J_\beta|$, $\varphi_\alpha = \pi$, $\varphi_\beta = \pi/4$, $U/|J_\alpha| = 2$ and $\mu = 0$. The $|\Delta_{\mathbf{k}}|^2$ corresponds to the ground state of the isolated Fermi system.

The peak is located at $\mathbf{k}a = (0.00, 1.78) \approx \left(0, \frac{\pi}{\sqrt{3}}\right)$.

solution $\bar{\Delta}/|J_\alpha| = 0.109$ for an infinite lattice. In Fig. 2.9 we see that even for the lattice of 60×60 sites there exists a clearly resolved peak at $\mathbf{k} \approx 2\mathbf{k}_0 = \left(0, \frac{\pi}{a\sqrt{3}}\right)$.

In conclusion, we have shown that the Fermi system can simulate classical magnetism, similar as was discussed in [10] for Bosons. Indeed, in a triangular lattice with complex tunnelings, the phase of the complex pairing function is the one that is mapped onto the orientation of the classical spins. It is a consequence of the fact that the pairing function is influenced by the shift of the minimum of dispersion relation for fermions, as seen in the Eq. (2.34).

2.5 Mixture of fermions and molecular dimers on the triangular lattice

2.5.1 The limit of dominant number of molecular dimers

In this section we consider a situation when the fermions coexist with molecular dimers – pairs of spin-up and spin-down fermions. The dimers form a Bose-Einstein

condensate. Such a mixture can be prepared by sweeping the system over a Feshbach resonance that creates a molecular BEC and leaves some fraction of unbound, repulsively interacting fermions. Then crossing a second Feshbach resonance one is able to change the interactions between fermions from repulsive to attractive, turning unbound fermions into BCS pairs [47]. The process does not affect the molecules at the same time. For this purpose Feshbach resonances at 202 G and 224 G for ^{40}K atoms [48] seem to be quite suitable. We also assume the presence of a weak Bose-Fermi coupling that transforms dimers into unbound fermions and vice versa. It can be realised via the photo-dissociation and photo-association. For a large molecular BEC the weak coupling does not influence significantly the condensate wave function and therefore we neglect dynamics of the BEC. The system under our consideration can be reduced to the following Hamiltonian

$$\hat{H} = \hat{H}_F + \hat{H}_{BF}, \quad (2.35)$$

with

$$\hat{H}_{BF} = \gamma \sum_i \left(\psi_i^* \hat{a}_{i\downarrow} \hat{a}_{i\uparrow} + \psi_i \hat{a}_{i\uparrow}^\dagger \hat{a}_{i\downarrow}^\dagger \right), \quad (2.36)$$

where the BEC wave function $\psi_i = \sqrt{n_B} e^{i\mathbf{q}_0 \cdot \mathbf{r}_i}$ is the ground state solution for bosons in the triangular lattice, i.e. \mathbf{q}_0 corresponds to the minimum of the dispersion relation Eq. (2.26). For reasons of simplicity but without loss of generality we choose the same dispersion relation for molecules and for fermions. In the system under consideration, the tunnelling amplitudes for molecules in a shaken optical lattice depend on a molecular state in the photo-association process. The coupling constant γ characterises the transfer of dimers into unbound fermions and vice versa. We consider real $\gamma \geq 0$.

In the presence of the condensate of dimers the BCS effective Hamiltonian (2.28) has to be supplemented with Eq. (2.36), that is

$$\hat{H}_{\text{eff}} = \hat{H}_{F,\text{eff}} + \hat{H}_{BF}. \quad (2.37)$$

In the presence of bosons, if $\mathbf{k}_0 = \mathbf{q}_0/2$, a simple analytical solution of the corresponding Bogoliubov-de Gennes equations Eqs. (2.30) exist. This solution need not correspond to the ground state of the system. However, we will see that for sufficiently strong coupling between bosons and fermions this becomes the ground-state solution. Employing Eqs. (2.30) with $\mathbf{k}_0 = \mathbf{q}_0/2$, we obtain the following equation for $\bar{\Delta}$:

$$\bar{\Delta} = \frac{U}{N_s} \sum_{\mathbf{k}} \frac{\bar{\Delta} + \gamma\sqrt{n_B}}{2\varepsilon_{\mathbf{k},+}} [1 - 2\theta(-\varepsilon_{\mathbf{k},+})], \quad (2.38)$$

where, in the present case, the excitation spectrum is

$$\varepsilon_{\mathbf{k},+} = \frac{E(\mathbf{k} + \mathbf{q}_0/2) - \tilde{E}(\mathbf{k} - \mathbf{q}_0/2)}{2} + \left[\frac{(E(\mathbf{k} + \mathbf{q}_0/2) + \tilde{E}(\mathbf{k} - \mathbf{q}_0/2) - 2\mu)^2}{4} + |\bar{\Delta} + \gamma\sqrt{n_B}|^2 \right]^{1/2}, \quad (2.39)$$

and the resulting pairing function

$$\Delta_i = e^{i\mathbf{q}_0 \cdot \mathbf{r}_i} \bar{\Delta}. \quad (2.40)$$

Let us concentrate on the triangular lattice with $|J_\beta|/|J_\alpha| = 1$, $\varphi_\alpha = \pi$ and $\varphi_\beta = \pi/4$ that corresponds to the dispersion relation plotted in Fig. 2.8(c). The dispersion relation reveals two non-equivalent degenerate minima (i.e. two minima that cannot be related by reciprocal vector), but the solution of the Gross-Pitaevskii equation for bosons chooses the Bloch wave with the quasi-momentum corresponding to one of the minima. The signatures of such a spontaneous symmetry breaking are observed experimentally [10]. We assume that Bose system chooses $\mathbf{q}_0 = \left(-\frac{2\pi}{3a}, \frac{\pi}{2a\sqrt{3}}\right)$ and analyse its influence on the Fermi system.

We consider the system with $\mu = 0$. If $\gamma = 0$ Cooper pairs with the quasi-momentum \mathbf{q}_0 do not exist, i.e. $\bar{\Delta} = 0$ is the only solution of Eq. 2.38. If coupling between bosons and fermions is present, but $\gamma\sqrt{n_B}/|J_\alpha| \leq 2.11$, the system reveals *gapless superfluidity*; see Sec. 1.5. Cooper pairs with the quasi-momentum \mathbf{q}_0

appear ($\bar{\Delta} \neq 0$), but there is no energy gap in the excitation spectrum. The system possesses quasi-momenta \mathbf{k} for which the excitation energies $\varepsilon_{\mathbf{k},+} < 0$ and consequently the corresponding quasi-particles are present even at $T = 0$.

Concerning the ground state of the system, numerical solutions of the Bogoliubov-de Gennes equations are analysed. It is found that an increase in the parameter γ causes a gradual enlargement of the peak at $\mathbf{k} = \mathbf{q}_0$ in the Fourier transform of the pairing function, together with a reduction of the peak at $\mathbf{k} = (0, \frac{\pi}{a\sqrt{3}})$ (the solution in the absence of bosons considered in the previous section).

When $\gamma\sqrt{n_B}/|J_\alpha| \approx 0.3$ we observe a crossover: the peak at $\mathbf{k} = (0, \frac{\pi}{a\sqrt{3}})$ becomes hardly visible and the ground state starts to be well reproduced by the pairing function Eq. (2.40).

For $\gamma\sqrt{n_B}/|J_\alpha| > 2.11$ an energy gap shows up, $\varepsilon_{\mathbf{k},+} > 0$. There is no quasi-particle at zero-temperature and the pairing function [Eq. (2.40)] is related to the ground state of the system.

In Fig. 2.10 we present numerical solutions for the triangular lattice of 60×60 sites for different values of $\gamma\sqrt{n_B}/|J_\alpha|$. In Fig. 2.10(a) the Fourier transform of the pairing function reveals two peaks at $\mathbf{k} \approx 2\mathbf{k}_0 = (0, \frac{\pi}{a\sqrt{3}})$ and $\mathbf{k} = \mathbf{q}_0 = (-\frac{2\pi}{3a}, \frac{\pi}{2a\sqrt{3}})$. The solution correspond to $\gamma\sqrt{n_B}/|J_\alpha| = 0.2$, for which the pairing function at the centre of the lattice is $|\Delta_i|/|J_\alpha| = 0.128$ and the energy gap in the excitation spectrum is close to zero ($\min(\varepsilon_{\mathbf{k},+}) \approx 0.00415|J_\alpha|$). In Fig. 2.10(b) the high peak of the pairing function in momentum space is clearly visible at $\mathbf{k} \approx \mathbf{q}_0$ due to the stronger coupling to bosons, $\gamma\sqrt{n_B}/|J_\alpha| = 2.3$. The pairing function at the centre of the lattice is $|\Delta_i|/|J_\alpha| = 0.891$ and the energy gap in the excitation spectrum is $0.187|J_\alpha|$. This numbers agree with the solutions for infinite system, $\bar{\Delta}/|J_\alpha| = 0.891$ and $\min(\varepsilon_{\mathbf{k},+}) = 0.194|J_\alpha|$.

2.5.2 Effects of variation of the number of molecular dimers

In the previous section we considered the Bose-Fermi mixture on the lattice with a weak coupling γ , that transforms dimers into unbound fermions and vice versa.

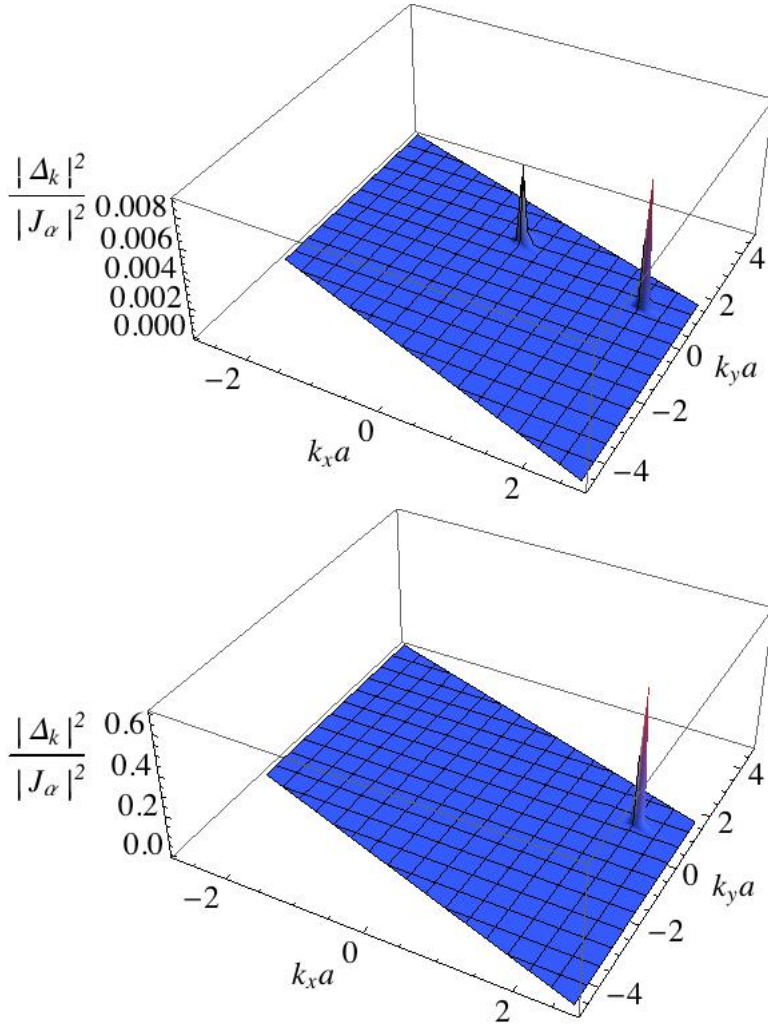


FIGURE 2.10: Modulus squared of the Fourier transform of the BCS pairing function $|\Delta_{\mathbf{k}}|^2$, where $\Delta_{\mathbf{k}} = \sum_i \Delta_i e^{-i\mathbf{k}\cdot\mathbf{r}_i} / \sqrt{N_s}$, obtained numerically for a finite system of 60×60 lattice sites for $|J_\alpha| = |J_\beta|$, $\varphi_\alpha = \pi$, $\varphi_\beta = \pi/4$, $U/|J_\alpha| = 2$ and $\mu = 0$. The Fermi system is coupled to the Bose-Einstein condensate, with wave function $\psi_i = \sqrt{n_B} e^{i\mathbf{q}_0 \cdot \mathbf{r}_i}$. Panel (a) shows $|\Delta_{\mathbf{k}}|^2$ with two peaks located at the positions $\mathbf{k}a = (0, \frac{\pi}{\sqrt{3}})$ and $\mathbf{k} = \mathbf{q}_0$. The coupling between fermions and molecule dimers is $\gamma\sqrt{n_B}/|J_\alpha| = 0.2$. In the panel (b) the peak is placed at

$$\mathbf{k}a = (2.09, 0.26) \approx \mathbf{q}_0 a = \left(-\frac{2\pi}{3}, -\frac{\pi}{2\sqrt{3}}\right) \text{ for } \gamma\sqrt{n_B}/|J_\alpha| = 2.3.$$

Due to the dominant number of bosons over fermions, the solutions for Gross-Pitaevskii equation were not influenced by the γ coupling. In this section we would like to analyse a system, in which we include also the stationary equations for dimers. The Hamiltonian for the fermions coexisting with molecular dimers in

the second quantisation formalism is:

$$\begin{aligned} \hat{H} = \int d^2r \left[\sum_{s=+,-} \left(\hat{\Psi}_{f,s}^\dagger(\mathbf{r}) H_{0,f}(\mathbf{r}) \hat{\Psi}_{f,s}(\mathbf{r}) - \frac{|g_{ff}|}{2} \hat{\Psi}_{f,s}^\dagger(\mathbf{r}) \hat{\Psi}_{f,-s}^\dagger(\mathbf{r}) \hat{\Psi}_{f,-s}(\mathbf{r}) \hat{\Psi}_{f,s}(\mathbf{r}) \right) \right. \\ \left. + \hat{\Psi}_b^\dagger(\mathbf{r}) H_{0,b}(\mathbf{r}) \hat{\Psi}_b(\mathbf{r}) + \frac{g_{bb}}{2} \hat{\Psi}_b^\dagger(\mathbf{r}) \hat{\Psi}_b^\dagger(\mathbf{r}) \hat{\Psi}_b(\mathbf{r}) \hat{\Psi}_b(\mathbf{r}) + \right. \\ \left. \Gamma \left(\hat{\Psi}_b^\dagger(\mathbf{r}) \hat{\Psi}_{f,\downarrow}(\mathbf{r}) \hat{\Psi}_{f,\uparrow}(\mathbf{r}) + \hat{\Psi}_b(\mathbf{r}) \hat{\Psi}_{f,\uparrow}^\dagger(\mathbf{r}) \hat{\Psi}_{f,\downarrow}^\dagger(\mathbf{r}) \right) \right], \end{aligned} \quad (2.41)$$

where $H_{0,f(b)}(\mathbf{r}) = -\frac{\hbar^2}{2m_{f(b)}} \nabla^2 - \mu_{f(b)} + V(\mathbf{r})$, and $V(\mathbf{r})$ is an optical lattice potential. The field operators of bosonic and fermionic atoms are denoted respectively by $\hat{\Psi}_b(\mathbf{r})$ and $\hat{\Psi}_{f,s}(\mathbf{r})$ where $s \in \{\uparrow, \downarrow\}$ indicates a spin state, $\mu_{f(b)}$ stands for the chemical potential of the Fermi and Bose sub-systems and m_b and m_f are masses of bosons and fermions, respectively. We consider the contact s-wave interaction among the species of the same kind, denoted by the parameter g_{ff} for fermions and g_{bb} for bosons. The term Γ , similarly as in the previous section, is responsible for the conversions between molecules and free fermions. The effective mean field Hamiltonian is expressed in the form:

$$\begin{aligned} \hat{H}_{eff} = \int d^2r \left[\sum_{s=+,-} \left(\hat{\Psi}_{f,s}^\dagger(\mathbf{r}) H_{0,f}(\mathbf{r}) \hat{\Psi}_{f,s}(\mathbf{r}) \right) + n_b \phi^*(\mathbf{r}) H_{0,b}(\mathbf{r}) \phi(\mathbf{r}) \right. \\ \left. + n_b^2 \frac{g_{bb}}{2} \phi^*(\mathbf{r}) \phi^*(\mathbf{r}) \phi(\mathbf{r}) \phi(\mathbf{r}) + \left(\Delta^\dagger(\mathbf{r}) \hat{\Psi}_{f,\downarrow}(\mathbf{r}) \hat{\Psi}_{f,\uparrow}(\mathbf{r}) + \Delta(\mathbf{r}) \hat{\Psi}_{f,\uparrow}^\dagger(\mathbf{r}) \hat{\Psi}_{f,\downarrow}^\dagger(\mathbf{r}) \right) \right. \\ \left. + \Gamma \sqrt{n_b} \left(\phi^*(\mathbf{r}) \hat{\Psi}_{f,\downarrow}(\mathbf{r}) \hat{\Psi}_{f,\uparrow}(\mathbf{r}) + \phi(\mathbf{r}) \hat{\Psi}_{f,\uparrow}^\dagger(\mathbf{r}) \hat{\Psi}_{f,\downarrow}^\dagger(\mathbf{r}) \right) \right], \end{aligned} \quad (2.42)$$

where the mean field pairing function is defined as

$$\Delta(\mathbf{r}) = -|g_{ff}| \langle \hat{\Psi}_{f,\downarrow}(\mathbf{r}) \hat{\Psi}_{f,\uparrow}(\mathbf{r}) \rangle. \quad (2.43)$$

We also replace the bosonic operator:

$$\langle \hat{\Psi}_b(\mathbf{r}) \rangle = \sqrt{n_b} \phi(\mathbf{r}), \quad (2.44)$$

where n_b is the number of bosons. We derive equations for eigen-functions $u_n(\mathbf{r})$, $v_n(\mathbf{r})$ using the standard BCS approach (see Sec. 1.4.2):

$$E_n u_n(\mathbf{r}) = H_{0,f}(\mathbf{r}) u_n(\mathbf{r}) + (\Delta(\mathbf{r}) + \Gamma \sqrt{n_b} \phi(\mathbf{r})) v_n(\mathbf{r}) \quad (2.45)$$

$$E_n v_n(\mathbf{r}) = -H_{0,f}^*(\mathbf{r}) v_n(\mathbf{r}) + (\Delta^\dagger(\mathbf{r}) + \Gamma \sqrt{n_b} \phi^*(\mathbf{r})) u_n(\mathbf{r}) \quad (2.46)$$

We assume that the molecular bosonic function is coupled to fermions by the pairing function $\Delta(\mathbf{r})$. Then the Gross-Pitaevskii equation can be written as:

$$\mu_b \phi(\mathbf{r}) = (H_{0,b}(\mathbf{r}) + n_b |g_{bb}| |\phi(\mathbf{r})|^2) \phi(\mathbf{r}) - \frac{\Gamma}{\sqrt{n_b} |g_{ff}|} \Delta(\mathbf{r}) \quad (2.47)$$

The discretisation of the space is done by expressing the functions $u_n(\mathbf{r})$, $v_n(\mathbf{r})$ and $\phi(\mathbf{r})$ in the Wannier's bases for the lowest energy band:

$$u_n(\mathbf{r}) = \sum_i w_f(\mathbf{r} - \mathbf{r}_i) u_n(\mathbf{r}_i) \quad (2.48)$$

$$v_n(\mathbf{r}) = \sum_i w_f(\mathbf{r} - \mathbf{r}_i) v_n(\mathbf{r}_i) \quad (2.49)$$

$$\phi(\mathbf{r}) = \sum_i w_b(\mathbf{r} - \mathbf{r}_i) \phi(\mathbf{r}_i), \quad (2.50)$$

The system can be then described by the following equations

$$E_n u_n(\mathbf{r}_i) = - \sum_{\langle i,j \rangle} J_{i,j} u_n(\mathbf{r}_j) - \mu_f u_n(\mathbf{r}_i) + [\Delta(\mathbf{r}_i) + \gamma \sqrt{n_b} \phi(\mathbf{r}_i)] v_n(\mathbf{r}_i) \quad (2.51)$$

$$E_n v_n(\mathbf{r}_i) = \sum_{\langle i,j \rangle} J_{i,j}^* v_n(\mathbf{r}_j) + \mu_f v_n(\mathbf{r}_i) + [\Delta^*(\mathbf{r}_i) + \gamma \sqrt{n_b} \phi^*(\mathbf{r}_i)] u_n(\mathbf{r}_i) \quad (2.52)$$

$$\mu_b \phi(\mathbf{r}_i) = - \sum_{\langle i,j \rangle} J_{i,j,b} \phi(\mathbf{r}_j) + U_b n_b \phi^*(\mathbf{r}_i) \phi(\mathbf{r}_i) \phi(\mathbf{r}_i) - \frac{\gamma}{\sqrt{n_b} U} \Delta(\mathbf{r}_i) \quad (2.53)$$

The bosonic function $\phi(\mathbf{r})$ is normalised to 1 and the fermionic functions u_n and v_n obey $|u_n|^2 + |v_n|^2 = 1$ for each n . The tunnelling amplitudes are defined as

$$J_{i,j} = \int d\mathbf{r}^2 w_f^*(\mathbf{r} - \mathbf{r}_i) H_{0,f} w_f(\mathbf{r} - \mathbf{r}_j) \quad (2.54)$$

$$J_{i,j,b} = \int d\mathbf{r}^2 w_b^*(\mathbf{r} - \mathbf{r}_i) H_{0,b} w_b(\mathbf{r} - \mathbf{r}_j) \quad (2.55)$$

We reduce the description of the system by using the nearest-neighbour-tunnelling and on-site-interactions, which are expressed the by following terms:

$$U = g_{ff} \int d\mathbf{r}^2 |w_f(\mathbf{r} - \mathbf{r}_i)|^4 \quad (2.56)$$

$$U_{bb} = g_{bb} \int d\mathbf{r}^2 |w_b(\mathbf{r} - \mathbf{r}_i)|^4 \quad (2.57)$$

$$\gamma = \Gamma \int d\mathbf{r}^2 w_b(\mathbf{r} - \mathbf{r}_i)^* w_f(\mathbf{r} - \mathbf{r}_i) w_f(\mathbf{r} - \mathbf{r}_i) = \gamma^* \quad (2.58)$$

The system is also subject to the time-periodic shaking, which leads to complex tunnelling elements $J_{i,j,(b)}$ (Sec. 2.3.1). In our calculations the stationary system is described by the equations (2.51) - (2.53). The system has many parameters that can be varied such as the chemical potential, number of bosonic particles, the fermion interaction U , the boson-boson repulsion strength U_{bb} , the coupling γ characterising the process of photo-association. The values of those constants are normalised to the amplitude of the tunnelling $|J_{i,j}|$ for fermionic atoms. For sake of simplicity we choose the same complex tunnelings for bosons and fermions; $J_{i,j,b}$ equals $J_{i,j}$.

The procedure to find the spatially varying pairing function $\Delta(\mathbf{r}_i)$ together with wave function $\phi(\mathbf{r}_i)$ is done in a self-consistent manner (for detail description see A.2)

2.5.2.1 Results

In this section we present the results obtained by solving Eqs. (2.51) - (2.53). The system is interesting due to its potential use as a simulator of classical magnetism. We focus on revealing what kind of spatially varying phases we are able to have for

fermions in two spin states coupled weakly to a condensate of dimers via Raman field in the triangular lattice with complex tunnelings. In this part of the thesis we analyse how the conclusions from Sec. 2.5.1 change when we add to the system the stationary equation for bosons and we then vary the number of those particles.

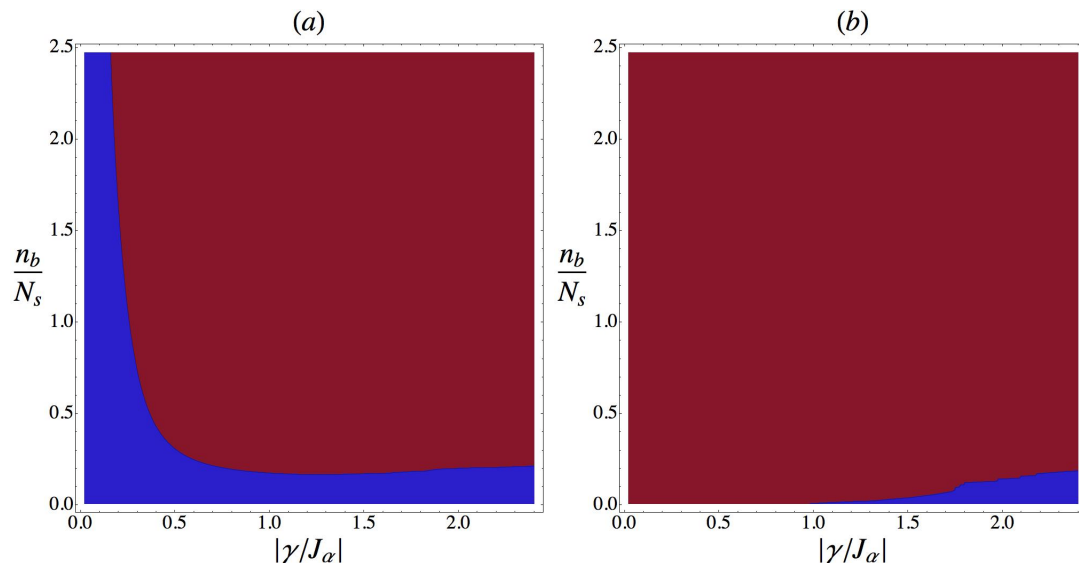


FIGURE 2.11: The effect of Bose-Fermi coupling on: (a) the BCS pairing function Δ and (b) the BEC wave function ϕ , for different values of the coupling strength γ and the number of bosons n_b . In absence of coupling Δ has its “natural” Fourier peak, i.e. maximum of $|\Delta_{\mathbf{k}}|^2$, at $\mathbf{k} = 2\mathbf{k}_0 = \left(0, \frac{\pi}{a\sqrt{3}}\right)$, while $|\phi_{\mathbf{k}}|^2$ has its natural peak at $\mathbf{q}_0 = \left(\pm \frac{2\pi}{3a}, \frac{\pi}{2a\sqrt{3}}\right)$, with one of the two possible \mathbf{q}_0 values spontaneously chosen. For sufficiently large γ one sub-system can impose its preferred spectral peak (i.e. its spatially varying phase) onto the other. In both panels red colour denotes the regime of “bosonic dominance”, where $|\Delta_{\mathbf{k}}|^2$ and $|\phi_{\mathbf{k}}|^2$ have a dominant (or only) peak at \mathbf{q}_0 . Conversely, blue colour denotes “fermionic dominance”, with main/only spectral peaks at $2\mathbf{k}_0$. The calculations were performed for a system of 10×10 lattice sites, with $|J_\alpha| = |J_\beta|$, $\varphi_\alpha = \pi$, $\varphi_\beta = \pi/4$, $U/|J_\alpha| = 2$, $U_{bb}/|J_\alpha| = 2$ and $\mu = 0$.

The main results are displayed in the Fig. 2.11. As in the section 2.5.1 we consider as an example a degenerate dispersion relation with two minima $\mathbf{k} = \left(\pm \frac{2\pi}{3a}, \frac{\pi}{2a\sqrt{3}}\right)$. It is realised by the following values of the complex hopping parameters: $|J_\beta|/|J_\alpha| = 1$ with $\varphi_\alpha = \pi$ and $\varphi_\beta = \pi/4$.

Previously we showed that without any transfer between fermions and bosons ($\gamma = 0$), the Fourier transform of the pairing function, $|\Delta_{\mathbf{k}}|^2$, exhibits a peak at

$\mathbf{k} = 2\mathbf{k}_0 = (0, \frac{\pi}{a\sqrt{3}})$ (see Fig. 2.9) according to Eq. (2.34). On the other hand, for $\gamma > 2.11$ and a large number of bosons the peak of $|\Delta_{\mathbf{k}}|^2$ is located at the position spontaneously chosen by the bosons, $\mathbf{k} = \mathbf{q}_0 = (\pm \frac{2\pi}{3a}, \frac{\pi}{2a\sqrt{3}})$ [Eq. (2.40)]. The

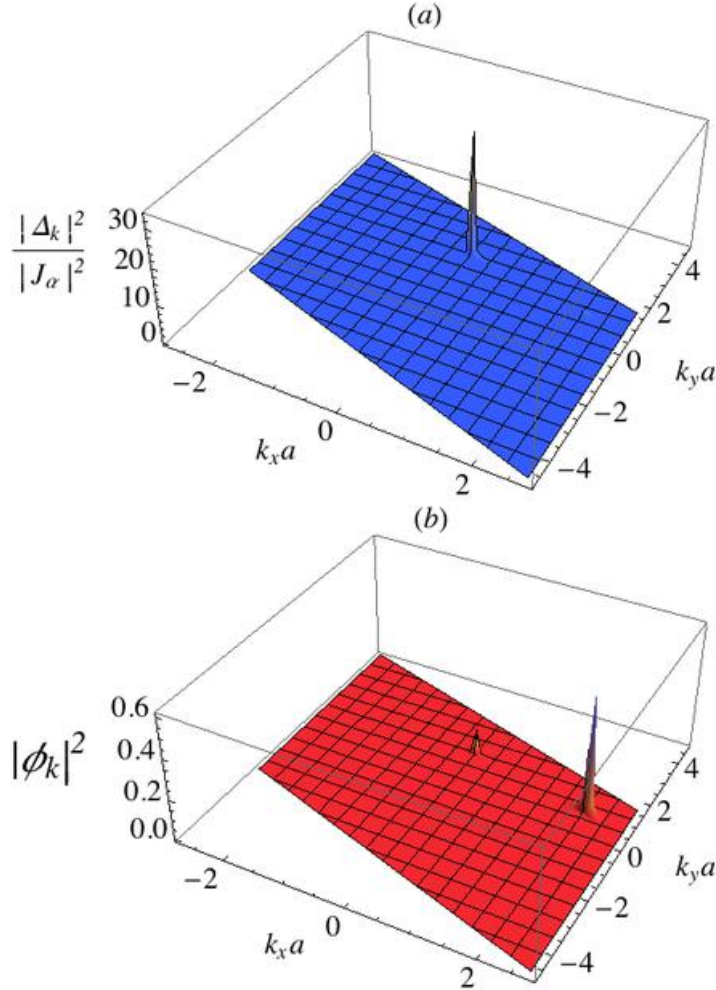


FIGURE 2.12: Modulus squared of the Fourier transform of the BCS pairing function $\Delta_{\mathbf{k}} = \sum_i \Delta_i e^{-i\mathbf{k}\cdot\mathbf{r}_i} / \sqrt{N_s}$ and the BEC wave function $\phi_{\mathbf{k}} = \sum_i \phi_i e^{-i\mathbf{k}\cdot\mathbf{r}_i} / \sqrt{N_s}$. The numerical calculation are proceeded for a finite system of 60×60 lattice sites for $|J_{\alpha}| = |J_{\beta}|$, $\varphi_{\alpha} = \pi$, $\varphi_{\beta} = \pi/4$, $U_{bb}/|J_{\alpha}| = 1$ and $\mu = 0$. The transfer between bosons and fermions and vice versa is equal to $\gamma/|J_{\alpha}| = 1.5$ with the number of bosons per site equal $n_b/N_s \approx 0.05$. Panel (a) presents $|\Delta_{\mathbf{k}}|^2$ that has a peak located at $\mathbf{k}a = (0, 1.78) \approx (0, \frac{\pi}{\sqrt{3}})$. Panel (b) presents the Bose-Einstein condensate wave function $|\phi_{\mathbf{k}}|^2$ with the peaks located at $\mathbf{k}a = (0, 1.78) \approx (0, \frac{\pi}{\sqrt{3}})$ and $\mathbf{k}a = (2.09, 0.89) \approx (\frac{2\pi}{3}, \frac{\pi}{2\sqrt{3}})$.

solutions of Eqs. (2.51) - (2.53) reproduce these results. Indeed, if the number of bosons is increased the relevant term grows like $\sqrt{n_b}$ in the equations [Eq. (2.51) - (2.52)], while the influence of the Fermi pairing function on the boson decreases as $1/\sqrt{n_b}$ [Eq. (2.53)]. In Fig. 2.11, this regime of “bosonic dominance” is denoted

by the red colour. Here, the dominant peaks of both $|\Delta_{\mathbf{k}}|^2$ and $|\phi_{\mathbf{k}}|^2$ is located at $\mathbf{k} = \mathbf{q}_0 = \left(\pm \frac{2\pi}{3a}, \frac{\pi}{2a\sqrt{3}}\right)$.

In Fig. 2.11 there are also minority regions denoted in blue. In this case the dominant peaks of both $|\Delta_{\mathbf{k}}|^2$ and $|\phi_{\mathbf{k}}|^2$ appear at $2\mathbf{k}_0$. This implies that the paring function has the solution governed by the dispersion relation for fermions and this solution is also imprinted on the bosons.

For simplicity, in Fig. 2.11 we have labeled different regimes (blue and red) according to the dominant Fourier peak of the BEC and the Fermi paring function. We note however that close to the boundary of the two regions both peaks are present (this is illustrated in Figs. 2.12 and 2.13). Sufficiently far from the boundary, each of the two wave functions has only one spectral peak, either its natural one or the one imposed by other subsystem. For example, for $\gamma/|J_{i,j}| > 2$ and $n_b/N_s \leq 0.1$, the coupling has no effect on the fermions and bosons posses a solution:

$$\phi_i = e^{i2\mathbf{k}_0 \cdot \mathbf{r}_i} |\bar{\phi}|. \quad (2.59)$$

This is a natural solution when we neglect the kinetic energy of the molecules, i.e. $J_{i,j}$ is not important when it is significantly smaller than γ . The dimers then simply have a phase which was a sum of the quasi-momenta of the two fermions that constitute them, even though this does not minimise dimers kinetic energy. This existence of this novel regime is qualitatively the main result of this section. More quantitatively, let us summarise all the various combinations of the solutions found by solving Eqs. (2.51) - (2.53):

1. For a small $\gamma/|J_\alpha|$ the BEC and the Fermi paring function are decoupled.
2. There exists a crossover regime for $\gamma/|J_\alpha| < 2.6$, for which the Fourier transforms of the paring function or the Bose function show two peaks at $2\mathbf{k}_0$ and \mathbf{q}_0 . The relative strength of this peaks depends of number of bosons, for examples look Figs. 2.12 and 2.13).

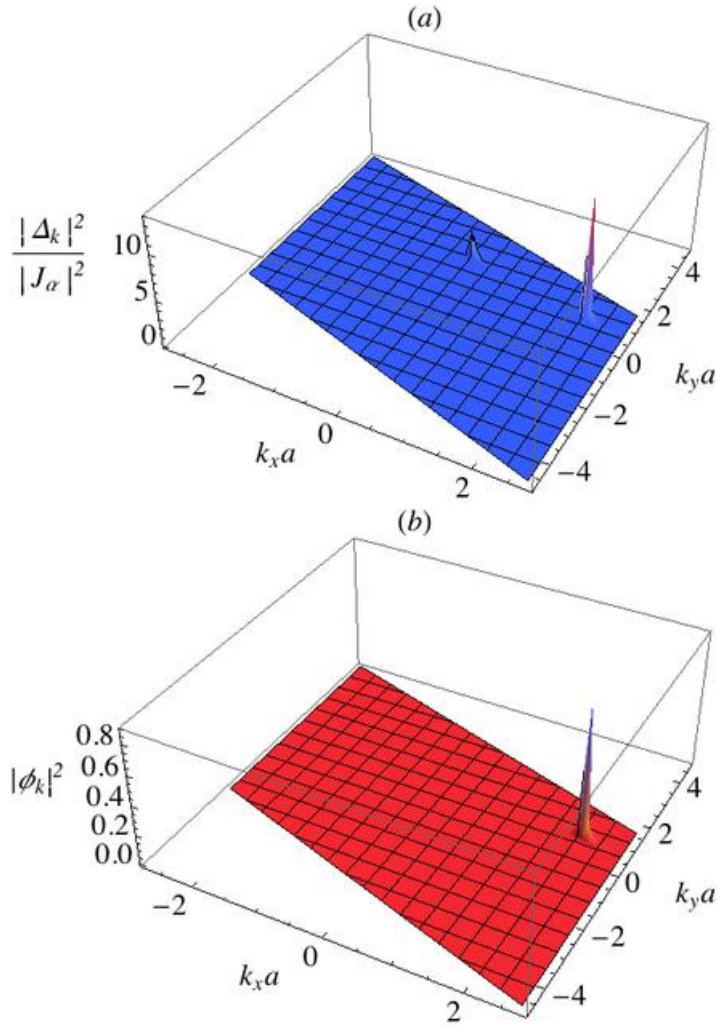


FIGURE 2.13: Modulus squared of the Fourier transform of the BCS pairing function and the BEC wave function. The solution are obtained for a system with the same parameters as in the Fig. 2.12, besides the transfer, which now is equal $\gamma/|J_\alpha| = 0.2$, with bosonic particles $n_b/N_s \approx 1.6$. In panel (a) $|\Delta_{\mathbf{k}}|^2$ is shown. There are the two peaks present at $\mathbf{k}a = (0.00, 1.78) \approx (0, \frac{\pi}{\sqrt{3}})$ and $\mathbf{k}a = (2.09, 0.89) \approx (\frac{2\pi}{3}, \frac{\pi}{2\sqrt{3}})$. Panel (b) presents a peak of the BEC wave function appearing at the position $\mathbf{k}a = (2.09, 0.89) \approx (\frac{2\pi}{3}, \frac{\pi}{2\sqrt{3}})$.

3. For strong coupling $\gamma/|J_\alpha| > 2$ one subsystem can control the other. When the number of bosons is small then their phase is controlled by fermions, while the number of bosons is large the opposite happens.

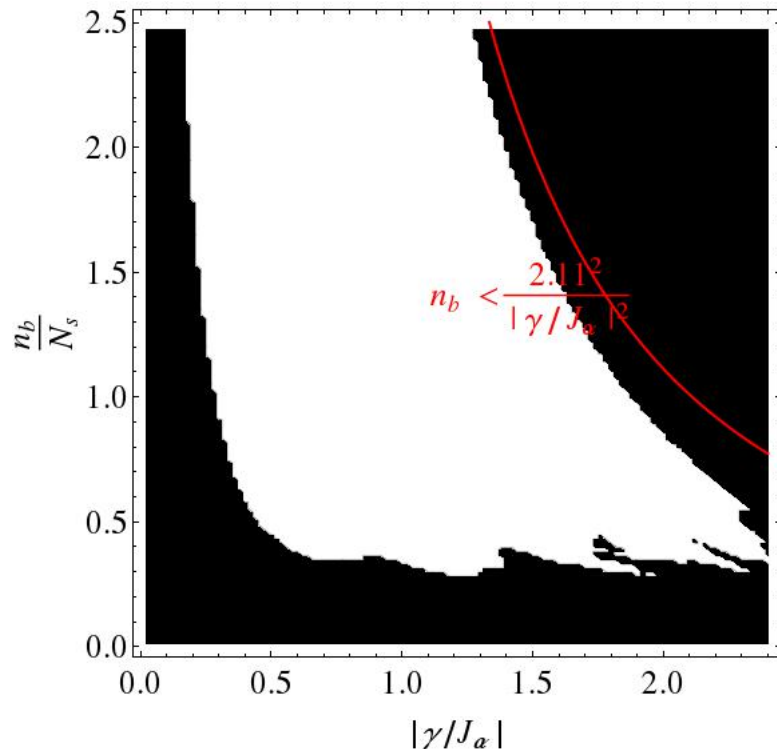


FIGURE 2.14: The region of gapless superfluidity. The figure presents a region, denoted by a white colour, for which the minimal positive excitation energy is less than 0.1 of the average value of the modulus of the pairing function in the configuration space. The results were obtained numerically for a small system of 10×10 lattice sites, with $|J_\alpha| = |J_\beta|$, $\varphi_\alpha = \pi$, $\varphi_\beta = \pi/4$, $U/|J_\alpha| = 2$ and $\mu = 0$. The red curve denotes the equality $n_b = \frac{(2.11)^2}{\gamma^2/|J_\alpha|^2}$

2.5.2.2 Gapless superfluidity

In the calculation for a small lattice size we capture the gapless superfluid⁵ regime described in the Sec. 1.5 and 2.5.1. In Fig. 2.14 the white region indicates the gapless regime, as a function of the number of bosons and the coupling between fermions and bosons. The energy gap disappears in the region starting from boson occupation number greater than $n_b/N_s \approx 0.2$ and for the coupling $0.2 < \gamma/|J_\alpha| < 2.6$.

In Sec. 2.5.1 we discussed the system, where the bosons were in majority. The gapless superfluidity was detected for $\gamma\sqrt{n_b}/|J_\alpha| < 2.11$. By looking at Fig. 2.14 we notice that the condition $n_b < \frac{(2.11)^2}{\gamma^2/|J_\alpha|^2}$ is qualitatively fulfilled. The difference

⁵The gapless superfluid regime is defined by the disappearance of the gap in the excitation spectrum. In our calculation it is assumed to appear when $\min(\varepsilon_{\mathbf{k},+}) < 0.1\bar{\Delta}$.

comes from the fact that the calculation we proceed in this section are done for much smaller lattice size ($N_s = 10$) rather than ($N_s = 60$) and the condition for gapless superfluid is less restrictive on the Fig. 2.14, i.e., $\min(\varepsilon_{\mathbf{k},+}) < 0.1\bar{\Delta}$.

To conclude, we considered the mean field description of a fermionic mixture coupled to bosonic molecules. We studied the competition between the solution governed by the single-particle dispersion relation and the one imposed by the transfer characterised by the term γ . We confirmed the solution from Sec. 2.5.1 and also found a new regime for small number of bosons where the pairing function imposed its phase on the wave function of the condensate.

2.6 Conclusions

We have studied a fermionic system as well as a Bose-Fermi mixture in a triangular lattice potential with complex tunnelings. In such a lattice the Bose system can simulate frustrated classical magnetism [10]. We have shown that this behaviour is similar for fermions where the pairing function acquires a complex phase. Assuming the presence of a coupling mechanism—an exchange of unbound fermions and bosonic molecules—we have shown that the complex phase of the Bose wave function can be imposed on the fermions, as reflected in the Fermi pairing function. We have also shown for small number of molecules the pairing function can force its phase on the bosons.

Chapter 3

Self-localisation of a small number of Bose particles in a superfluid Fermi system

3.1 Introduction

In this chapter we study the phenomenon of self-localisation of impurities of a condensed bosonic species in a homogeneous balanced mixture of fermions in two different internal states. This process occurs due to nonlinear interaction effects. It causes a deformation of the density profile of the majority particles in a form of a trapping potential for the impurity.

The behaviour of a small object immersed in a degenerate quantum gas has been investigated by several authors [49–65].

There are also many recent experimental realisations that explore the impurity physics either in the weakly [66–70] or the strongly interacting regime [71–74].

For example, weak interactions between a single impurity atom and particles of a large BEC can be described by perturbation theory [75], but for stronger interactions the effective mass of the impurity atom diverges, indicating the breakdown

of the perturbative approach and the self-localisation of the impurity [76, 77]. This process shares similarities with the small polaron problem. Indeed, in solid state physics a movement of an electron through a crystal lattice causes distortions (Fig. 3.1), resulting in the formation of the polaron - an entity composed of the electron and a cloud of virtual phonons. The polaron shows a tendency to self-trap itself in a form of localised states [78].

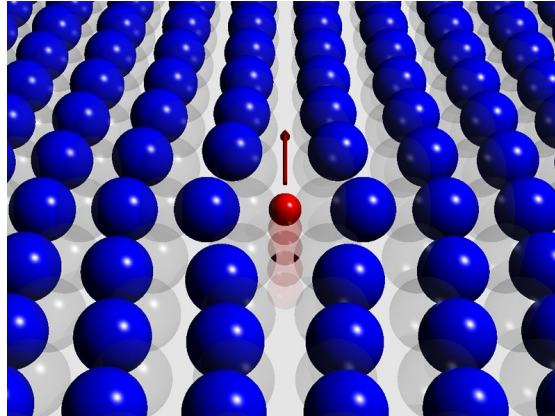


FIGURE 3.1: An electron (red) moving in a crystal lattice of ions (blue) creates a distortion, which leads to formation of a polaron. Adopted from <http://www.research.gov/>

When an impurity injected into a BEC interacts even more strongly (than in the regime that resembles behaviour of a polaron), it enters a regime where yet another mapping into a condensed-matter phenomenon can be made. In this regime a complete space separation between condensate and immersed particles is observed. This behaviour closely relates to electron bubbles in helium [79], which are formed by excess electrons in liquid helium. Helium atoms are pushed away by the quantum kinetic pressure exerted by the trapped electron and this pressure is balanced by surface tension and hydrostatic pressure [80].

Additionally, interesting physics can be studied when impurities interact among themselves. Two polarons can form a bound state (bipolaron) [81]. N impurities can crystallise for a certain set of parameters [56].

In ultra-cold *fermionic* gases polaron effects with a small number of spin-up fermions immersed in a large cloud of spin-down Fermi particles have been studied theoretically [60–65] and experimentally [82–84]. Employing a Feshbach resonance,

experimentalists have been able to investigate a transition from the nearly non-interacting case, through the polaron regime, to the limit where pairs of unlike fermions form tightly bound molecules. For example, on the repulsive side of the Feshbach resonance, strongly interacting fermions might form repulsive polarons [84]. This state can lead to creation of exotic quantum phases [85–88]. (Note that on the positive side of the Feshbach resonance fermions are unstable against decay into a bound molecular state, but nevertheless, this regime has proven to be experimentally accessible.)

Similar polaronic regime appears in a resonant Bose-Fermi mixture, involving one spin state each of bosonic and fermionic atoms. For a small number of bosons ($n_b < n_f$), Monte-Carlo calculations suggest a first-order quantum phase transition between condensed polaronic regime and a molecular phase in which molecules are formed by one bosonic and one fermionic atom, and interact weakly with unpaired fermions [89–91].

Another interesting theme is to study a “magnetic” impurity localised (by an external potential) in a superfluid fermionic mixture. By this we mean that the impurity interacts differently with spin-up and spin-down atoms. At the mean-field level this leads to pairs of bound states in the superconducting gap as well as bound states below the Fermi sea for repulsive interactions [72]. Complimentary to this work, here we consider a small number of Bose particles immersed in a large, homogeneous, superfluid and balanced mixture of spin-up and spin-down fermions.

This chapter is organised as follows. In Sec. 3.3 we begin with an explanation of the concept of instability of a Bose-Fermi mixture, and then introduce the theoretical model used in our description of Bose-Fermi mixtures. The results for the case of three-dimensional and one-dimensional systems are collected in Sec. 3.4. We describe the self-localisation of both interacting and non-interacting impurities. In the one-dimensional space we particularly focus on soliton-like states.

3.2 Instability of Bose-Fermi mixtures

In this section we would like to investigate how a weak contact interaction can make a homogeneous binary mixture unstable. Specifically, we are interested in bosonic impurity immersed in a fermionic system. Another limit, already investigated in the literature, concerns mixtures with a number of bosons comparable to (or even larger than) the number of fermions [92–101]. In that regime the instability of a homogeneous solution appears when boson-fermion interaction reaches a critical strength. Here, in the case of small boson numbers, the boson-boson interactions can be neglected and the uniform density solution is unstable for any *non-zero* boson-fermion coupling.

As an illustration of how interactions can lead to a phase separation, let us discuss a simple model of N_f fermions in one spin state and a small population, N_b , of bosonic particles. The system is initially homogeneous. The instability is introduced in a system if one finds a deviation of density that lowers the total energy. The total *canonical* energy in the model depends on the densities of bosons, $n_b = N_b/V$, and fermions, $n_f = N_f/V$, where V is the three-dimensional volume:

$$E = \int dr^3 \mathcal{E} [n_b, n_f], \quad (3.1)$$

where \mathcal{E} is the energy density. Due to the Pauli principle, there is no interaction between the fermions. We also assume that the bosonic kinetic energy is negligible in the thermodynamic limit. Finally, we also omit the boson-boson interaction. This leads to:

$$\mathcal{E} = \left(\frac{3}{5} n_f E_f + g_{bf} n_b n_f \right) \quad \text{and} \quad E = V \mathcal{E}, \quad (3.2)$$

where $E_f = [\hbar^2/2m_f](6\pi^2)^{2/3} n_f^{2/3} = A n_f^{2/3}$ stands for the Fermi energy, m_f is the fermion mass, g_{bf} denotes the interaction strength between the bosonic and fermionic atoms. The first term in the energy density [Eq. (3.2)] is the energy of fermions and the second expression denotes the interaction energy.

We now consider small changes in densities of the two species. First-order variation of Eq. (3.2) has to vanish, due to the particle number conservation. The second order variation of E with respect to densities fluctuations δn_i has a form

$$\delta^2 E = V \left(\frac{2}{3} A n_f^{-1/3} \delta^2 n_f + 2 g_{bf} \delta n_b \delta n_f \right). \quad (3.3)$$

For an energy minimum the expression in Eq. (3.3) has to be positive. More formally, all the minors of the energy functional have to be non-negative:

$$\frac{\partial^2 \mathcal{E}}{\partial n_f^2} \geq 0, \quad \frac{\partial^2 \mathcal{E}}{\partial n_b^2} \geq 0 \quad (3.4)$$

and

$$\frac{\partial^2 \mathcal{E}}{\partial n_f^2} \frac{\partial^2 \mathcal{E}}{\partial n_b^2} - \left(\frac{\partial^2 \mathcal{E}}{\partial n_f \partial n_b} \right)^2 \geq 0. \quad (3.5)$$

In our model $\left(\frac{\partial^2 \mathcal{E}}{\partial n_f \partial n_b} \right) = g_{bf}$ and $\frac{\partial^2 \mathcal{E}}{\partial n_b^2} = 0$, so in order for the system to stay homogeneously mixed we would need

$$g_{bf}^2 \leq 0. \quad (3.6)$$

We thus conclude, that for any sign of non-zero value of g_{bf} the system becomes unstable. Note that in our simple model, there is neither bosonic pressure (coming from the kinetic energy) nor boson-boson interactions to suppress the density fluctuations.

Let us show a simple example of a configuration that lowers the energy compared to the energy of a homogenous system. We consider a three-dimensional box filled with the Bose-Fermi mixture considered above, with repulsive inter-species interactions. We then divide the box into two halves and assume that a small number of fermions moves from one half of the container to the other. Consequently, the density is lowered by $-\delta n_f$ in one half and elevated by δn_f in the other. Due to the repulsive interactions some bosons δn_b move to the half where there is less fermions. We then calculate the total energy as a sum of the energy in the two

halves:

$$E = \frac{3 N_f E_f}{5} \frac{1}{2} \left[\left(1 + \frac{\delta n_f}{n_f} \right)^{5/3} + \left(1 - \frac{\delta n_f}{n_f} \right)^{5/3} \right] + \frac{g_{bf} V}{2} \left[n_f \left(1 + \frac{\delta n_f}{n_f} \right) n_b \left(1 - \frac{\delta n_b}{n_b} \right) + n_f \left(1 - \frac{\delta n_f}{n_f} \right) n_b \left(1 + \frac{\delta n_b}{n_b} \right) \right]. \quad (3.7)$$

For a large enough box the energy is given by:

$$E = \frac{3 N_f E_f}{5} \frac{1}{2} \left[\left(1 + \frac{\delta n_f}{n_f} \right)^{5/3} + \left(1 - \frac{\delta n_f}{n_f} \right)^{5/3} \right] + g_{bf} V \left[n_f n_b \left(1 - \frac{\delta n_f}{n_f} \frac{\delta n_b}{n_b} \right) \right]. \quad (3.8)$$

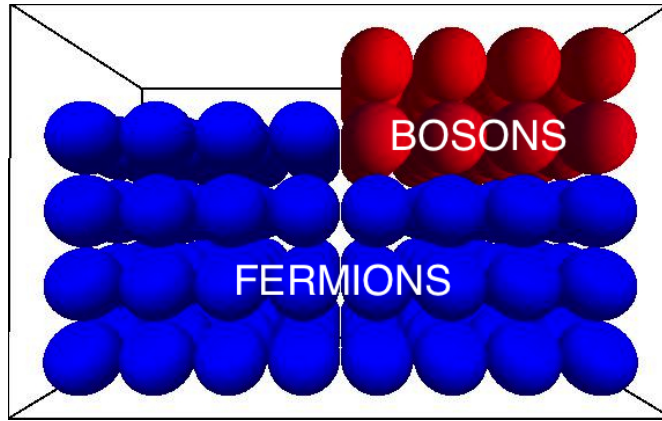


FIGURE 3.2: A box with an imbalanced number of fermions in the two halves. The repulsive interaction leads bosons to move into the half with lower fermion number. This configuration has lower energy than a homogeneous mixture of the two species.

In the presence of any fermionic density fluctuations, $\delta n_b = n_b$ minimises the energy, as illustrated in a Fig. 3.2. We still have to prove that this is a favourable configuration for the fermions. In order to do this, we calculate the total energy difference between systems with and without the fluctuations, for $\delta n_b = n_b$:

$$E [n_b \pm \delta n_b |_{\delta n_b = n_b}, n_f \pm \delta n_f] - E [n_b, n_f] = \quad (3.9)$$

$$\frac{3 N_f E_f}{5} \frac{1}{2} \left[\left(1 + \frac{\delta n_f}{n_f} \right)^{5/3} + \left(1 - \frac{\delta n_f}{n_f} \right)^{5/3} - 2 \right] - g_{bf} V n_f n_b \frac{\delta n_f}{n_f}. \quad (3.10)$$

An expansion of the fermion kinetic energy, up to the quadratic term in δn_f , leads to maximal value of $\delta n_f = g_{bf} \frac{3n_b}{2E_f}$ that lessens the energy of the system

for $\delta n_b = n_b$. Thus, for any positive value of g_{bf} some non-zero fluctuation of the fermion density, combined with bosons fully localising in one half of the box, lowers the total energy of the system.

One should stress that in this simple illustration we do not calculate the absolute lowest energy state. We just point out that there is a lower energy state than a homogeneous mixture of bosons and fermions.

It is also important to stress that the simple phase separation of bosons presented above is not what we will call *self-localisation*. In these calculations we have neglected the kinetic energy of condensed bosons, which grows if they are localised to one half of the box, and the importance of this effect depends on the total size of the system. In contrast, we define self-localisation as a phenomena that does not depend on the boundary conditions, i.e. the volume to which the particles are localised stays constant when we change the volume of the whole system. Also, the Bose-Fermi mixture we used as the example of an instability caused by interactions is much simpler than the model we would like to discuss throughout this work. First of all, we will like to consider a mutually interacting fermionic mixture in two different internal states. We will also take into account the bosonic pressure and, later on, also the repulsive interaction between the bosons.

3.3 Model description of Bose-Fermi mixtures

Let us consider a small number, N_b , of bosonic atoms in a condensed state, immersed in a 3D, homogeneous, dilute and balanced mixture of fermions in two different internal (spin) states. Interactions between ultra-cold atoms can be described via contact potentials $\mathcal{V}_{ij}(\mathbf{r}) = g_{ij}\delta(\mathbf{r})$, with strengths given in terms of s -wave scattering lengths a_{ij} , according to $g_{ij} = 2\pi\hbar^2 a_{ij}/m_{ij}$, where m_{ij} is the reduced mass of a pair of interacting atoms. In our model we consider attractive interactions between fermions in different spin states, i.e. $g_{ff} < 0$. Interactions between bosons and fermions are determined by the spin-independent g_{bf} . For the main part of this work, we neglect mutual interactions of bosonic atoms, on

the assumption that either their density remains sufficiently small or the coupling constant is negligible. We will later verify the validity of this assumption in Sec. 3.4.1.4.

The system is described by the following Hamiltonian:

$$\hat{H} = \int d^3r \left[\hat{\Psi}_b^\dagger \left(-\frac{\hbar^2}{2m_b} \nabla^2 \right) \hat{\Psi}_b + \sum_{s=+,-} \left(\hat{\Psi}_{f,s}^\dagger H_0 \hat{\Psi}_{f,s} - \frac{|g_{ff}|}{2} \hat{\Psi}_{f,s}^\dagger \hat{\Psi}_{f,-s}^\dagger \hat{\Psi}_{f,-s} \hat{\Psi}_{f,s} + g_{bf} \hat{\Psi}_{f,s}^\dagger \hat{\Psi}_{f,s} \hat{\Psi}_b^\dagger \hat{\Psi}_b \right) \right], \quad (3.11)$$

where $H_0 = -\frac{\hbar^2}{2m_f} \nabla^2 - \mu$. $\hat{\Psi}_b$ and $\hat{\Psi}_{f,s}$ refer, respectively, to the field operators of bosonic and fermionic atoms, with $s \in \{+, -\}$ indicating the spin state. μ stands for the chemical potential of the Fermi sub-system, and m_b and m_f are masses of bosons and fermions, respectively.

We look for a thermal equilibrium state assuming that the Bose and Fermi sub-systems are separable. For instance in the limit of zero temperature it is given by a product ground state

$$|\Psi\rangle = |\psi\rangle_f |\phi\rangle_b. \quad (3.12)$$

This ansatz was used by Landau and Pekar to describe polaron wave-function in the strong-coupling regime. It implies that the impurity (usually light and therefore fast) adiabatically follows the motion of the heavy particles. Similar to the Born-Oppenheimer approximation, we freeze the coordinates of the slow system and solve the Hamiltonian of the fast moving objects. The energy of the fast particles then enters the effective Hamiltonian for the slow system as a potential energy term. For the impurity in ultra-cold alkali gases the mass ratio is usually close to unity. In this case, the justification for the ansatz in Eq. (3.12), which assumes lack of correlations between the impurity and the environment, comes from the fact that the interaction energy is small compared to the chemical potential of the majority species [51, 52].

We also postulate that the Fermi sub-system can be described by the BCS mean-field approximation [20], with the pairing field

$$\Delta(\mathbf{r}) = |g_{ff}| \langle \hat{\psi}_{f,+} \hat{\psi}_{f,-} \rangle \quad (3.13)$$

and the Hartree-Fock potential

$$W(\mathbf{r}) = -|g_{ff}| \langle \hat{\psi}_{f,+}^\dagger \hat{\psi}_{f,+} \rangle = -|g_{ff}| \langle \hat{\psi}_{f,-}^\dagger \hat{\psi}_{f,-} \rangle \quad (3.14)$$

affected by a potential proportional to the density of bosons $N_b |\phi(\mathbf{r})|^2$.

Assuming a spherical symmetry of particle densities, the description of the system reduces to the Bogoliubov-de Gennes equations for fermions

$$\begin{aligned} (H_0 + W + g_{bf} N_b |\phi|^2) u_{nlm} + \Delta v_{nlm} &= E_{nl} u_{nlm} \\ \Delta^* u_{nlm} - (H_0 + W + g_{bf} N_b |\phi|^2) v_{nlm} &= E_{nl} v_{nlm}, \end{aligned} \quad (3.15)$$

where l and m stand for angular momentum quantum numbers and

$$W = -|g_{ff}| \sum_{nlm} |v_{nlm}(\mathbf{r})|^2, \quad (3.16)$$

$$\Delta = |g_{ff}| \sum_{nlm} u_{nlm}(\mathbf{r}) v_{nlm}^*(\mathbf{r}), \quad (3.17)$$

which have to be solved together with the Gross-Pitaevskii equation for bosons

$$\left[-\frac{\hbar^2}{2m_b} \nabla^2 + V(\mathbf{r}) \right] \phi(\mathbf{r}) = \mu_b \phi(\mathbf{r}), \quad (3.18)$$

where

$$V(\mathbf{r}) = -\frac{2g_{bf}}{|g_{ff}|} W(\mathbf{r}) = g_{bf} \rho_f(\mathbf{r}). \quad (3.19)$$

The effective potential $V(\mathbf{r})$ for bosons comes from contact interactions between bosons and fermions. ρ_f is the density of fermions and μ_b is the chemical potential for bosons. We consider a temperature much lower than the critical temperature for Bose-Einstein condensation, so we can neglect thermal excitations of bosons.

The coupled Eqs. (3.15) and (3.18) are solved numerically in a self-consistent manner. We start with choosing an initial function for an impurity, a pairing function and a density for fermions. Each iteration step involves first solving the eigenvalue problem of the Bogoliubov de Gennes equations (3.15) modified by the interaction with bosons. This action has to be repeated until Δ and W converge. A new value of a bosonic wave function is then obtained by inserting the fermion density into Eq. (3.18) and then diagonalising. The iterations proceed until all the quantities converge on a self-consistent solution.

In the calculations and in all the figures we adopt

$$\begin{aligned} E_0 &= 2E_F = \frac{\hbar^2 k_F^2}{m_f}, \\ l_0 &= \frac{1}{k_F}, \end{aligned} \quad (3.20)$$

units for energy and length, respectively, where $k_F = (3\pi^2 n_0)^{1/3}$ is the Fermi wave-number of a uniform ideal Fermi gas of density n_0 . In these units the coupling constants are

$$\begin{aligned} g_{ff} &= 4\pi k_F a_{ff}, \\ g_{bf} &= 2\pi k_F a_{bf} \left(1 + \frac{m_f}{m_b}\right), \end{aligned} \quad (3.21)$$

and we deal with six independent parameters in the system: number of bosons N_b , chemical potential of the Fermi sub-system μ , ratio of the masses m_b/m_f , scattering lengths $k_F a_{ff}$ and $k_F a_{bf}$, and the radius R of the 3D volume we consider.

In the 3D case the coupling constant g_{ff} in Δ [Eq. (1.30)] has to be regularised in order to avoid ultraviolet divergences. That is, $g_{ff} \rightarrow g_{\text{eff}}$, where

$$\frac{1}{|g_{\text{eff}}|} = \frac{1}{|g_{ff}|} - \frac{1}{2\pi^2} \left(\frac{1}{2} \ln \frac{\sqrt{E_C} + \sqrt{\mu}}{\sqrt{E_C} - \sqrt{\mu}} - \sqrt{\frac{E_C}{\mu}} \right). \quad (3.22)$$

The logarithmic term in the Eq. (3.22) results from the sum over Bogoliubov modes corresponding to the energy above a numerical cutoff E_C , performed in the spirit of the local density approximation; see Sec. B.2 for details.

3.4 Results in three dimensions

Without interactions between bosons and fermions, the ground state of the system corresponds to uniform particle densities. For a non-zero coupling constant g_{bf} , the uniform solution become unstable and, depending on the sign of g_{bf} , the bosonic and fermionic clouds tend to either separate from each other or stick together. For sufficiently strong interactions, the effect of self-localisation may be expected (for a similar problem in the case of an impurity atom immersed in a large Bose-Einstein condensate see Refs. [50–52]). Indeed, for $g_{bf} > 0$ bosons repel fermions and create a potential well in their vicinity where they may localise if the well is sufficiently large. For attractive interactions the density of fermions increases in the vicinity of Bose particles. Due to the fact that $g_{bf} < 0$, the bosons experience the density deformation as a potential well in which they may localise.

We begin with the 3D model and focus on the repulsive boson-fermion interactions¹. Analysis of both the zero-temperature limit and the thermal effects are performed. We also discuss the possibility of the effect of self-localisation being a signature of fermionic superfluidity. Finally, we also comment on the effects of including the boson-boson interaction, and on the case of attractive boson-fermion interactions.

3.4.1 Repulsive boson-fermion interaction

3.4.1.1 General characteristics of self-localisation

Figure 3.3 shows the densities of bosons and fermions and the pairing function corresponding to the ground state of the system for $g_{bf} = 0$ and $g_{bf} = 10$. Without boson-fermion interactions, the quantities are flat and uniform (except for a small region close to the edge of the 3D volume due to assumed open boundary conditions). However, when considerable interactions are turned on, it becomes

¹Note that our model neglects a possible weakly bound Bose-Fermi molecular state, that can be found for repulsive interactions between fermionic and bosonic species [72].

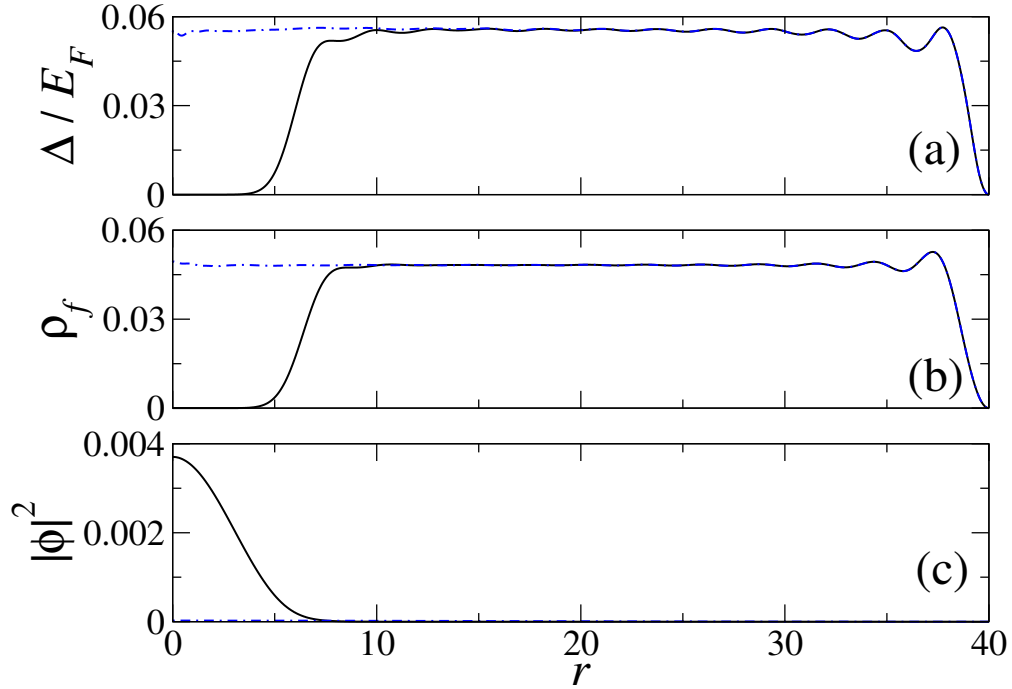


FIGURE 3.3: Self-localisation of ^{23}Na atoms in a superfluid mixture of ^{40}K atoms. Panel (a) shows the pairing function $\Delta(r)$, panel (b) the fermion density $\rho_f(r)$ and panel (c) the density of bosons $|\phi(r)|^2$. Solid black lines correspond to boson-fermion interaction strength $g_{bf} = 10$ and dotted-dashed blue lines to $g_{bf} = 0$. In panel (c) the dotted-dashed blue line is hardly visible because for $g_{bf} = 0$ bosons are delocalised and their density is very small. Number of bosons is $N_b = 100$, number of fermions is $N_f \approx 12000$ (chemical potential $\mu = E_F$) and the fermion-fermion coupling constant is $g_{ff} = -5.5$.

energetically favourable to separate bosons and fermions. The density $\rho_f(\mathbf{r})$ is depleted around the centre and bosons form a bound state localised in a small area around $\mathbf{r} = 0$. It is clear that the localisation effect is the result of boson-fermion interactions. It relies on a local deformation of the density of fermions and is not affected by the boundary conditions. However, note that the choice of boundary conditions and the origin makes the point $\mathbf{r} = 0$ special. In a real physical system, the impurity could be localised at any point in space, spontaneously breaking the translational symmetry of the system.

The response of the Fermi sub-system to bosons, which tend to localise, can be investigated by monitoring the deformation of the Bogoliubov quasiparticle modes. The density of fermions is a sum of the Bogoliubov modes $\rho_f(\mathbf{r}) = 2 \sum_{nlm} |v_{nlm}(\mathbf{r})|^2$. The factor of two comes from the two symmetric spectra of eigenvalues of the Bogoliubov de Gennes equations. The modes with zero angular

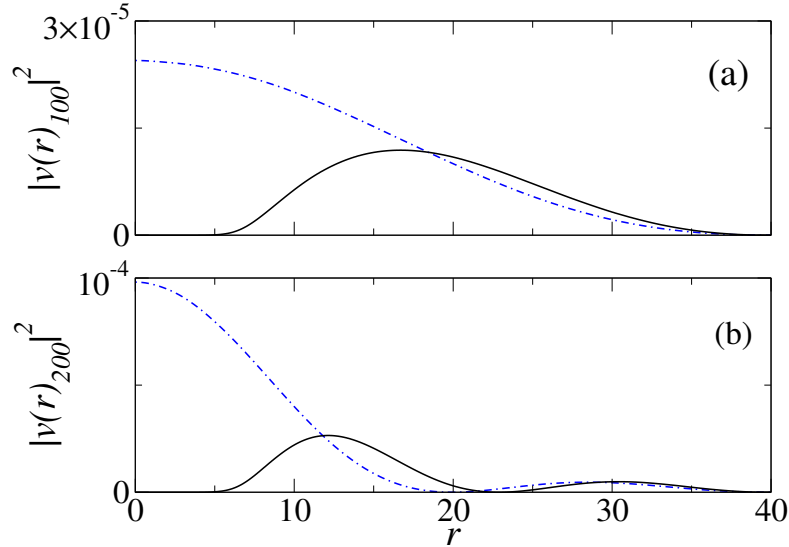


FIGURE 3.4: Probability densities $|v_{nlm}(r)|^2$ of two fermion pairs at the bottom of the Fermi sea with angular momentum $l = 0$. Panel (a) corresponds to the ground state ($n = 1$) of the radial degree of freedom and panel (b) to the first excited state ($n = 2$). Solid black lines correspond to boson-fermion interaction strength $g_{bf} = 10$ and dotted-dashed blue lines to $g_{bf} = 0$. All parameters are the same as in Fig. 3.3.

momentum contribute only to the density around $\mathbf{r} = 0$. Consequently, the modification of these modes is primarily responsible for preparation of the potential well in which the bosons localise. In Fig. 3.4 we illustrate the deformation of two modes with $l = 0$ corresponding to fermions at the bottom of the Fermi sea, but we should keep in mind that all modes with $l = 0$ are affected by the interactions with bosons. The deformation of modes for fermions at the Fermi level is reflected by a change in the shape of the pairing field, visible in Fig. 3.3, because those modes contribute mainly to $\Delta(\mathbf{r})$.

The data in Figs. 3.3 and 3.4 are for $N_b = 100$ ^{23}Na atoms and a mixture of $N_f \approx 12000$ ^{40}K atoms (chemical potential $\mu = E_F$) in two different hyperfine states. We set the scattering lengths $g_{ff} = -5.5$ and $g_{bf} = 10$, with the assumption that they can be realised using Feshbach resonances (e.g., magnetic resonance for fermions and optical resonance between bosons and fermions [20, 102]).

In Fig. 3.5 we show the average radius of the Bose cloud, $\langle r \rangle$, and its standard deviation, $\sigma = (\langle r^2 \rangle - \langle r \rangle^2)^{1/2}$, as a function of the coupling constant g_{bf} . The self-localisation means that both $\langle r \rangle$ and σ are much smaller than the radius of

the 3D volume. One can see that there is a critical non-zero value of g_{bf} leading to self-localisation. In the case of a small Bose sub-system considered here, this critical g_{bf} is distinctly different from the critical value for the instability of the homogeneous solution in the Sec. 3.2. The latter, for the case without boson-boson interactions, corresponds to $g_{bf} > 0$ [Eq. (3.6)].

The replacement of sodium atoms by the lighter ${}^7\text{Li}$ atoms causes an increase of the critical value g_{bf} for the emergence of self-localisation. This is a consequence of taking into account the bosonic pressure; compressing the cloud of the light lithium particles costs more energy than in the case of heavier sodium atoms.

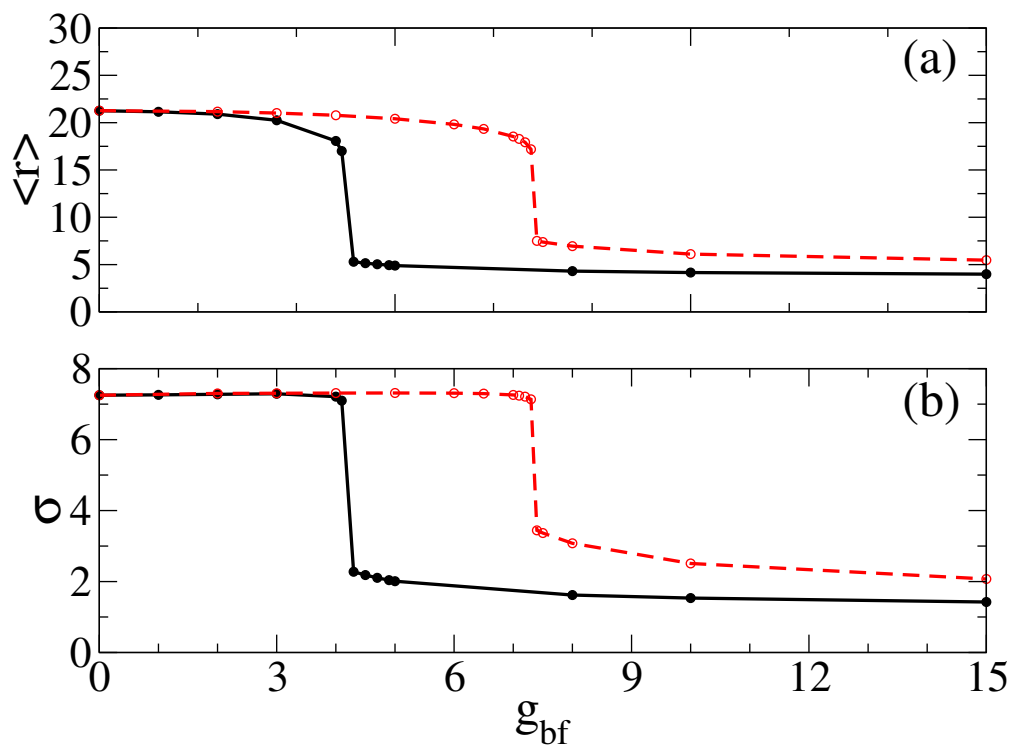


FIGURE 3.5: The average radius of the Bose cloud $\langle r \rangle$ [panel (a)] and the standard deviation $\sigma = (\langle r^2 \rangle - \langle r \rangle^2)^{1/2}$ [panel (b)] versus boson-fermion coupling constant g_{bf} . Black full symbols correspond to a mixture of ${}^{23}\text{Na}$ and ${}^{40}\text{K}$ atoms, while red open symbols correspond to a mixture of ${}^7\text{Li}$ and ${}^{40}\text{K}$ atoms. Note the abrupt transitions to localised states when critical values of g_{bf} are reached.

All the other parameters are the same as in Figs. 3.3-3.4.

3.4.1.2 Non-zero temperature

A small non-zero temperature mostly affects superfluidity and has little effect on the self-localisation phenomenon. At a temperature greater than zero, the

momentum distribution of fermions is smeared out; fermions above the Fermi level appear. The Hartree–Fock term and the pairing function defined in Eqs. (3.16) and (3.17) then change according to:

$$W = -|g_{ff}| \sum_{nlm} [f_{nl}|u_{nlm}(\mathbf{r})|^2 + (1 - f_{nl})|v_{nlm}(\mathbf{r})|^2], \quad (3.23)$$

$$\Delta = |g_{ff}| \sum_{nlm} (1 - 2f_{nl})u_{nlm}(\mathbf{r})v_{nlm}^*(\mathbf{r}), \quad (3.24)$$

with the Fermi-Dirac distribution

$$f_{nl} = \frac{1}{\exp(E_{nl}/k_{\text{B}}T) + 1}. \quad (3.25)$$

For Bosons, we solve the Gross–Pitaevskii equation (Eq. 3.18). Note that the temperatures we consider are still well below the critical temperature for condensation. Eqs. (3.23)–(3.24) and Eqs. (3.15)–(3.18) are solved in a self-consistent manner, according to the procedure described in Sec. 3.3, with just a small modification. To keep the number of fermions in the system constant, we have to additionally adjust the chemical potential. However, because the temperatures are still very low, we can estimate the value of μ . Let us look at the particle number for the ideal Fermi gas in the limit $T \rightarrow 0$ [103]:

$$N(T, V, z) = g \frac{2\pi V}{h^3} (2m_f)^{3/2} \int_0^\infty d\epsilon \frac{\epsilon^{3/2}}{z^{-1} \exp(\epsilon/k_{\text{B}}T) + 1}, \quad (3.26)$$

where ϵ is energy, g is the number of spin states ($g = 2s + 1$) and $z = \exp(\mu/k_{\text{B}}T)$ is the fugacity. The correction to Eq. (3.26) for small, but non-vanishing temperatures ($z \gg 1$) can be written as an expansion of the function $f_{3/2}$ ²:

$$\frac{N}{V} = \frac{4\pi g}{3} \left(\frac{2m_f}{h^2} \right)^{3/2} (k_{\text{B}}T \ln z)^{3/2} \left(1 + \frac{\pi^2}{8} (\ln z)^{-2} \right). \quad (3.27)$$

²The function f_n is defined as $f_n = \frac{1}{\Gamma(n)} \int_0^\infty \frac{x^{n-1} dx}{z^{-1} e^x + 1}$, where $0 \leq z \leq \infty$.

The equation for the chemical potential then reads:

$$\mu \approx E_F \left(1 - \frac{\pi^2 k_B T}{12 E_F} \right). \quad (3.28)$$

Instead of solving many times set of Eqs. (3.15) together with calculating Eqs. (3.23)-(3.24) to find the chemical potential for a given number of fermions, we use the approximate value of μ from Eq. (3.28).

In Fig. 3.6 we see that even for $T = 0.028 T_F$, when the pairing function is very small, the densities of bosons and fermions hardly change. Increasing the temperature to $T = T_F$ (which is still much smaller than the critical temperature for Bose–Einstein condensation of $N_b = 100$ atoms localised in a volume of radius $\langle r \rangle \approx 4$, $T_{BEC} \approx 6 T_F$) we observe effects of thermal fluctuations in the fermion density and a modification of the density of bosons, but the self-localisation persists. Thus, bosons self-localise in both the normal and the superfluid phase of the Fermi sub-system.

3.4.1.3 Self-localisation as a probe of superfluidity?

So far we have seen that self-localisation has little influence on the existence of the pairing function. Specifically, the interaction of fermions and the impurity Bose particles influences the pairing function Δ only locally, as seen in Fig. 3.3. This implies that the superfluidity is not destroyed even when the interaction is so strong that the strong confinement of the impurity object takes place. Qualitatively, let us say that self-localisation does not influence superfluidity.

We can also ask the reverse question - does superfluidity affect the self-localisation? This is in principle a separate question, especially if we consider a small number of bosonic impurities, which might not influence superfluidity of a large Fermi cloud, but can be influenced by it. So far, we have also seen that self-localisation persist at temperatures higher than the critical temperature for superfluidity (Fig. 3.6). This, again qualitatively, suggests that the answer to this questions is also “no”. However, we can investigate this question in a bit more detail. What we have seen

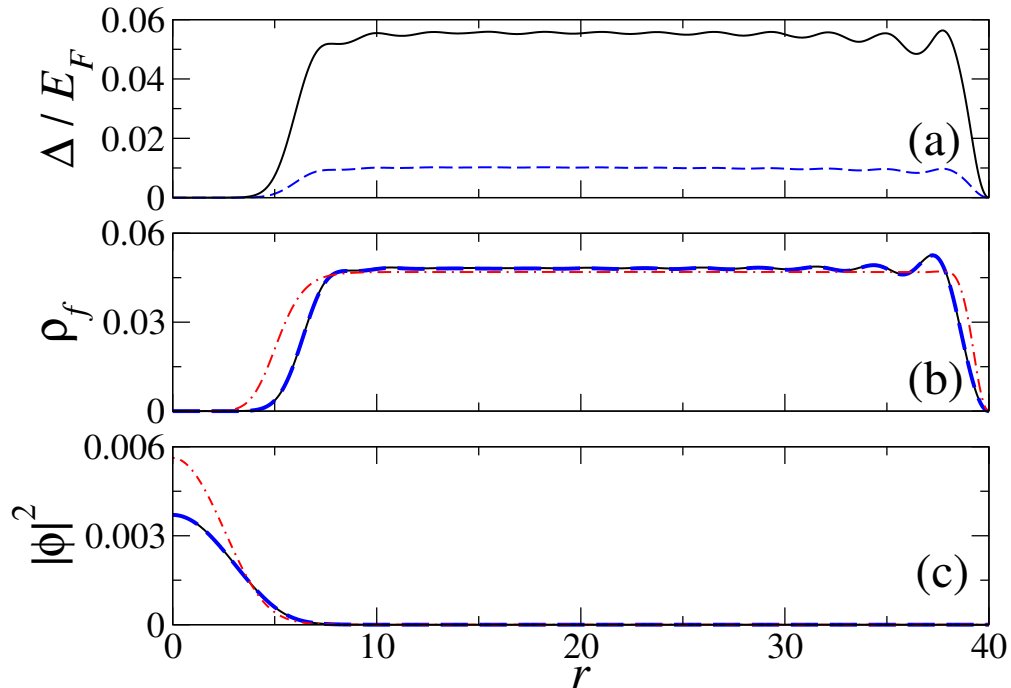


FIGURE 3.6: Self-localisation of ^{23}Na atoms in a mixture of ^{40}K atoms at non-zero temperature. Panel (a) shows the pairing function $\Delta(r)$, panel (b) the fermion density $\rho_f(r)$ and panel (c) the density of bosons $|\phi(r)|^2$. Solid black lines correspond to $T = 0$ and $\mu = E_F$, blue dashed lines to $T = 0.028 T_F$ and $\mu \approx E_F$, and red dotted-dashed lines to $T = T_F$ and $\mu = 0.16 E_F$. Boson-fermion interaction strength is $g_{bf} = 10$, fermion-fermion coupling constant is $g_{ff} = -5.5$, and the numbers of bosons and fermions are $N_b = 100$ and $N_f \approx 12000$. In panel (a) the dotted-dashed red line is not visible because at $T = T_F$ the pairing function is equal zero. In panels (c) and (d) the solid black and dashed blue lines are hardly distinguishable.

so far is that if g_{bf} is sufficiently large then self-localisation does not rely on the Fermi component of the system being superfluid. We can still question whether the *critical* value of g_{bf} depends on whether the Fermi component is superfluid.

If this is the case, then it is very interesting because it could potentially provide an experimental probe of fermionic superfluidity. This would be very exciting because such reliable, and experimentally feasible, probes are actually very rare. Let us briefly explain this point before coming back to our results and proposal (we also note that a related proposal was made in Ref. [98]).

Superfluidity is commonly associated with a range of different phenomena and has many theoretical definitions. Often these various definitions are introduced because specific experimental signatures are available in specific systems. For

example, superfluidity is associated with some form of condensation or transport without dissipation. However, neither of these phenomena is necessarily tied to superfluidity [20]. For example, an ideal Bose gas can display condensation without superfluidity.

Similarly, fermionic superfluidity is conceptually associated with pair formation, but pair formation in itself does not guarantee it. There are exotic states of highly imbalanced spin mixtures of fermions in which pairing occurs, but superfluidity does not, even at zero temperature. In this system, radio frequency spectroscopy, commonly used to detect pairing, cannot distinguish between normal and superfluid paired states [104].

In ultra-cold atoms the most convincing argument for superfluidity is the formation of ordered Abrikosov lattices of *quantised* vortices in rotating gasses [105–108]. Performing such experiments for ultra-cold fermions is however extremely challenging, as seen in the fact that the MIT group which originally performed them [108] is still the only one ever to use this probe. In comparison, detection (by imaging) of the self-localisation of bosonic impurities should be relatively easy. So, our goal here is to see whether in some situation bosons will become localised *only* if the Fermi gas around them is superfluid (or, conversely, only if it is not). We take the simplest model in which we work at zero temperature and compare the self-trapping of bosons in a non-interacting mixture of fermions and an attractively interacting one. In this simple scenario, since we are at $T = 0$, we know *a priori* that the non-interacting Fermi gas is normal and the interacting one is superfluid. In Fig. 3.7 we see that the critical value of the boson-fermion coupling is shifted by 20% between these two cases, with smaller value of coupling g_{bf} being sufficient to induce the localisation of bosons in a superfluid system.

This observation is for now only qualitative, because of the simplicity of the model, but still it is very encouraging. It implies that, when changing the interaction g_{ff} , the easily-detectable appearance of self-localisation could serve as a signature of fermionic superfluidity. Of course, we need to stress again that in our simple $T = 0$ model we already know that any non-zero g_{ff} will lead to superfluidity

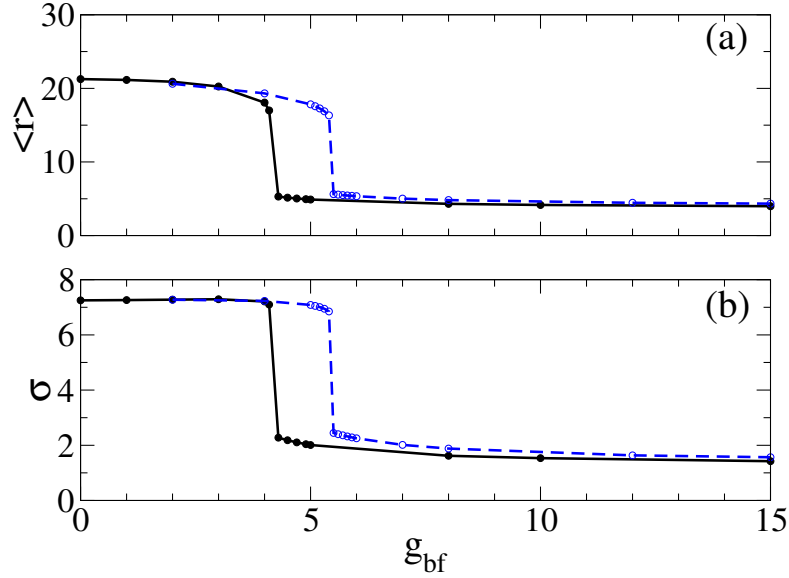


FIGURE 3.7: The average radius of the Bose cloud $\langle r \rangle$ [panel (a)] and the standard deviation $\sigma = (\langle r^2 \rangle - \langle r \rangle^2)^{1/2}$ [panel (b)] versus boson-fermion coupling constant g_{bf} . Black full symbols correspond to a mixture of ^{23}Na and superfluid ^{40}K atoms ($g_{ff} = -5.5$), while blue open symbols correspond to a mixture of ^{23}Na and normal ^{40}K atoms ($g_{ff} = 0$). The value of the critical g_{bf} at which the self-localisation occurs differs by 20%. All the other parameters are the same as in Figs. 3.3-3.4.

for a homogeneous system. The bigger hope, which would need more work to be confirmed, is that this qualitative picture carries over to non-zero temperature, where the critical g_{ff} for superfluidity depends on T , or conversely the critical temperature depends on g_{ff} . Then, tuning g_{ff} at constant T (or vice versa), in the presence of bosonic impurities, could be a way to detect when exactly superfluidity emerges, and thus map out the critical values of coupling/temperature.

3.4.1.4 The effects of the inclusion of boson-boson interactions

In our model we so far neglected the boson-boson interactions, assuming that their number and/or their local density remains sufficiently small. In order to scrutinise this assumption, we can include the interaction into Eq. (3.18); this leads to the usual Gross-Pitaevskii equation [Eq. (1.17)]:

$$\left[-\frac{\hbar^2}{2m_b} \nabla^2 + V(\mathbf{r}) + g_{bb} N_b |\phi(\mathbf{r})|^2 \right] \phi(\mathbf{r}) = \mu_b \phi(\mathbf{r}), \quad (3.29)$$

where $V(\mathbf{r})$ is given in Eq. (3.19), g_{bb} is the boson-boson coupling and ϕ is normalised to 1. With the units adopted in this thesis [Eq. (3.20)] the coupling parameter g_{bb} is expressed by:

$$g_{bb} = 4\pi k_F a_{bb} \frac{m_f}{m_b}. \quad (3.30)$$

The ground state of Eq. (3.29) is found using the method of imaginary time evolution (See A.1). For a system consisting of a Fermi spin-mixture and interacting bosons we need to solve numerically the coupled equations (3.15) and (3.29) in a self-consistent manner.

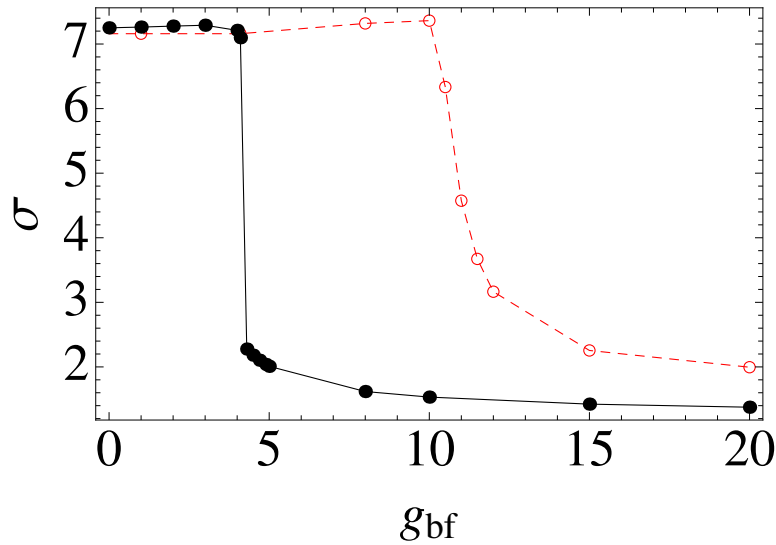


FIGURE 3.8: The standard deviation σ of the Bose cloud versus boson-fermion coupling constant g_{bf} , for non-zero boson-boson interactions (red open symbols). Calculations are done for a mixture of ^{23}Na atoms and superfluid ^{40}K atoms ($g_{ff} = -5.5$). There are two bosons in the system. Black full symbols correspond to the case of no boson repulsion ($g_{bb} = 0$) and red open symbols to $g_{bb} = 27$. The critical value of g_{bf} is shifted for repulsively interacting bosons and the self-localisation does not appear as abruptly. All the other parameters are the same as in Figs. 3.3-3.4.

Qualitatively, we expect that the critical value of g_{bf} for the self-localisation to occur is greater for $g_{bb} > 0$ than for $g_{bb} = 0$. There is an additional energy needed to overcome the mutual repulsion between the bosons in order for the self-localisation to appear. Indeed, this is what we observe.

In Fig. 3.8 we present the standard deviation of the boson density distribution as a function of g_{bf} . There are two noticeable effects. First, the critical value of g_{bf} for

which the self-localisation occurs is shifted for bosons with non-zero g_{bb} . Second, the reduction of the standard deviation signalling the trapping of the impurity is less sharp. Note, however, that here we used a very large $g_{bb} = 27$. For a small number of bosons the value of the repulsive Bose-Bose coupling constant has to be much larger than any other interaction parameter in the system in order to make a visible difference.

We thus conclude that in the system with a small number of bosons immersed in the Fermi mixture, the model without the boson-boson interaction should qualitatively and quantitatively describe the effect of self-localisation.

Finally, let us notice that we only discussed a process of going from a homogeneous system to self-localisation near $\mathbf{r} = 0$. For a system with boson-boson repulsion and many bosons, we could also consider another scenario, with the bosons distributed between many different self-localisation points in space. This could be an energetically beneficial arrangement, as it would minimise the energy of the Bose-Bose repulsion.

3.4.2 Attractive boson-fermion interaction

In a system consisting of a trapped Bose-Einstein condensate coexisting with a normal degenerate Fermi gas, attractive interactions can lead to a collapse [109]. Indeed, if the attraction is sufficiently strong, and density high enough, the breakdown of the mean-field was predicted for example in [95, 110]. We observe a similar effect in a homogeneous mixture of superfluid fermions and a small number of bosons.

Up to this point, we considered the repulsive boson-fermion interaction. For the attractive interaction, we do not observe self-localisation regardless of the phase of the Fermi sub-system. For $g_{bf} < 0$ the particle densities can collapse to a Dirac- δ distribution. Indeed, the growing of the interactions causes a mutual accumulation of the density of fermions and bosons around $r = 0$, to the point when the attraction counteracts the Fermi pressure. For sufficiently small $|g_{bf}|$, a

metastable state may appear. However, it turns out that the existence of such a metastable state is not the result of self-localisation in the system. Indeed, it is an effect of a compromise between the requirement of minimal kinetic energies and restrictions related to the boundary conditions.

It is also interesting to ask if a repulsive interaction between the bosons can prevent the breakdown of the mean-field picture for an attractively interacting mixture of fermions and bosons. We indeed find such a g_{bb} and g_{bf} (greater than for a system without boson-boson interaction) for which system is not homogeneous, but the standard deviation for this solution is sensitive to any change of the system size. The bosonic density goes towards a uniform distribution for increasing volume and towards a Dirac- δ distribution for reducing volume. We conclude that this is just a metastable state. The repulsive interaction between bosons can prevent the breakdown of mean-field for some values of g_{bf} , but we do not observe the self-localisation.

3.5 Results in one dimension

In one-dimensional systems physics is dramatically different from the “normal” physics of interacting particles in 3D. The dynamics in 1D is integrable and thus the system cannot reach thermal equilibrium. From a theoretical point of view there have been many interesting developments in this field, for example the theory of Luttinger liquids [111] or the important progress in the exact solutions such as those relying on the Bethe ansatz [112]. One-dimensional systems were historically mostly a theorists’ toy. However, in ultra-cold atomic systems they are now experimentally accessible. In Sec. 2.2.1.3 we showed that use of a deep optical lattice enables experimentalists to reduce dimensionality of a system from 3D to 2D. Adding another set of lattice beams can lower the dimensionality to 1D. Indeed, if in x and y directions we apply harmonic potentials characterised by trapping frequency ω_{\perp} , and $\hbar\omega_{\perp}$ is much greater than other energy scales in the problem (chemical potential, temperature), the transverse degrees of freedom are

frozen out (i.e. the system is confined to the ground state along these directions) and the system becomes effectively one-dimensional. A simple illustration of the effects of such reduced dimensionality was the observation of a “quantum Newton’s cradle” [113]. The behaviour of the well-known classical toy was mimicked by a trapped 1D Bose gas, and it was observed that despite numerous collisions performed by hundreds of atoms the system does not approach an equilibrium. Other, more intricate 1D many-body effects that have been observed include the realisation of a Tonks-Girardeau gas [114, 115], in which, due to strong repulsion, bosons in many ways behave like fermions.

For repulsive boson-fermion interactions, we observe self-localisation of bosons with the behaviour of the particle densities similar to that in the 3D case. Therefore, here we focus on the case of attractive interactions, where the collapse does not occur and we encounter qualitatively new phenomena, in particular appearance of *vector* soliton.

Assuming that Bose and Fermi particles are in the ground states of the two-dimensional potential in the transverse direction and performing integration over x and y in the Hamiltonian of Eq. (3.11), we obtain the 1D version of Eqs. (3.15)-(3.19):

$$\begin{aligned} \left(-\frac{1}{2m_f}\partial_x^2 - \mu + W(x) + g_{bf}\phi(x)^2\right) u_n(x) + \Delta(x)v_n(x) &= E_n u_n(x) \\ \Delta(x)u_n(x) - \left(-\frac{1}{2}\partial_x^2 - \mu + W(x) + g_{bf}\phi(x)^2\right) v_n(x) &= E_n v_n(x) \end{aligned} \quad (3.31)$$

$$\left(-\frac{1}{2}\partial_x^2 + g_{bf}\rho_f(x)\right) \phi(x) = E\phi(x) \quad (3.32)$$

with the following coupling constants

$$\begin{aligned} g_{ff} = g_{ff}^{1D} &= \frac{g_{ff}}{2\pi\sigma_f^2} = 2\hbar\omega_\perp a_{ff}, \\ g_{bf} = g_{bf}^{1D} &= \frac{g_{bf}}{\pi(\sigma_f^2 + \sigma_b^2)} = 2\hbar\omega_\perp a_{bf}, \end{aligned} \quad (3.33)$$

where $\sigma_b = \sqrt{\hbar/m_b\omega_\perp}$ and $\sigma_f = \sqrt{\hbar/m_f\omega_\perp}$ are the length scales for the ground-state transverse spatial extension for the Fermi and Bose particles. In our units [Eq. (3.20)], the 1D coupling constants are

$$\begin{aligned} g_{ff}^{1D} &= \frac{g_{ff}^{3D}}{2\pi\sigma_f^2} = \frac{2m_f\omega_\perp}{\hbar k_F} a_{ff}, \\ g_{bf}^{1D} &= \frac{g_{bf}^{3D}}{2\pi(\sigma_f^2 + \sigma_b^2)} = \frac{2m_f\omega_\perp}{\hbar k_F} a_{bf}. \end{aligned} \quad (3.34)$$

In the 1D case, there is no ultraviolet divergence and the pairing function does not require regularisation. Nevertheless, numerical simulations converge much faster if the Bogoliubov modes above a numerical cutoff energy E_C are included in the spirit of the local density approximation. That is, the coupling constant in Δ is substituted by (see [116], App. B.1)

$$\frac{1}{|g_{\text{eff}}^{1D}|} = \frac{1}{|g_{ff}^{1D}|} - \frac{1}{2\pi} \ln \frac{\sqrt{E_C} + \sqrt{\mu}}{\sqrt{E_C} - \sqrt{\mu}}. \quad (3.35)$$

3.5.1 Attractive boson-fermion interactions

Figure 3.9 shows the results for $g_{bf} = -20$, obtained with periodic boundary conditions for fermions and open boundary conditions for bosons. For the attractive interactions, bosons and fermions try to stick together, which leads to an increase of the fermion density in the vicinity of the boson concentration and the creation of a potential well for the localisation of the Bose particles.

Analysing the Bogoliubov modes $v_k(z)$ (see Fig. 3.10) we find that the probability density $v_0^2(z)$ of a pair of fermions at the bottom of the Fermi sea becomes strongly localised. The Bogoliubov mode $v_1(z)$ of the next fermion pair forms also a bound state. Since $v_1(z)$ is an antisymmetric function it is nearly zero in the area around $z = 0$. Probability densities of other fermions are deformed and almost all of them drop to zero in the region where $v_0(z)$ is localised. This can be interpreted as a real-space manifestation of the Pauli exclusion principle.

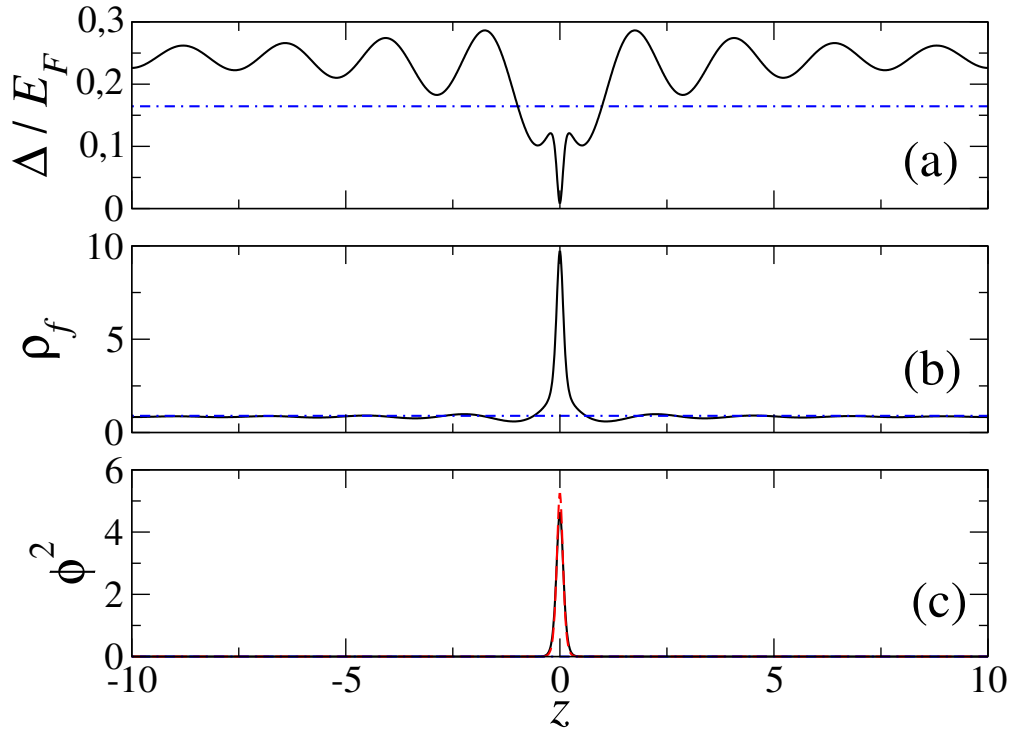


FIGURE 3.9: Self-localisation of a single boson ($N_b = 1$) in a superfluid mixture of fermions in 1D space. Panel (a) shows the pairing function $\Delta(z)$, panel (b) the fermion density $\rho_f(z)$ and panel (c) the boson density $|\phi(z)|^2$. Solid black lines correspond to boson-fermion interaction strength $g_{bf} = -20$ and dotted-dashed blue lines to $g_{bf} = 0$. Number of fermions is $N_f \approx 20$ (chemical potential $\mu = E_F$) and fermion-fermion coupling constant is $g_{ff} = -1$. Ratio of the masses of Bose and Fermi particles, m_b/m_f , fulfils Eq. (3.38). The configuration space extends from $z = -10$ to $z = 10$. In panel (c) the dotted-dashed blue line is hardly visible, because the boson is delocalised and its density is very small for $g_{bf} = 0$. Red dashed line in panel (c) indicates the solitonic solution of Eq. (3.39).

In the BCS limit only particles close to the Fermi level contribute to the pairing function Δ , and there is practically no contribution from the fermions located deeply in the Fermi sea. That is why $\Delta(z)$, contrary to the fermion density, reveals a minimum at $z = 0$, as seen in Fig. 3.9.

3.5.1.1 Simple model

The analysis of the Bogoliubov modes suggests a simple model of self-localisation in the case of attractive boson-fermion interactions. It belongs to a class of general solutions of nonlinear wave equations - solitons. Solitons are stable localised solutions that interact by a phase shift with each other [117] and move without

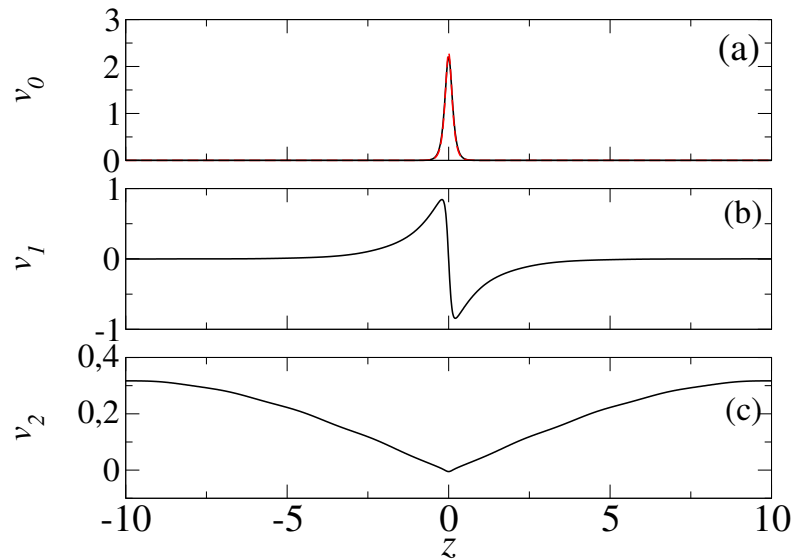


FIGURE 3.10: Bogoliubov modes $v_k(z)$ corresponding to fermion pairs located close to the bottom of the Fermi sea. Panel (a) is related to the pair of fermions at the bottom of the Fermi sea, panel (b) and (c) to the next pairs. Solid black lines correspond to the numerical solutions. Red dashed line in panel (a) indicates solitonic solution of Eq. (3.39). All the others parameters are the same as in Fig. 3.9.

spreading. This makes them intriguing macroscopic particle-like objects, suitable for probing the system they move in. Their non-spreading feature is based on the existence of non-linear interaction which compensates the spreading due to dispersion. The Gross–Pitaevskii equation describing the evolution of the condensate wave function exhibits both *dark* and *bright* soliton solutions. Dark solitons are an excitation in a stable BEC and represent a local decrease in the density of particles. They have, for example, been predicted and recently observed in a strongly interacting superfluid of fermionic atoms [116, 118]. Bright solitons are 1D self-trapped wave-packets formed in ultra-cold bosons with an attractive interaction. They have been studied theoretically in Bose and Fermi degenerate gases, in the regime where the number of bosons dominates over the number of fermions [119]. For an impurity atom in a large BEC considered in Ref. [52], the 1D system is described by a parametric soliton with the state of the impurity atom given by the hyperbolic secant squared function. These type of solitons belong to a separate class, in which one of the matter fields propagates inside a nonlinear medium of the other, and each of them propagates as a soliton [120].

Let us then discuss the soliton-like solutions in the case of the attractive boson-fermion interactions in the regime of a small number of BEC particles. We suppose that in the vicinity of the localised bosons we may neglect the pairing field and the density of all fermions except that of a fermion pair at the bottom of the Fermi sea.

We then obtain the following set of equations:

$$(\mu - E_0)v_0 = \left[-\frac{1}{2}\partial_z^2 - |g_{ff}|v_0^2 - |g_{bf}|N_b\phi^2 \right] v_0, \quad (3.36)$$

$$\mu_b\phi = \left[-\frac{m_f}{2m_b}\partial_z^2 - 2|g_{bf}|v_0^2 \right] \phi. \quad (3.37)$$

For

$$\frac{m_b}{m_f} = \frac{N_b}{2} + \frac{|g_{ff}|}{2|g_{bf}|}, \quad (3.38)$$

there exists an analytical solution of Eqs. (3.36) - (3.37):

$$\phi(z) = v_0(z) = \sqrt{\frac{\alpha}{2}} \operatorname{sech}(\alpha z), \quad (3.39)$$

with

$$\begin{aligned} \alpha &= |g_{bf}| \frac{m_b}{m_f}, \\ E_0 &= \mu + \frac{g_{bf}^2 m_b^2}{2m_f^2}, \\ \mu_b &= -\frac{g_{bf}^2 m_b}{2m_f}. \end{aligned} \quad (3.40)$$

Such a solution resembles vector solitons. They appear in non-linear optics when interactions of several field components are described by a set of coupled non-linear Schrödinger equations [120].

Comparison of the analytical solution of Eq. (3.39) with numerical results of the full set of equations is shown in Figs. 3.9-3.10. The agreement is very good and increases with the strength of boson-fermion interactions. Indeed, for strong interactions, due to the Pauli exclusion, there is negligible probability density to

find any fermions other than the localised bottom-of-the-sea pair in the vicinity of $z = 0$. As a consequence, the localised bosons interact almost exclusively with the localised fermion pair and the set of Eqs. (3.36)-(3.37) becomes exact.

Figure 3.10(b) shows that the Bogoliubov mode $v_1(z)$ forms an antisymmetric bound state. Indeed, in the vicinity of $z = 0$ (where the fermion density is dominated by v_0^2 and the pairing function drops to zero) this mode should fulfil an equation similar to Eq. (3.36), that is

$$(\mu - E_1)v_1 = \left[-\frac{1}{2}\partial_z^2 - |g_{ff}|v_0^2 - |g_{bf}|N_b\phi^2 \right] v_1. \quad (3.41)$$

If ϕ and v_0 are given by Eq. (3.39) the antisymmetric solution of Eq. (3.41) forms a marginally (zero-energy) bound state, given by the solution:

$$v_1(z) \sim \tanh(\alpha z), \quad (3.42)$$

$$E_1 = \mu. \quad (3.43)$$

In the full description of the system, the state governed by Eqs. (3.31)-(3.32) may become either truly bound or unbound, due to the existence of all the other modes. In the considered system, it turns out that the state is pushed towards a true bound state as visible in Fig. 3.10(b).

When the boson-fermion coupling constant $|g_{bf}|$ is decreased, we observe an increasing discrepancy between the analytical and numerical solutions (of approximate and exact equations, respectively), as shown in Fig. 3.11. The width of the boson probability density distribution obtained numerically is significantly greater than the corresponding analytical value. This is due to the fact that in the effective potential experienced by the bosons a considerable contribution comes from other fermions, and not only from the pair at the bottom of the Fermi sea. The density of such fermions, contrary to the localised fermion pair, possesses a minimum at $z = 0$ and thus effectively makes the potential well for bosons weaker. Consequently, bosons occupy a much larger space than can be expected on the basis of the solution in Eq. (3.39).

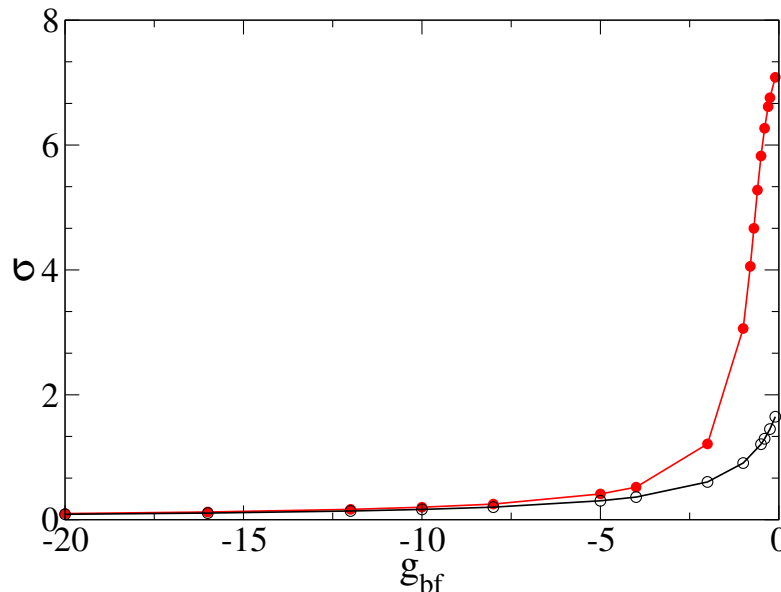


FIGURE 3.11: Width of the boson density distribution, $\sigma = (\langle z^2 \rangle - \langle z \rangle^2)^{1/2}$, versus boson-fermion coupling constant g_{bf} . Red full symbols correspond to the numerical values and black open symbols to the solutions Eq. (3.39). The configuration space extends from $z = -20$ to $z = 20$. All the other parameters are the same as in Fig. 3.9.

3.5.1.2 Simple model with inclusion of boson-boson interactions

In the previous section we argued that the discrepancy between the analytical solution of Eq. (3.39) and the numerical solution of the Eqs. (3.31)-(3.32) is caused by the interaction of bosonic particles with more than one pair of fermions near the bottom of the Fermi sea. The stronger is the attraction between the fermions and the bosons, the greater is the reduction of the spatial extent of the densities of both bosons and the lowest-energy Fermi pair. Hence the elimination of the other fermions from the space where the self-localisation occurs (due to the Pauli exclusion principle) is more complete and the agreement with the simple model is better.

If we also include attractive interactions between the bosons, we expect the self-localisation to be stronger, and hence also the agreement with the simple analytical model, based on considering just the lowest-energy Fermi pair, to be better. Now

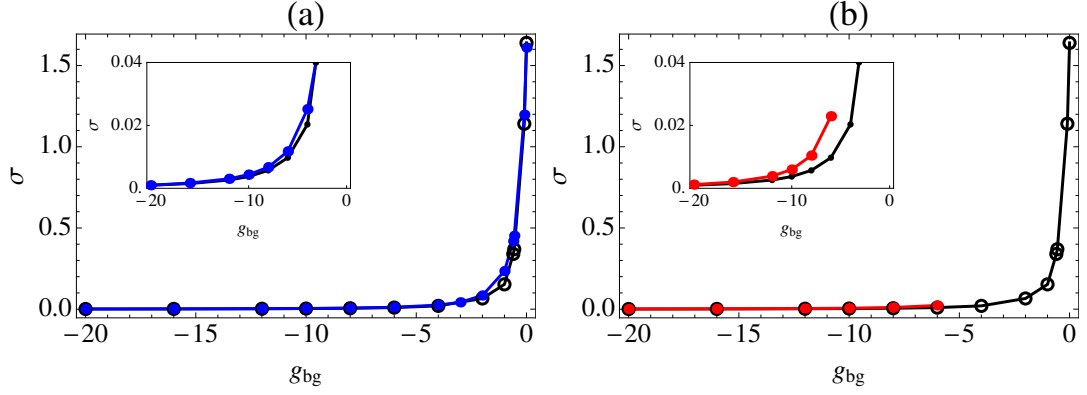


FIGURE 3.12: Width of the boson density, i.e. $\sigma = (\langle z^2 \rangle - \langle z \rangle^2)^{1/2}$, versus boson-fermion coupling constant g_{bf} , for different boson-boson interactions. In panel (a) blue solid symbols correspond to the numerical values and black open symbols to the solutions of Eq. (3.48), both for an attractive boson-boson interaction $g_{bb} = -3.5$. Panel (b) shows the behaviour of a system with repulsion between the bosons, $g_{bb} = 3.5$. Red solid symbols show numerical results and black open symbols analytical solutions of Eq. (3.48). In the case of repulsive boson-boson interactions we see stronger discrepancy between analytical and numerical calculations. Ratio of the masses of Bose and Fermi particles, m_b/m_f , fulfils Eq. (3.47). The configuration space extends from $z = -10$ to $z = 10$. Number of fermions is $N_f \approx 20$ (chemical potential $\mu = E_F$), number of bosons is $N_b = 2$ and the fermion-fermion coupling constant is $g_{ff} = -1$.

our simple model reads:

$$(\mu - E_0)v_0 = \left[-\frac{1}{2}\partial_z^2 - |g_{ff}|v_0^2 - |g_{bf}|N_b\phi^2 \right] v_0, \quad (3.44)$$

$$\mu_b\phi = \left[-\frac{m_f}{2m_b}\partial_z^2 - 2|g_{bf}|v_0^2 + g_{bb}N_b\phi^2 \right] \phi, \quad (3.45)$$

with the boson-boson interaction in the units used in the thesis:

$$g_{bb} = g_{bb}^{1D} = \frac{g_{bb}^{3D}}{2\pi\sigma_b^2} = \frac{2m_f\omega_\perp}{\hbar k_F} a_{bb}. \quad (3.46)$$

This model also has a solitonic solution. Indeed, we discover that for

$$\frac{m_b}{m_f} = \frac{|g_{bf}|N_b + |g_{ff}|}{2|g_{bf}| - g_{bb}N_b} \quad (3.47)$$

we can find an analytical solution of Eqs. (3.44)-(3.45):

$$\phi(z) = v_0(z) = \sqrt{\frac{\alpha}{2}} \operatorname{sech}(\alpha z), \quad (3.48)$$

with

$$\alpha = \frac{(2|g_{bf}| - g_{bb}N_b) m_b}{2 m_f} = \frac{|g_{bf}|N_b + |g_{ff}|}{2},$$

$$E_0 = \mu + \frac{g_{bf}^2 m_b^2}{2m_f^2}, \quad \mu_b = -\frac{g_{bf}^2 m_b}{2m_f}. \quad (3.49)$$

In Fig 3.12 we see that the numerical solutions of Eqs. (3.31)-(3.32), with g_{bb} included analogously to Eq. (3.29), indeed agrees better with the analytical result in Eq. (3.48) for the attraction $g_{bf} < 0$ than for the repulsion $g_{bf} > 0$.

Finally, let us notice that in the case of the repulsive boson-boson interaction, the soliton solution in Eq. (3.48) exists only when $g_{bb}N_b < 2|g_{bf}|$. Mathematically, this can be most easily seen from the requirement that $m_b/m_f > 0$ in Eq. (3.47). Physically, this condition is necessary for the effective nonlinear term for bosons in Eq. (3.45) to be attractive.

In conclusion, in the case of attraction between the bosonic particles we can also find a simple model with the vector solitons for one-dimensional mixture of bosons and fermions.

3.6 Final remarks

To realise experimentally the self-localisation of bosons in a Fermi system, ultra-cold clouds of bosons and fermions have to be prepared in a laboratory. For a sufficiently large boson-fermion coupling constant, that can be achieved by means of a Feshbach resonance, the self-localisation takes place. Signatures of the self-localisation can be visible in the expansion of the atomic clouds after trapping potentials are turned off. That is, if during the time of flight the boson-fermion interactions are kept negligibly weak, the initially strongly localised boson cloud will show much faster expansion than the Fermi cloud due to the release of a large kinetic energy. The simplest experiment would employ a Fermi sub-system in a normal phase. In order to observe the self-localisation in a superfluid Fermi

mixture a manipulation of the fermion-fermion coupling constant is also needed and two Feshbach resonances must be employed, e.g. one resonance controlled by magnetic field and the other by optical means.

We have considered a small number of bosons immersed in a superfluid mixture of fermions in two different spin states. With negligible boson-boson interactions, homogeneous densities of the particles become unstable as soon as the boson-fermion coupling constant is non-zero, this effect corresponding to "simple" phase separation. We showed that in 3D space, for sufficiently strong repulsive boson-fermion interactions, a dramatic form of phase separation (i.e. the self-localisation of Bose particles) takes place. That is, the repulsion between particles creates a local potential well for bosons where, if the well is sufficiently large, they can localise. The difference between critical values of the boson-fermion interaction strength for the instability of a homogeneous solution and for the self-localisation is very clear if the boson-boson interactions are negligible.

The self-localisation is present both for the superfluid and the normal state of fermions. It modifies properties of the Fermi sub-system locally without destroying the superfluidity. Low non-zero temperature affects the pairing function but does not destroy the self-localisation phenomenon. However, the presence of the superfluidity shifts the critical g_{bf} for self-localisation, and this could be used as a tool for detecting fermionic superfluidity.

We do not observe self-localisation for attractive boson-fermion interactions in the 3D case. In this context the self-localisation requires sufficiently strong boson-fermion interactions. However, for strong attractive interactions no metastable state of the system has been found and the densities of the atoms collapse to Dirac-delta distributions, indicating a breakdown of the description with the contact interaction potentials.

In the 1D case there is no collapse for attractive boson-fermion interactions. The self-localisation of bosons is accompanied by localisation of a pair of fermions at the bottom of the Fermi sea. This phenomenon can be described by a simple model where the self-localisation is related to the existence of a vector soliton solution.

Appendix A

Appendix for Chapter 2

A.1 The steepest-descent method

The method of steepest descent has been widely use to obtain the ground state of the Gross-Pitaevskii equation. It is simply done by the replacement of the real time variable t in the time-dependent Gross-Pitaevskii equation with the imaginary value $-it$. To gain the intuition how this method works, let us consider a linear problem:

$$i\hbar \frac{d\Psi}{dt} = \left[-\frac{\hbar^2}{2m_b} \nabla^2 + V(\mathbf{r}) \right] \Psi(\mathbf{r}) = H\Psi(\mathbf{r}), \quad (\text{A.1})$$

where we substitute time variable $t \rightarrow -it$. The wave function can be express as a superposition of eigenstates ϕ_n of the equation $H\phi_n = E_n\phi_n$ with eigenvalues E_n :

$$\Psi(t) = \sum_n c_n \exp \frac{-iE_n t}{\hbar} \phi_n, \quad (\text{A.2})$$

the c_n coefficient are defined by the expansion of the initial condition $\Psi(t = 0) = \sum_n c_n \phi_n$. The imaginary time evolution of the Eq. A.1 and Eq. A.2 leads to an exponential decay of the wave function, and a corresponding decay of the eigenstates. The evolution is non unitary. The algorithm requires to renormalise

the resulting wave function after each step using the normalisation condition:

$$1 = \int d^3r |\Psi(\mathbf{r})|^2. \quad (\text{A.3})$$

Crucially, the eigenenergy governs the decay rate, and so the eigenstate with the lowest energy, i.e. the ground state of the system, decays slowest. For the Gross-Pitaevskii the expansion Eq. A.2 cannot be used. However, from some trial wave function (which should ideally be a rough guess of the final solution), and by suitable renormalisation of the wave-function (by fixing the norm) during the imaginary time propagation, the wave function will tend towards the ground state of the system of weakly interacting Bose gas [121]. In our calculation the condition for reaching the stationary state is given not just by the relative difference in the chemical potential between two consecutive steps, but by the speed in the difference $(|\mu_b(k+1) - \mu_b(k)|/\mu_b(k))/(dt) < 10^{-16}$, where dt is the time step in the imaginary time evolution, k is a number of steps.

A.2 Calculation for the Sec. 2.5.2

The solution in the section 2.5.2 are obtained using the following procedure:

1. We begin with some initial functions $\Delta_o(\mathbf{r}_i)$ and $\phi_o(\mathbf{r}_i)$. For the $\phi_o(\mathbf{r}_i)$ the equations 2.51 and 2.52 are solved by finding the eigenfunctions $u_n(\mathbf{r}_i), v_n(\mathbf{r}_i)$, from which we construct the new $\Delta(\mathbf{r}_i)$. This step is repeated until the relative change of the pairing function $(|\bar{\Delta}_o - \bar{\Delta}|/\bar{\Delta}_o)$ between each diagonalisation is less than 10^{-3} (the same condition is obtained for the density for fermions).
2. The new $\Delta(\mathbf{r}_i)$ we insert into Eq. (2.53). The algorithm for the steepest-descent method A.1 is used to find the ground state for the dimers wave function $\phi(\mathbf{r}_i)$. The Eq. (2.53) is inhomogeneous, but it turns out that if it

is written in the form:

$$\mu_b \phi(\mathbf{r}_i) = - \sum_{\langle i,j \rangle} J_{i,j,b} \phi(\mathbf{r}_j) + \left(U_b n_b |\phi(\mathbf{r}_i)|^2 - \frac{\gamma}{\sqrt{n_b} U} \frac{\Delta(\mathbf{r}_i)}{\phi(\mathbf{r}_i)} \right) \phi(\mathbf{r}_i) \quad (\text{A.4})$$

the same procedure, as used for a standard GP equation, allows as to find the desired solution also for this case. The decaying to the ground state is ceased when a speed of the relative changes of the chemical potential $|\mu_b(k+1) - \mu_b(k)|/\mu_b(k)/dt$ is less then 10^{-16} , where dt is the time step in the imaginary time evolution, k is a number of steps.

3. The new functions $\Delta(\mathbf{r}_i)$ and $\phi(\mathbf{r}_i)$ takes the roles of $\Delta_o(\mathbf{r}_i)$ and $\phi_o(\mathbf{r}_i)$ for the procedures in the points (1.) and (2.). The procedure is repeated until their values reach the saturation. The saturation is expected when the relative difference after the steps (1.) and (2.) of $\Delta(\mathbf{r}_i)$ and $\phi(\mathbf{r}_i)$ being less than 10^{-3} .

Appendix B

Appendix for Chapter 3

B.1 Paring function in one dimension

In the numerical calculations, the sum in the expression for $\Delta(\mathbf{x})$ is truncated, with some energy cutoff Λ . In $1D$ system the large cut-off is enough for the paring function to converge. However, in order to accelerate the calculations we use a procedure presented in [116]. It gives an analytical expression for the term above the cut-off. For a large number of particles, the system can be treated locally as uniform (LDA). The small correction that contains the modes above Λ is added as follow:

$$\Delta(x) \approx g \sum_{n=1}^{\Lambda} u_n v_n^* + g \int_{|k| > k_{\Lambda}(x)} \frac{dk}{2\pi} \frac{\Delta(x)}{2E(k, x)} \quad (\text{B.1})$$

The term $E(k, x) = \sqrt{\epsilon(k, x)^2 + \Delta(x)^2}$ is a local quasiparticle energy with $\epsilon(k, x) = \hbar^2 k^2 / (2m) + W(x) - \mu$. The local energy cut off corresponds to the momentum $k_{\Lambda} = \sqrt{2E_{\Lambda} + 2\mu - 2W(x)}$. It is defined for just positive values, for the negative it is equal 0.

When k_Λ is dominant over the Fermi momentum $k_f = \sqrt{2\mu - 2W(x)}$ a term under the integral in the equation (B.1) can be expand in powers of Δ . We will take into account just two leading terms, which after an integration have a form:

$$\Delta(x) = g \sum_{n=1}^{\Lambda} u_n(x)v_n^*(x) + g \frac{\Delta(x)}{2\pi k_f(x)} \ln \left(\frac{k_\Lambda(x) + k_f(x)}{k_\Lambda(x) - k_f(x)} \right), \quad (\text{B.2})$$

It effectively leads to

$$\Delta(x) = g_{ef}(x) \sum_{n=1}^{\Lambda} u_n(x)v_n^*(x), \quad (\text{B.3})$$

where the local value of the interaction constant $g_{ef}(x)$ is given as follow

$$g_{ef}(x) = \frac{g}{1 - \frac{g}{2\pi k_f(x)} \ln \left(\frac{k_\Lambda(x) + k_f(x)}{k_\Lambda(x) - k_f(x)} \right)}. \quad (\text{B.4})$$

Fig.B.1 depicts the $\Delta(x)$ from the equation B.3 for different cut offs Λ .

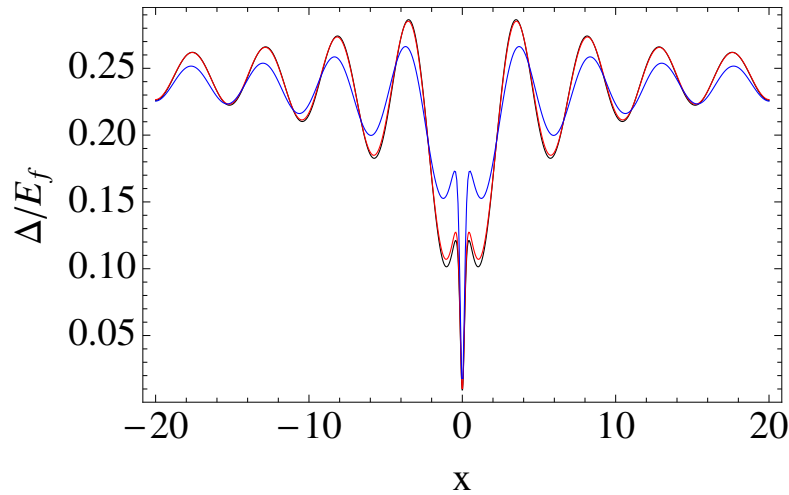


FIGURE B.1: The one dimensional regularised paring function $\Delta(x)$ for different cutoffs for the Bose-Fermi mixture with the same parameters as in the Fig. 3.9. The black, red and blue lines corresponds to the following energy cutoffs $\Lambda = 15000$, $\Lambda = 7500$, $\Lambda = 5000$

B.2 The regularisation of the paring function in 3D

In 3D the contact potential leads to an unphysical divergency for a two body problem, which then also appears in the paring function. The regularisation prescription relies on using a pseudo-potential:

$$\Delta(\mathbf{R}) = |g_{ff}| \lim_{r \rightarrow 0} \frac{\partial}{\partial r} \left[r \left\langle \hat{\psi}_{f,\uparrow} \left(\mathbf{R} + \frac{\mathbf{r}}{2} \right) \hat{\psi}_{f,\downarrow} \left(\mathbf{R} - \frac{\mathbf{r}}{2} \right) \right\rangle \right], \quad (\text{B.5})$$

where \mathbf{r} is a relative position between two particle, \mathbf{R} is the centre of mass position. The operator $\frac{\partial}{\partial r}[r \cdot]$ is necessary as the expectation value $\left\langle \hat{\psi}_{f,\uparrow} \hat{\psi}_{f,\downarrow} \right\rangle$ diverges as $1/r$ for $r \rightarrow 0$. This can be shown by calculating the time derivative of $\left\langle \hat{\psi}_{f,\uparrow} \hat{\psi}_{f,\downarrow} \right\rangle$ [122], which for the steady-state approach of BCS theory has to equal zero (for a description of BCS theory look Sec. 1.4.2). By doing so, it becomes apparent that the compensation of the divergence of $\left\langle \hat{\psi}_{f,\uparrow} \hat{\psi}_{f,\downarrow} \right\rangle$ can be done, if for $r \rightarrow 0$ we have a following equality:

$$\left\langle \hat{\psi}_{f,\uparrow} \left(\mathbf{R} + \frac{\mathbf{r}}{2} \right) \hat{\psi}_{f,\downarrow} \left(\mathbf{R} - \frac{\mathbf{r}}{2} \right) \right\rangle = \frac{m}{4\pi\hbar^2 r} \Delta(\mathbf{R}) + F_{reg} + O(r). \quad (\text{B.6})$$

Now we inset $\left\langle \hat{\psi}_{f,\uparrow} \left(\mathbf{R} + \frac{\mathbf{r}}{2} \right) \hat{\psi}_{f,\downarrow} \left(\mathbf{R} - \frac{\mathbf{r}}{2} \right) \right\rangle$ into the definition of $\Delta(\mathbf{R})$ [Eq. B.5]

$$\Delta(\mathbf{R}) = |g_{ff}| F_{reg} = |g_{ff}| \lim_{r \rightarrow 0} \left[\left\langle \hat{\psi}_{f,\uparrow} \left(\mathbf{R} + \frac{\mathbf{r}}{2} \right) \hat{\psi}_{f,\downarrow} \left(\mathbf{R} - \frac{\mathbf{r}}{2} \right) \right\rangle - \frac{m}{4\pi\hbar^2 r} \Delta(\mathbf{R}) \right]. \quad (\text{B.7})$$

For a uniform and infinite system (see Sec. 1.4.2.1) we can calculate the value of $\left\langle \hat{\psi}_{f,\uparrow} \hat{\psi}_{f,\downarrow} \right\rangle$:

$$\left\langle \hat{\psi}_{f,\uparrow} \left(\mathbf{R} + \frac{\mathbf{r}}{2} \right) \hat{\psi}_{f,\downarrow} \left(\mathbf{R} - \frac{\mathbf{r}}{2} \right) \right\rangle = \frac{\Delta}{2} \int d^3k \frac{e^{i\mathbf{k}\mathbf{r}}}{E_k} (1 - f(E_k)), \quad (\text{B.8})$$

where $f(E_k)$ is the Fermi-Dirac distribution and $E_k = \sqrt{\Delta^2 + (\hbar^2 k^2 / 2m - \mu)^2}$. To calculate the paring function according to the Eq. (B.7) we substitute the $1/r$ term by a function $G(\mathbf{r})$ for which we know a solution (It is the same as adding and subtracting the the term $\Delta(\mathbf{R})G(\mathbf{r})/2$ from $\left\langle \hat{\psi}_{f,\uparrow} \hat{\psi}_{f,\downarrow} \right\rangle$). We use for this purpose

the single particle Green's function associated with Hamiltonian H_o , that satisfied the equation $[-\hbar^2/(2m)\nabla^2 - \mu]G(\mathbf{r}) = \delta(\mathbf{r})$:

$$G(\mathbf{r}) = \frac{m}{2\pi\hbar^2} \frac{e^{ik_f\mathbf{r}}}{r} \rightarrow \frac{m}{2\pi\hbar^2 r} + i \frac{m}{2\pi\hbar^2} k_f. \quad (\text{B.9})$$

Then, we can write the final expression for the pairing function

$$\Delta = \Delta \frac{|g_{ff}|}{2} \int d^3\mathbf{k} \left[\frac{1}{E_k} (1 - f(E_k)) - P \frac{1}{\epsilon_k} \right], \quad (\text{B.10})$$

where $\epsilon_k = \hbar^2 k^2 / 2m - \mu$. Indeed, $G(\mathbf{r}) = \lim_{\eta \rightarrow 0^+} \int d^3\mathbf{k} \frac{e^{i\mathbf{k}\mathbf{r}}}{\epsilon_k - i\eta}$, behaves similar as, for $r \rightarrow 0$, the integrand of the Eq. B.8 and the imaginary part cancel with the regularised part of the momentum truncated propagator ($1/(X - i\eta) = P(1/X) + i\pi\delta$).

For not necessary uniform and finite systems with some energy cutoff E_C the generalisations of the above procedure have been done [122–125]. The results have to be independent of E_C and the observables should be not effected by the procedure. It first of all requires that the value E_c has to be chosen sufficiently far from the Fermi level. For a great number of particle the system can be treated locally as infinite, which allows us to estimate the regulator (Eq. B.9) as follow:

$$\Delta(\mathbf{r}) = |g_{ff}| \sum_{E_n < E_C} v_n^*(\mathbf{r}) u_n(\mathbf{r}) (1 - f(E_n)) + i \frac{\Delta(\mathbf{r}) k_f(\mathbf{r}) m}{4\pi\hbar^2} + \frac{\Delta(\mathbf{r})}{4\pi^2} \int_0^{k_c(\mathbf{r})} k^2 dk \frac{1}{\epsilon_k}. \quad (\text{B.11})$$

In the unites use in the thesis we get the final expression:

$$\Delta(\mathbf{r}) = |g_{ff}| \sum_{E_n < E_C} v_n^*(\mathbf{r}) u_n(\mathbf{r}) - \frac{\Delta(\mathbf{r})}{2\pi} \left(\frac{1}{2} \ln \frac{\sqrt{E_C} + \sqrt{\mu}}{\sqrt{E_C} - \sqrt{\mu}} - \sqrt{\frac{E_C}{\mu}} \right), \quad (\text{B.12})$$

which leads to the regularised expression for $\Delta(\mathbf{r})$:

$$\Delta(\mathbf{r}) = |g_{\text{eff}}| \sum_{E_n < E_C} v_n^*(\mathbf{r}) u_n(\mathbf{r}), \quad (\text{B.13})$$

where $|g_{\text{eff}}|$ is define as:

$$\frac{1}{|g_{\text{eff}}|} = \frac{1}{|g_{ff}|} - \frac{1}{2\pi^2} \left(\frac{1}{2} \ln \frac{\sqrt{E_C} + \sqrt{\mu}}{\sqrt{E_C} - \sqrt{\mu}} - \sqrt{\frac{E_C}{\mu}} \right). \quad (\text{B.14})$$

In the Fig B.2 we present the pairing function for the Fermi system discuss in the Sec. 3.3. We notice that once the regularisation procedure is used the system is independent from the cutoff E_C .

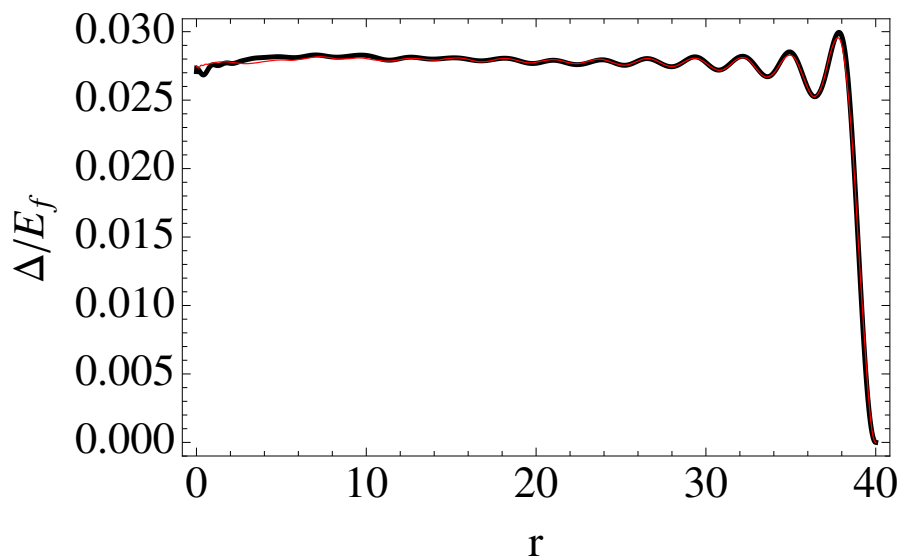


FIGURE B.2: The 3D pairing function Δ for a different cutoffs applied to the Fermi mixture with the same parameters as in the Fig. 3.3 ($g_{ff} = -5.5, \mu = E_f$). The black and red lines corresponds to Δ with the g_{eff} with the energy cutoff $E = 20E_f, E = 2E_f$ respectively. The difference are hardly visible.

Bibliography

- [1] M. H. Anderson, J. R. Ensher, M. R. Matthews, C. E. Wieman, and E. A. Cornell. Observation of Bose–Einstein condensation in a dilute atomic vapor. *Science*, 269:198–201, 1995.
- [2] K. B. Davis, M. O. Mewes, M. R. Andrews, N. J. van Druten, D. S. Durfee, D. M. Kurn, and W. Ketterle. *Phys. Rev. Lett.*, 75:3969, 1995.
- [3] C. C. Bradley, C. A. Sackett, J. J. Tollett, and R. G. Hulet. Evidence of Bose–Einstein condensation in an atomic gas with attractive interactions. *Phys. Rev. Lett.*, 75:1687, 1995.
- [4] W. D. Phillips. Laser cooling and trapping of neutral atoms. *Rev. Mod. Phys.*, 70:721, 1998.
- [5] Cheng Chin, R. Grimm, P. Julienne, and E. Tiesinga. Feshbach resonances in ultracold gases. *Rev. Mod. Phys.*, 82(2):1225–1286, 2010.
- [6] A. Görlitz, J. M. Vogels, A. E. Leanhardt, C. Raman, T. L. Gustavson, J. R. Abo-Shaer, A. P. Chikkatur, S. Gupta, S. Inouye, T. Rosenband, and W. Ketterle. Realization of Bose–Einstein condensates in lower dimensions. *Phys. Rev. Lett.*, 87:130402, 2001.
- [7] I. Bloch. Ultracold quantum gases in optical lattices. *Nature Physics*, 1: 23–30, 2005.
- [8] Alexander L. Gaunt, Tobias F. Schmidutz, Igor Gotlibovych, Robert P. Smith, and Zoran Hadzibabic. Bose-Einstein Condensation of Atoms in a Uniform Potential. *Phys. Rev. Lett.*, 110(20):200406, May 2013. ISSN

- 0031-9007. doi: 10.1103/PhysRevLett.110.200406. URL <http://link.aps.org/doi/10.1103/PhysRevLett.110.200406>.
- [9] C Becker, P Soltan-Panahi, J Kronjager, S Dorscher, K Bongs, and K Sengstock. Ultracold quantum gases in triangular optical lattices. *New Journal of Physics*, 12(6):065025, 2010. URL <http://stacks.iop.org/1367-2630/12/i=6/a=065025>.
- [10] J. Struck, C. Ölschläger, R. Le Targat, P. Soltan-Panahi, A. Eckardt, M. Lewenstein, P. Windpassinger, and K. Sengstock. Quantum simulation of frustrated classical magnetism in triangular optical lattices. *Science*, 2011. doi: 10.1126/science.1207239. URL <http://www.sciencemag.org/content/early/2011/07/20/science.1207239.abstract>.
- [11] I. Bloch, J. Dalibard, and W. Zwerger. Many-body physics with ultracold gases. *Rev. Mod. Phys.*, 80(3):885, 2008.
- [12] M. Greiner, M. O. Mandel, T. Esslinger, T. Hänsch, and I. Bloch. Quantum phase transition from a superfluid to a mott insulator in a gas of ultracold atoms. *Nature*, 415:39, 2002.
- [13] C. A. Regal, M. Greiner, and D. S. Jin. Observation of resonance condensation of fermionic atom pairs. *Phys. Rev. Lett.*, 92:040403, 2004.
- [14] A. L. Fetter and J. D. Walecka. *Quantum Theory of Many-Particle Systems*. McGraw-Hill, New York, 1971.
- [15] C.J. Pethick and H. Smith. *Bose–Einstein Condensation in Dilute Gases*. Cambridge University Press, Cambridge, 2002.
- [16] K. Huang. *Statistical Mechanics*. Wiley, New York, 1987.
- [17] Mohit Randeria, Ji-Min Duan, and Lih-Yir Shieh. Bound states, Cooper pairing, and Bose condensation in two dimensions. *Phys. Rev. Lett.*, 62: 981–984, Feb 1989. doi: 10.1103/PhysRevLett.62.981. URL <http://link.aps.org/doi/10.1103/PhysRevLett.62.981>.

- [18] W. Zwerger, editor. *BCS-BEC Crossover and the Unitary Fermi Gas*, volume 836 of *Lecture Notes in Physics*. Springer, Berlin, 2011.
- [19] S. Inouye, M. R. Andrews, J. Stenger, H.-J. Miesner, D. M. Stamper-Kurn, and W. Ketterle. Observation of Feshbach resonances in a Bose–Einstein condensate. *Nature*, 392:151–154, 1998.
- [20] W. Ketterle and M. Zwierlein. in *Ultra Cold Fermi Gases*, volume CLXIV of *Proceedings of the International School of Physics “Enrico Fermi”*, Edts M. Inguscio, W. Ketterle and C. Salomon. IOS Press, 2007.
- [21] Alexandrov A. S. *Theory of Superconductivity, From Weak to Strong Coupling*. Institute of Physics Publishing, Bristol, 2003.
- [22] L. P. Gor’kov. Microscopic derivation of the Ginzburg–Landau equations in the theory of superconductivity. *Soviet Phys. JETP*, 9:1364, 1959.
- [23] E. M. Lifshitz and L. P. Pitaevskii. *Statistical Physics*. Pergamon Press, Oxford, 1980.
- [24] D. Jaksch and P. Zoller. The cold atoms Hubbard toolbox. *Ann. Phys. (N.Y.)*, 315:52, 2005.
- [25] M. Lewenstein, A. Sanpera, V. Ahufinger, B. Damski, A. Sen De, and U. Sen. Ultracold atomic gases in optical lattices: mimicking condensed matter physics and beyond. *Adv. Phys.*, 56(2):243–379, 2007.
- [26] Thomas M Hanna, Eite Tiesinga, and Paul S Julienne. Creation and manipulation of Feshbach resonances with radiofrequency radiation. *New Journal of Physics*, 12(8):083031, 2010. URL <http://stacks.iop.org/1367-2630/12/i=8/a=083031>.
- [27] D. Jaksch, C. Bruder, J. I. Cirac, C. W. Gardiner, and P. Zoller. Cold bosonic atoms in optical lattices. *Phys. Rev. Lett.*, 81:3108, 1998.
- [28] M. Greiner, M. O. Mandel, T. Hänsch, and I. Bloch. Collapse and revival of the matter wave field of a Bose–Einstein condensate. *Nature*, 419:51, 2002.

- [29] Andre Eckardt, Christoph Weiss, and Martin Holthaus. Superfluid-insulator transition in a periodically driven optical lattice. *Phys. Rev. Lett.*, 95(26):260404, 2005. doi: 10.1103/PhysRevLett.95.260404. URL <http://link.aps.org/abstract/PRL/v95/e260404>.
- [30] H. Lignier, C. Sias, D. Ciampini, Y. Singh, A. Zenesini, O. Morsch, and E. Arimondo. Dynamical control of matter-wave tunneling in periodic potentials. *Phys. Rev. Lett.*, 99:220403, Nov 2007. doi: 10.1103/PhysRevLett.99.220403. URL <http://link.aps.org/doi/10.1103/PhysRevLett.99.220403>.
- [31] Alessandro Zenesini, Hans Lignier, Donatella Ciampini, Oliver Morsch, and Ennio Arimondo. Coherent control of dressed matter waves. *Physical Review Letters*, 102(10):100403, 2009. doi: 10.1103/PhysRevLett.102.100403. URL <http://link.aps.org/abstract/PRL/v102/e100403>.
- [32] A. Eckardt, P. Hauke, P. Soltan-Panahi, C. Becker, K. Sengstock, and M. Lewenstein. Frustrated quantum antiferromagnetism with ultracold bosons in a triangular lattice. *EPL (Europhysics Letters)*, 89(1):10010, 2010. URL <http://stacks.iop.org/0295-5075/89/i=1/a=10010>.
- [33] Arkadiusz Kosior and Krzysztof Sacha. Simulation of frustrated classical xy models with ultracold atoms in three-dimensional triangular optical lattices. *Phys. Rev. A*, 87:023602, Feb 2013. doi: 10.1103/PhysRevA.87.023602. URL <http://link.aps.org/doi/10.1103/PhysRevA.87.023602>.
- [34] Krzysztof Sacha, Katarzyna Targońska, and Jakub Zakrzewski. Frustration and time-reversal symmetry breaking for Fermi and Bose-Fermi systems. *Phys. Rev. A*, 85:053613, May 2012. doi: 10.1103/PhysRevA.85.053613. URL <http://link.aps.org/doi/10.1103/PhysRevA.85.053613>.
- [35] J. Struck, C. Ölschläger, M. Weinberg, P. Hauke, J. Simonet, A. Eckardt, M. Lewenstein, K. Sengstock, and P. Windpassinger. Tunable gauge potential for neutral and spinless particles in driven optical lattices. *Phys. Rev.*

- Lett.*, 108:225304, May 2012. doi: 10.1103/PhysRevLett.108.225304. URL <http://link.aps.org/doi/10.1103/PhysRevLett.108.225304>.
- [36] Philipp Hauke, Olivier Tieleman, Alessio Celi, Christoph Ölschläger, Juliette Simonet, Julian Struck, Malte Weinberg, Patrick Windpassinger, Klaus Sengstock, Maciej Lewenstein, and André Eckardt. Non-abelian gauge fields and topological insulators in shaken optical lattices. *Phys. Rev. Lett.*, 109:145301, Oct 2012. doi: 10.1103/PhysRevLett.109.145301. URL <http://link.aps.org/doi/10.1103/PhysRevLett.109.145301>.
- [37] N. D. Mermin and H. Wagner. Absence of ferromagnetism or antiferromagnetism in one- or two-dimensional isotropic Heisenberg models. *Phys. Rev. Lett.*, 17:1133, 1966.
- [38] N. W. Ashcroft and N. D. Mermin. *Solid State Physics*. Holt, Rinehardt and Winston, New York, 1976.
- [39] J. Hubbard. Electron correlations in narrow energy bands. *Proc. R. Soc. A*, 276:238–257, November 1963.
- [40] G. Floquet. Sur les équations différentielles linéaires à coefficients périodiques. *Annales de l'École Normale Supérieure*, 12:47, 1883.
- [41] Jon H. Shirley. Solution of the Schrödinger equation with a Hamiltonian periodic in time. *Phys. Rev.*, 138:B979–B987, May 1965. doi: 10.1103/PhysRev.138.B979. URL <http://link.aps.org/doi/10.1103/PhysRev.138.B979>.
- [42] Zel'dovich. The quasienergy of a quantum-mechanical system subjected to a periodic action. *Sov. Phys. JETP*, 1967.
- [43] Ennio Arimondo, Donatella Ciampini, André Eckardt, Martin Holthaus, and Oliver Morsch. Chapter 10 - KiloHertz-Driven Bose–Einstein Condensates in Optical Lattices. In Ennio Arimondo Paul Berman and Chun Lin, editors, *Advances in Atomic, Molecular, and Optical Physics*, volume 61 of *Advances In Atomic, Molecular, and Optical Physics*, pages 515 – 547. Academic Press, 2012. doi: <http://dx.doi.org/10.1016/B978-0-12-396482-3>.

- 00010-7. URL <http://www.sciencedirect.com/science/article/pii/B9780123964823000107>.
- [44] A G Fainshtein, N L Manakov, and L P Rapoport. Some general properties of quasi-energetic spectra of quantum systems in classical monochromatic fields. *Journal of Physics B: Atomic and Molecular Physics*, 11(14):2561, 1978. URL <http://stacks.iop.org/0022-3700/11/i=14/a=020>.
- [45] F. Haake. *Quantum Signatures of Chaos*. Springer-Verlag, 2nd edition, 2001.
- [46] Mateusz Lacki and Jakub Zakrzewski. Fast dynamics for atoms in optical lattices. *Phys. Rev. Lett.*, 110:065301, Feb 2013. doi: 10.1103/PhysRevLett.110.065301. URL <http://link.aps.org/doi/10.1103/PhysRevLett.110.065301>.
- [47] A. Niederberger, J. Wehr, M. Lewenstein, and K. Sacha. Disorder-induced phase control in superfluid Fermi-Bose mixtures. *EPL (Europhysics Letters)*, 86(2):26004, 2009. URL <http://stacks.iop.org/0295-5075/86/i=2/a=26004>.
- [48] C. A. Regal and D. S. Jin. Measurement of positive and negative scattering lengths in a Fermi gas of atoms. *Phys. Rev. Lett.*, 90:230404, 2003.
- [49] D. K. K. Lee and J. M. F. Gunn. Polarons and Bose decondensation: A self-trapping approach. *Phys. Rev. B*, 46:301–307, Jul 1992. doi: 10.1103/PhysRevB.46.301. URL <http://link.aps.org/doi/10.1103/PhysRevB.46.301>.
- [50] Ryan M. Kalas and D. Blume. Interaction-induced localization of an impurity in a trapped Bose-Einstein condensate. *Phys. Rev. A*, 73:043608, Apr 2006. doi: 10.1103/PhysRevA.73.043608. URL <http://link.aps.org/doi/10.1103/PhysRevA.73.043608>.
- [51] F. M. Cucchietti and E. Timmermans. Strong-coupling polarons in dilute gas Bose-Einstein condensates. *Phys. Rev. Lett.*, 96:210401, Jun 2006. doi: 10.

- 1103/PhysRevLett.96.210401. URL <http://link.aps.org/doi/10.1103/PhysRevLett.96.210401>.
- [52] Krzysztof Sacha and Eddy Timmermans. Self-localized impurities embedded in a one-dimensional Bose-Einstein condensate and their quantum fluctuations. *Phys. Rev. A*, 73:063604, Jun 2006. doi: 10.1103/PhysRevA.73.063604. URL <http://link.aps.org/doi/10.1103/PhysRevA.73.063604>.
- [53] M. Bruderer, W. Bao, and D. Jaksch. Self-trapping of impurities in Bose-Einstein condensates: Strong attractive and repulsive coupling. *EPL (Europhysics Letters)*, 82(3):30004, 2008. URL <http://stacks.iop.org/0295-5075/82/i=3/a=30004>.
- [54] M Bruderer, A Klein, S R Clark, and D Jaksch. Transport of strong-coupling polarons in optical lattices. *New Journal of Physics*, 10(3):033015, 2008. URL <http://stacks.iop.org/1367-2630/10/i=3/a=033015>.
- [55] D. H. Santamore and Eddy Timmermans. Fermion-mediated interactions in a dilute Bose-Einstein condensate. *Phys. Rev. A*, 78:013619, Jul 2008. doi: 10.1103/PhysRevA.78.013619. URL <http://link.aps.org/doi/10.1103/PhysRevA.78.013619>.
- [56] David C. Roberts and Sergio Rica. Impurity crystal in a Bose-Einstein condensate. *Phys. Rev. Lett.*, 102:025301, Jan 2009. doi: 10.1103/PhysRevLett.102.025301. URL <http://link.aps.org/doi/10.1103/PhysRevLett.102.025301>.
- [57] Alexey Novikov and Mikhail Ovchinnikov. A diagrammatic calculation of the energy spectrum of quantum impurity in degenerate Bose-Einstein condensate. *Journal of Physics A: Mathematical and Theoretical*, 42(13):135301, 2009. URL <http://stacks.iop.org/1751-8121/42/i=13/a=135301>.
- [58] J. Tempere, W. Casteels, M. K. Oberthaler, S. Knoop, E. Timmermans, and J. T. Devreese. Feynman path-integral treatment of the BEC-impurity polaron. *Phys. Rev. B*, 80:184504, Nov 2009. doi: 10.1103/PhysRevB.80.184504. URL <http://link.aps.org/doi/10.1103/PhysRevB.80.184504>.

- [59] Alexey Novikov and Mikhail Ovchinnikov. Variational approach to the ground state of an impurity in a Bose–Einstein condensate. *Journal of Physics B: Atomic, Molecular and Optical Physics*, 43(10):105301, 2010. URL <http://stacks.iop.org/0953-4075/43/i=10/a=105301>.
- [60] F. Chevy. Universal phase diagram of a strongly interacting Fermi gas with unbalanced spin populations. *Phys. Rev. A*, 74:063628, Dec 2006. doi: 10.1103/PhysRevA.74.063628. URL <http://link.aps.org/doi/10.1103/PhysRevA.74.063628>.
- [61] R. Combescot, A. Recati, C. Lobo, and F. Chevy. Normal state of highly polarized Fermi gases: Simple Many-Body approaches. *Phys. Rev. Lett.*, 98:180402, May 2007. doi: 10.1103/PhysRevLett.98.180402. URL <http://link.aps.org/doi/10.1103/PhysRevLett.98.180402>.
- [62] M. Punk and W. Zwerger. Theory of rf-spectroscopy of strongly interacting fermions. *arXiv:0707.0792*, 2007.
- [63] Nikolay Prokof'ev and Boris Svistunov. Fermi-polaron problem: Diagrammatic Monte Carlo method for divergent sign-alternating series. *Phys. Rev. B*, 77:020408, Jan 2008. doi: 10.1103/PhysRevB.77.020408. URL <http://link.aps.org/doi/10.1103/PhysRevB.77.020408>.
- [64] N. V. Prokof'ev and B. V. Svistunov. Bold diagrammatic Monte Carlo: A generic sign-problem tolerant technique for polaron models and possibly interacting many-body problems. *Phys. Rev. B*, 77:125101, Mar 2008. doi: 10.1103/PhysRevB.77.125101. URL <http://link.aps.org/doi/10.1103/PhysRevB.77.125101>.
- [65] M. Punk, P. T. Dumitrescu, and W. Zwerger. Polaron-to-molecule transition in a strongly imbalanced Fermi gas. *Phys. Rev. A*, 80:053605, Nov 2009. doi: 10.1103/PhysRevA.80.053605. URL <http://link.aps.org/doi/10.1103/PhysRevA.80.053605>.
- [66] Nicolas Spethmann, Farina Kindermann, Shincy John, Claudia Weber, Dieter Meschede, and Artur Widera. Dynamics of single neutral impurity

- atoms immersed in an ultracold gas. *Phys. Rev. Lett.*, 109:235301, Dec 2012. doi: 10.1103/PhysRevLett.109.235301. URL <http://link.aps.org/doi/10.1103/PhysRevLett.109.235301>.
- [67] Arne Härter, Artjom Krüchow, Andreas Brunner, Wolfgang Schnitzler, Stefan Schmid, and Johannes Hecker Denschlag. Single ion as a three-body reaction center in an ultracold atomic gas. *Phys. Rev. Lett.*, 109:123201, Sep 2012. doi: 10.1103/PhysRevLett.109.123201. URL <http://link.aps.org/doi/10.1103/PhysRevLett.109.123201>.
- [68] Lothar Ratschbacher, Christoph Zipkes, Carlo Sias, and Michael Kohl. Controlling chemical reactions of a single particle. *Nat Phys*, 8(9):649–652, 09 2012. URL <http://dx.doi.org/10.1038/nphys2373>.
- [69] N. Spethmann, F. Kindermann, S. John, C. Weber, D. Meschede, and A. Widera. Inserting single Cs atoms into an ultracold Rb gas. *Applied Physics B*, 106(3):513–519, 2012. ISSN 0946-2171. doi: 10.1007/s00340-011-4868-6. URL <http://dx.doi.org/10.1007/s00340-011-4868-6>.
- [70] J. Catani, G. Lamporesi, D. Naik, M. Gring, M. Inguscio, F. Minardi, A. Kantian, and T. Giamarchi. Quantum dynamics of impurities in a one-dimensional Bose gas. *Phys. Rev. A*, 85:023623, Feb 2012. doi: 10.1103/PhysRevA.85.023623. URL <http://link.aps.org/doi/10.1103/PhysRevA.85.023623>.
- [71] Tetsu Takekoshi, Markus Debatin, Raffael Rameshan, Francesca Ferlaino, Rudolf Grimm, Hanns-Christoph Nägerl, C. Ruth Le Sueur, Jeremy M. Hutson, Paul S. Julienne, Svetlana Kotochigova, and Eberhard Tiemann. Towards the production of ultracold ground-state rbc molecules: Feshbach resonances, weakly bound states, and the coupled-channel model. *Phys. Rev. A*, 85:032506, Mar 2012. doi: 10.1103/PhysRevA.85.032506. URL <http://link.aps.org/doi/10.1103/PhysRevA.85.032506>.

- [72] Jee Woo Park, Cheng-Hsun Wu, Ibon Santiago, Tobias G. Tiecke, Sebastian Will, Peyman Ahmadi, and Martin W. Zwierlein. Quantum degenerate Bose-Fermi mixture of chemically different atomic species with widely tunable interactions. *Phys. Rev. A*, 85:051602, May 2012. doi: 10.1103/PhysRevA.85.051602. URL <http://link.aps.org/doi/10.1103/PhysRevA.85.051602>.
- [73] T. Schuster, R. Scelle, A. Trautmann, S. Knoop, M. K. Oberthaler, M. M. Haverhals, M. R. Goosen, S. J. J. M. F. Kokkelmans, and E. Tiemann. Feshbach spectroscopy and scattering properties of ultracold Li + Na mixtures. *Phys. Rev. A*, 85:042721, Apr 2012. doi: 10.1103/PhysRevA.85.042721. URL <http://link.aps.org/doi/10.1103/PhysRevA.85.042721>.
- [74] M. Repp, R. Pires, J. Ulmanis, R. Heck, E. D. Kuhnle, M. Weidemüller, and E. Tiemann. Observation of interspecies ${}^6\text{Li}$ - ${}^{133}\text{Cs}$ Feshbach resonances. *Phys. Rev. A*, 87:010701, Jan 2013. doi: 10.1103/PhysRevA.87.010701. URL <http://link.aps.org/doi/10.1103/PhysRevA.87.010701>.
- [75] H. Fröhlich. Electrons in lattice fields. *Advances in Physics*, 3(11):325–361, 1954. doi: 10.1080/00018735400101213. URL <http://www.tandfonline.com/doi/abs/10.1080/00018735400101213>.
- [76] S. I. Pekar L. D. Landau. *Zh. Eksp. Teor. Fiz.*, 16:341, 1946.
- [77] S. I. Pekar L. D. Landau. *Zh. Eksp. Teor. Fiz.*, 18:419, 1948.
- [78] G. D. Mahan. *Many-Particle Physics*. Plenum Press, 1981.
- [79] A. A. Blinova, M. G. Boshier, and E. Timmermans. Single impurities in a Bose-Einstein condensate can make two polaron flavors. *ArXiv e-prints*, April 2013.
- [80] C. G. Kuper. Theory of negative ions in liquid Helium. *Phys. Rev.*, 122:1007–1011, May 1961. doi: 10.1103/PhysRev.122.1007. URL <http://link.aps.org/doi/10.1103/PhysRev.122.1007>.

- [81] Jozef T Devreese and Alexandre S Alexandrov. Fröhlich polaron and bipolaron: recent developments. *Reports on Progress in Physics*, 72(6):066501, 2009. URL <http://stacks.iop.org/0034-4885/72/i=6/a=066501>.
- [82] André Schirotzek, Cheng-Hsun Wu, Ariel Sommer, and Martin W. Zwierlein. Observation of Fermi polarons in a tunable Fermi liquid of ultracold atoms. *Phys. Rev. Lett.*, 102:230402, Jun 2009. doi: 10.1103/PhysRevLett.102.230402. URL <http://link.aps.org/doi/10.1103/PhysRevLett.102.230402>.
- [83] S. Nascimbène, N. Navon, K. J. Jiang, L. Tarruell, M. Teichmann, J. McKeever, F. Chevy, and C. Salomon. Collective oscillations of an imbalanced Fermi gas: Axial compression modes and polaron effective mass. *Phys. Rev. Lett.*, 103:170402, Oct 2009. doi: 10.1103/PhysRevLett.103.170402. URL <http://link.aps.org/doi/10.1103/PhysRevLett.103.170402>.
- [84] C. Kohstall, M. Zaccanti, M. Jag, A. Trenkwalder, P. Massignan, G. M. Bruun, F. Schreck, and R. Grimm. Metastability and coherence of repulsive polarons in a strongly interacting Fermi mixture. *Nature*, 485(7400):615–618, 05 2012. URL <http://dx.doi.org/10.1038/nature11065>.
- [85] R. A. Duine and A. H. MacDonald. Itinerant ferromagnetism in an ultracold atom Fermi gas. *Phys. Rev. Lett.*, 95:230403, Nov 2005. doi: 10.1103/PhysRevLett.95.230403. URL <http://link.aps.org/doi/10.1103/PhysRevLett.95.230403>.
- [86] G. J. Conduit, A. G. Green, and B. D. Simons. Inhomogeneous phase formation on the border of itinerant ferromagnetism. *Phys. Rev. Lett.*, 103:207201, Nov 2009. doi: 10.1103/PhysRevLett.103.207201. URL <http://link.aps.org/doi/10.1103/PhysRevLett.103.207201>.
- [87] Gyu-Boong Jo, Ye-Ryoung Lee, Jae-Hoon Choi, Caleb A. Christensen, Tony H. Kim, Joseph H. Thywissen, David E. Pritchard, and Wolfgang Ketterle. Itinerant ferromagnetism in a Fermi gas of ultracold atoms.

- Science*, 325(5947):1521–1524, 2009. doi: 10.1126/science.1177112. URL <http://www.sciencemag.org/content/325/5947/1521.abstract>.
- [88] P. Massignan and G.M. Bruun. Repulsive polarons and itinerant ferromagnetism in strongly polarized Fermi gases. *The European Physical Journal D*, 65(1-2):83–89, 2011. ISSN 1434-6060. doi: 10.1140/epjd/e2011-20084-5. URL <http://dx.doi.org/10.1140/epjd/e2011-20084-5>.
- [89] Elisa Fratini and Pierbiagio Pieri. Pairing and condensation in a resonant Bose-Fermi mixture. *Phys. Rev. A*, 81:051605, May 2010. doi: 10.1103/PhysRevA.81.051605. URL <http://link.aps.org/doi/10.1103/PhysRevA.81.051605>.
- [90] Elisa Fratini and Pierbiagio Pieri. Mass imbalance effect in resonant Bose-Fermi mixtures. *Phys. Rev. A*, 85:063618, Jun 2012. doi: 10.1103/PhysRevA.85.063618. URL <http://link.aps.org/doi/10.1103/PhysRevA.85.063618>.
- [91] G. Bertaina, E. Fratini, S. Giorgini, and P. Pieri. Quantum Monte Carlo study of a resonant Bose-Fermi mixture. *Phys. Rev. Lett.*, 110:115303, Mar 2013. doi: 10.1103/PhysRevLett.110.115303. URL <http://link.aps.org/doi/10.1103/PhysRevLett.110.115303>.
- [92] K. Mølmer. Phase collapse and excitations in Bose-Einstein condensates. *Phys. Rev. A*, 58:566, 1998.
- [93] L. Viverit, C. J. Pethick, and H. Smith. Zero-temperature phase diagram of binary boson-fermion mixtures. *Phys. Rev. A*, 61:053605, Apr 2000. doi: 10.1103/PhysRevA.61.053605. URL <http://link.aps.org/doi/10.1103/PhysRevA.61.053605>.
- [94] S. Yip. Collective modes in a dilute Bose-Fermi mixture. *Physical Review A*, 64(2):2–5, lipca 2001. ISSN 1050-2947. doi: 10.1103/PhysRevA.64.023609. URL <http://link.aps.org/doi/10.1103/PhysRevA.64.023609>.

- [95] Robert Roth. Structure and stability of trapped atomic boson-fermion mixtures. *Phys. Rev. A*, 66:013614, Jul 2002. doi: 10.1103/PhysRevA.66.013614. URL <http://link.aps.org/doi/10.1103/PhysRevA.66.013614>.
- [96] Han Pu, Weiping Zhang, Martin Wilkens, and Pierre Meystre. Phonon spectrum and dynamical stability of a dilute quantum degenerate Bose-Fermi mixture. *Phys. Rev. Lett.*, 88:070408, Feb 2002. doi: 10.1103/PhysRevLett.88.070408. URL <http://link.aps.org/doi/10.1103/PhysRevLett.88.070408>.
- [97] Sadhan K. Adhikari and Luca Salasnich. One-dimensional superfluid bose-fermi mixture: Mixing, demixing, and bright solitons. *Phys. Rev. A*, 76:023612, Aug 2007. doi: 10.1103/PhysRevA.76.023612. URL <http://link.aps.org/doi/10.1103/PhysRevA.76.023612>.
- [98] S. G. Bhongale and H. Pu. Phase separation in a mixture of a Bose-Einstein condensate and a two-component Fermi gas as a probe of Fermi superfluidity. *Phys. Rev. A*, 78:061606, Dec 2008. doi: 10.1103/PhysRevA.78.061606. URL <http://link.aps.org/doi/10.1103/PhysRevA.78.061606>.
- [99] Dirk-Sören Lühmann, Kai Bongs, Klaus Sengstock, and Daniela Pfannkuche. Self-Trapping of Bosons and Fermions in Optical Lattices. *Physical Review Letters*, 101(5):1–4, lipca 2008. ISSN 0031-9007. doi: 10.1103/PhysRevLett.101.050402. URL <http://link.aps.org/doi/10.1103/PhysRevLett.101.050402>.
- [100] Yu-Li Lee and Yu-Wen Lee. The stability of the low-dimensional mixtures of dilute quantum gases. *Journal of the Physical Society of Japan*, 80(4):044003, 2011. doi: 10.1143/JPSJ.80.044003. URL <http://jpsj.ipap.jp/link?JPSJ/80/044003/>.
- [101] Jun Liang Song, Mohammad S. Mashayekhi, and Fei Zhou. Fermi-Bose mixtures near broad interspecies Feshbach resonances. *Phys. Rev. Lett.*, 105:195301, Nov 2010. doi: 10.1103/PhysRevLett.105.195301. URL <http://link.aps.org/doi/10.1103/PhysRevLett.105.195301>.

- [102] M. Theis, G. Thalhammer, K. Winkler, M. Hellwig, G. Ruff, R. Grimm, and J. Hecker Denschlag. Tuning the scattering length with an optically induced Feshbach resonance. *Phys. Rev. Lett.*, 93:123001, 2004.
- [103] W. Greiner. *Thermodynamics and Statistical Mechanics*. Springer-Verlag, 1995.
- [104] C. H. Schunck, Y. Shin, A. Schirotzek, M. W. Zwierlein, and W. Ketterle. Pairing of strongly interacting fermions without superfluidity. *cond-mat/0702066*, 2007.
- [105] M. R. Matthews, B. P. Anderson, P. C. Haljan, D. S. Hall, C. E. Wieman, and E. A. Cornell. Vortices in a Bose–Einstein condensate. *Phys. Rev. Lett.*, 83:2498, 1999.
- [106] K. W. Madison, F. Chevy, W. Wohlleben, and J. Dalibard. Vortex formation in a stirred Bose–Einstein condensate. *Phys. Rev. Lett.*, 84:806, 2000.
- [107] J. R. Abo-Shaer, C. Raman, J. M. Vogels, and W. Ketterle. Observation of vortex lattices in Bose-Einstein condensates. *Science*, 292(5516):476–479, 2001. doi: 10.1126/science.1060182. URL <http://www.sciencemag.org/content/292/5516/476.abstract>.
- [108] M. W. Zwierlein, J. R. Abo-Shaer, A. Schirotzek, C. H. Schunck, and W. Ketterle. Vortices and superfluidity in a strongly interacting Fermi gas. *Nature*, 435:1047, 2005.
- [109] Giovanni Modugno, Giacomo Roati, Francesco Riboli, Francesca Ferlaino, Robert J. Brecha, and Massimo Inguscio. Collapse of a degenerate Fermi gas. *Science*, 297(5590):2240–2243, 2002. doi: 10.1126/science.1077386. URL <http://www.sciencemag.org/content/297/5590/2240.abstract>.
- [110] R. Roth and H. Feldmeier. Mean-field instability of trapped dilute boson-fermion mixtures. *Phys. Rev. A*, 65:021603, Jan 2002. doi: 10.1103/PhysRevA.65.021603. URL <http://link.aps.org/doi/10.1103/PhysRevA.65.021603>.

- [111] F. D. M. Haldane. Effective harmonic-fluid approach to low-energy properties of one-dimensional quantum fluids. *Phys. Rev. Lett.*, 47:1840, 1981.
- [112] M. Takahashi. *Thermodynamics of One-Dimensional Solvable Models*. Cambridge University Press, 1999.
- [113] T. Kinoshita, T. Wenger, and D. S. Weiss. A quantum Newton's cradle. *Nature*, 440:900–903, 2006.
- [114] T. Kinoshita, T. Wenger, and D. S. Weiss. Observation of a one-dimensional Tonks-Girardeau gas. *Science*, 305:1125–1128, 2004.
- [115] B. Paredes, A. Widera, V. Murg, O. Mandel, S. Fölling, J. I Cirac, G. V. Shlyapnikov, T. W. Hänsch, and I. Bloch. Tonks-Girardeau gas of ultracold atoms in an optical lattice. *Nature*, 429:277 – 281, 2004.
- [116] Jacek Dziarmaga and Krzysztof Sacha. Gap soliton in superfluid Fermi gas at zero and finite temperature. *Laser Physics*, 15:674, 2005.
- [117] Johnson R. S. Drazin P. G. *Soliton:an introduction*. Cambridge University Press, 1989.
- [118] Tarik Yefsah, Ariel T. Sommer, Mark J. H. Ku, Lawrence W. Cheuk, Wenjie Ji, Waseem S. Bakr, and Martin W. Zwierlein. Heavy solitons in a fermionic superfluid. *Nature*, 499(7459):426–430, 07 2013. URL <http://dx.doi.org/10.1038/nature12338>.
- [119] Tomasz Karpiuk, Mirosław Brewczyk, and Kazimierz Rzazewski. Bright solitons in Bose-Fermi mixtures. *Physical Review A*, 73(5):1–6, maja 2006. ISSN 1050-2947. doi: 10.1103/PhysRevA.73.053602. URL <http://link.aps.org/doi/10.1103/PhysRevA.73.053602>.
- [120] Y. S. Kivshar and G. P. Agrawal. *Optical Solitons*. Elsevier, 2003.
- [121] M. Holland and J. Wachter. in *Ultra Cold Fermi Gases*, volume CLXIV of *Proceedings of the International School of Physics "Enrico Fermi"*, Edts M. Inguscio, W. Ketterle and C. Salomon. IOS Press, 2007.

-
- [122] G. Bruun, Y. Castin, R. Dum, and K. Burnett. Bcs theory for trapped ultracold fermions. *The European Physical Journal D - Atomic, Molecular, Optical and Plasma Physics*, 7(3):433–439, 1999. ISSN 1434-6060. doi: 10.1007/s100530050587. URL <http://dx.doi.org/10.1007/s100530050587>.
- [123] Aurel Bulgac and Yongle Yu. Renormalization of the Hartree-Fock-Bogoliubov equations in the case of a zero range pairing interactions. *Phys. Rev. Lett.*, 88:042504, Jan 2002. doi: 10.1103/PhysRevLett.88.042504. URL <http://link.aps.org/doi/10.1103/PhysRevLett.88.042504>.
- [124] Marcella Grasso and Michael Urban. Hartree-Fock-Bogoliubov theory versus local-density approximation for superfluid trapped fermionic atoms. *Phys. Rev. A*, 68:033610, Sep 2003. doi: 10.1103/PhysRevA.68.033610. URL <http://link.aps.org/doi/10.1103/PhysRevA.68.033610>.
- [125] A. Niederberger, J. Wehr, M. Lewenstein, and K. Sacha. Disorder-induced phase control in superfluid Fermi-Bose mixtures. *EPL (Europhysics Letters)*, 86(2):26004, 2009. URL <http://stacks.iop.org/0295-5075/86/i=2/a=26004>.